# Catenated covalent organic frameworks constructed from polyhedra

Tianqiong Ma[1,2,3], Yi Zhou[4,5], Christian S. Diercks[1,2,3], Junpyo Kwon[6,7], Felipe Gándara[8], Hao Lyu[1,2,3], Nikita Hanikel[1,2,3], Pilar P. Sánchez[8], Yuzhong Liu[1,2,3], Nicolas J. Diercks[1,2,3], Robert O. Ritchie[6,7,9], Davide M. Proserpio[10], Osamu Terasaki[4,5] and Omar M. Yaghi[1,2,3]*

[1]Department of Chemistry, University of California, Berkeley, CA 94720, United States.

[2]Kavli Energy NanoScience Institute, Berkeley, CA 94720, United States.

[3]Bakar Institute of Digital Materials for the Planet, Division of Computing, Data Science, and Society, University of California, Berkeley, CA 94720, United States.

[4]Center for High-Resolution Electron Microscopy (C*ħ*EM), School of Physical Science and Technology, ShanghaiTech University, Shanghai 201210, People's Republic of China.

[5]Shanghai Key Laboratory of High-Resolution Electron Microscopy, ShanghaiTech University, Shanghai 201210, People's Republic of China.

[6]Department of Mechanical Engineering, University of California, Berkeley, CA 94720, United States.

[7]Materials Science Division, Lawrence Berkeley National Laboratory, Berkeley, CA 94720, United States.

[8]Department of New Architectures in Materials Chemistry, Materials Science Institute of Madrid, Consejo Superior de Investigaciones Científicas, Madrid 28049, Spain.

[9]Department of Materials Science and Engineering, University of California, Berkeley, CA 94720, United States.

[10]Dipartimento di Chimica, Università di Milano, Via Golgi 19, Milano 20133, Italy.

*Corresponding author. Email: yaghi@berkeley.edu

**Abstract:** Although the synthetic chemistry leading to interlocking molecular [*n*]catenanes of organic polyhedra (*n* = 2–3) and rings (*n* = 2–130) is established, the analogous chemistry pertaining to infinite three-dimensional systems ([∞]catenane) remains undeveloped. We report a series of [∞]catenane covalent organic frameworks (termed catena-COFs). These were synthesized by linking 4,4'-(1,10-phenanthroline-2,9-diyl)dibenzaldehyde (PDB) to either of tris-(4-aminophenyl)-amine (TAPA), -methane (TAPM), or -methanol (TAPMol) through imine condensation. These combinations give discrete adamantane-like polyhedra, catenated by virtue of the copper(I) ions templating a mutually embracing arrangement of PDBs (points-of-catenation) and ultimately resulting in infinite catena-COF-805, -806, and -807. The crystal structures of these COFs obtained from electron microscopy and x-ray diffraction were determined to be isoreticular and to adopt the **bor-y** structure type.

Synthetic molecular architectures in which polyhedra or rings are held together through mechanical interlocking rather than chemical bonding are referred to as [*n*]catenanes (*n* denotes the number of mechanically linked units)[1–6]. In such catenated molecules, the constituents can move freely within the confines of their mechanically linked counterpart without parting company. This interlocking provides for large-amplitude motion at the molecular level without the need for making or breaking chemical bonds and has thus enabled the development of molecular machines[7–11]. Facilitating dynamics through interlocking is also known in nature where, for example, the viral capsid of bacteriophage HK97 comprises catenated proteins having the required structural flexibility for passage of genomic material[12]. Thus, discrete interlocking molecules of increasing complexity have been synthesized including catenanes of interlocking rings[1–4] and cages[13–16],

rotaxanes[17–19], and one-dimensional poly[*n*]catenanes[20,21] or Olympic gels[22,23]. In contrast, the chemistry of [∞]catenane frameworks is undeveloped: several metal-organic frameworks containing interlocking are known[24–33]; however, their design remains elusive. The challenge of making such systems is further highlighted by the complete absence of organic [∞]catenane frameworks where discrete organic molecular constituents are linked by mechanical interlocking. Here, we report a series of [∞]catenane covalent organic frameworks (COFs), termed catena-COF-805, -806, and -807, which are formed through mechanical interlocking of discrete organic adamantane-like polyhedra. The crystal structures of the three catena-COFs were solved by a combination of transmission electron microscopy (TEM) techniques and powder x-ray crystallography. Based on their crystal structure and the average particle size, it can be calculated that each individual COF crystal is composed of millions of interlocking organic polyhedra.

The design of an [∞]catenane framework commenced with the identification of a topology that can be formed from the interlocking of rings or polyhedra (Supplementary Section 1). We targeted the **bor** topology[34] in which 3- and 4-connected vertices are linked alternately to produce an infinite 3D arrangement. Reticulation of the tetrahedral $[Cu(PDB)_2]BF_4$ (where PDB = 4,4'-(1,10-phenanthroline-2,9-diyl)dibenzaldehyde)[35] with tritopic tris-(4-aminophenyl)amine (TAPA), tris-(4-aminophenyl)methane (TAPM), and tris-(4-aminophenyl)methanol (TAPMol) linkers yields catena-COF-805, -806, and -807 with interlocking **bor-y** topology (the underlying **bor** topology, Fig. 1). In $[Cu(PDB)_2]BF_4$, the copper centers pre-organize two PDB ligands in a mutually embracing manner, such that their appended aldehyde groups approximate a tetrahedral geometry in order to meet the interlocking requirement for adjacent adamantane-like polyhedra. The angles between the two aldehyde functionalities of each phenanthroline ligand and the angles between amino functionalities of TAPA, TAPM, or TAPMol are close to the target angles of an adamantane-like polyhedron (70.5° and 120°). The minor deviation of the angles can be

compensated for by rotation of the imine bonds connecting the building units, as well as by additional flexibility imparted by the central atoms (−N, −CH, −COH) of the three tritopic amine linkers. The PDB forms one of the six corners of the adamantane-like polyhedron, where each polyhedron is interlocked with six adjacent polyhedra through the copper(I) templates, with the tetrafluoroborate anions ($BF_4^-$) occupying the void spaces in and between the polyhedra to maintain charge balance, thus yielding a 3D [∞]catenane (Fig. 2). Since catena-COF-805, -806, and -807 have isoreticular structures, we present below the details pertaining to the exemplar compound catena-COF-805 and only discuss -806 and -807 where differences are notable. The detailed synthesis and analysis of the three compounds and the corresponding methods and data are disclosed in Methods and Supplementary Information.

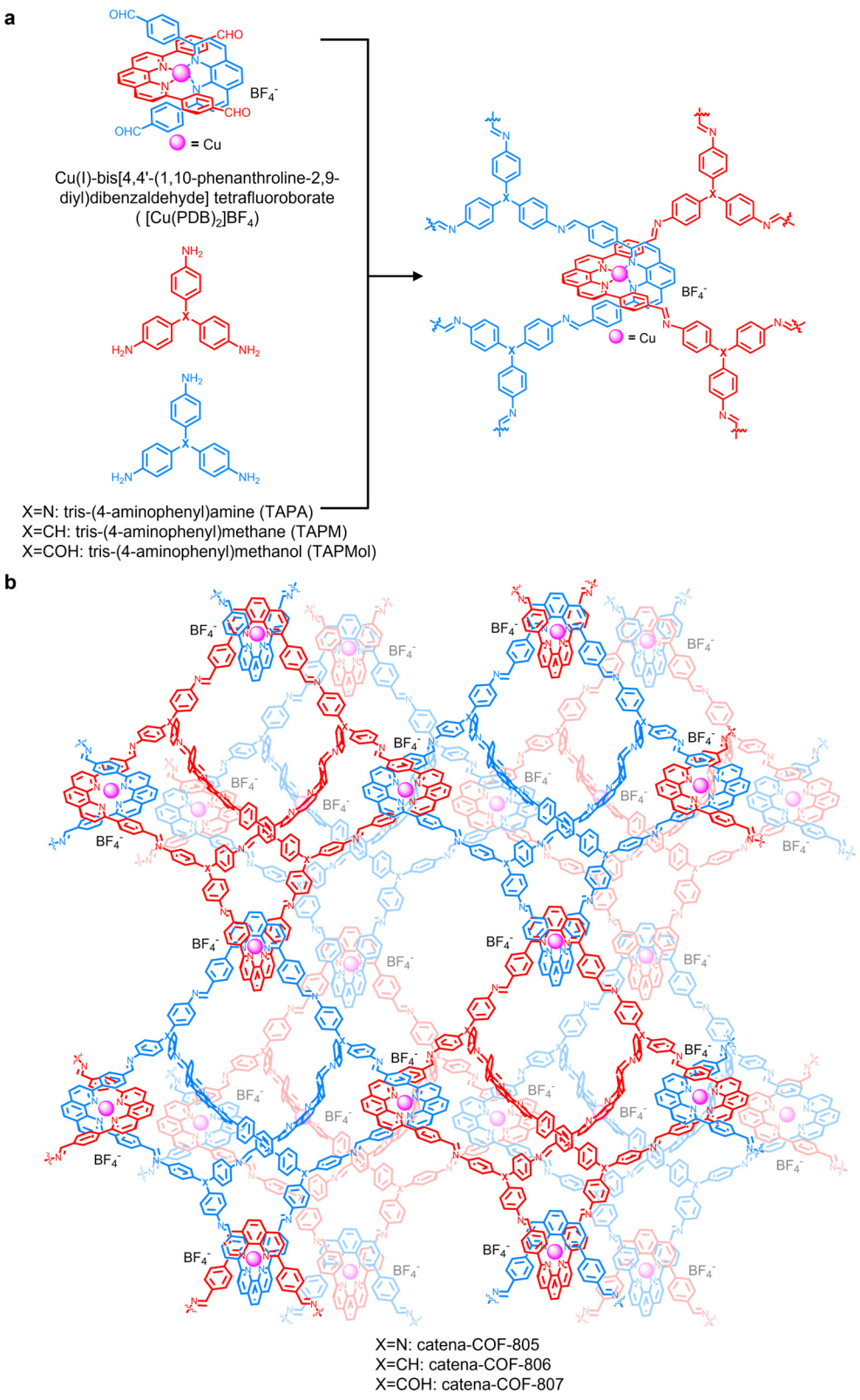


**Fig. 1 | Synthetic strategy and design of the 3D [∞]catenane COFs.** Catena-COF-805, -806 and -807 were synthesized by imine-formation reactions between tetrahedral $[Cu(PDB)_2]BF_4$ and

tritopic TAPA, TAPM or TAPMol, respectively (a), forming extended structures of interlocking organic polyhedra with Cu(I) templating and $BF_4^-$ as counter anions (b). Two colours of red and blue were used to illustrate interlocking between each two polydedra.

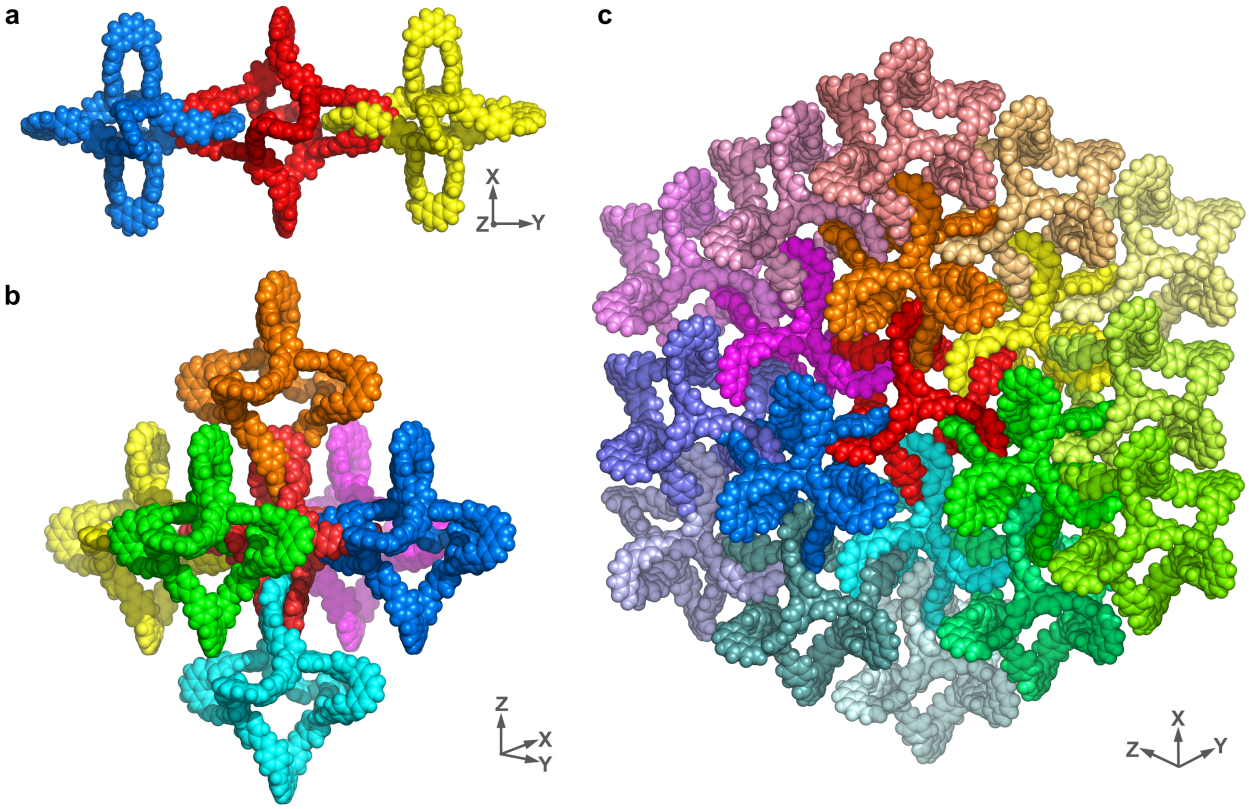


**Fig. 2 | Perspectives of the crystal structure of catena-COF-805.** The discrete polyhedra are represented by various colors. **a**, A fragment containing three interlocking organic adamantane-like polyhedra in catena-COF-805. **b**, In the 3D [∞]catenane framework of catena-COF-805, each adamantane-like polyhedron is interlocked with six adjacent polyhedra through the Cu(I) templates, where each PDB serves as one of the six corners of a polyhedron, with the $BF_4^-$ occupying the void spaces in and between the polyhedra for charge balance. Cu(I) ions and $BF_4^-$ anions are omitted for clarity. **c**, The overall crystal structure of the extended framework constructed entirely of interlocking covalent polyhedra.

## Results and discussion

**Synthesis and characterization of catena-COFs.** Catena-COF-805 was synthesized by linking $[Cu(PDB)_2]BF_4$ (8.0 mg, 0.008 mmol) with TAPA (3.3 mg, 0.011 mmol) in a mixture of 1,4-dioxane and mesitylene (*v*/*v* = 1:1, 0.5 mL). Aqueous acetic acid (6 mol/L, 50 μL) was added as a catalyst and 4-bromoaniline (27.5 mg, 20 equiv.) was added as a mono-functional amine modulator[36]. The reaction was carried out in a sealed pyrex tube and heated at 150°C for 3 days. The resulting precipitate was collected by centrifugation, washed with *N,N*-dimethylformamide and tetrahydrofuran, and then activated at 120°C for 12 hours to yield a reddish-brown solid (yield: 8.1 mg, 75.7%. Methods and Supplementary Section 2). Thermogravimetric analysis indicates that the solid has a high thermal stability up to 500°C (Supplementary Fig. 3), in agreement with previous findings for imine COFs.

The formation of imine linkages in catena-COF-805 was confirmed by Fourier-transform infrared (FT-IR) spectroscopy and solid-state nuclear magnetic resonance (SSNMR) spectroscopy (Supplementary Sections 4,5). When compared with those of the linkers, *i.e.*, $[Cu(PDB)_2]BF_4$ and TAPA, the FT-IR spectrum of the COF shows both attenuation of the C=O stretching vibration at ~1693 $cm^{-1}$, and the N−H stretch around 3300 $cm^{-1}$ and 3400 $cm^{-1}$ (Supplementary Figs. 4–6), thus confirming conversion of the aldehyde and amine starting materials. Comparison of the $^{13}C$ cross-polarization magic-angle spinning (CP/MAS) NMR spectra of the linkers with that of catena-COF-805 confirmed that the COF product featured characteristic signals of, as expected, both starting building units (Supplementary Figs. 7−9). In addition, the signal corresponding to the aldehyde carbon at ~192 ppm, as well as the signals of the carbon atoms adjacent to the amino group in TAPA at 116−118 ppm are strongly attenuated, further corroborating imine condensation between the aldehyde and amine building units. Attempts to observe the formed imine bonds (HC=N, expected at 154−156 ppm) by $^{13}C$ CP/MAS spectroscopy was complicated by the fact that the

118 $[Cu(PDB)_2]BF_4$ linker itself contains C=N bonds (~155 ppm). However, direct evidence for the
119 formation of new imine bonds can be obtained by $^{1}H$-$^{13}C$ heteronuclear correlation (HETCOR)
120 spectroscopy since the imine bonds (HC=N) contain H while the C=N functionality in PDB does
121 not. Here, the overlaid 2D spectra (Supplementary Figs. 10−12) show that for catena-COF-805, a
122 new $^{1}H$-$^{13}C$ correlation signal is observed at ~155 ppm of $^{13}C$ and ~9 ppm of $^{1}H$. In contrast, no
123 correlation signal is observed around these chemical shifts in the spectra of the $[Cu(PDB)_2]BF_4$
124 linker.

125 **Structure determination of catena-COFs.** Powder x-ray diffraction (PXRD), discussed further
126 below, of catena-COF-805 indicated a highly crystalline phase with a diffraction pattern distinct
127 from those of the corresponding linkers (Supplementary Figs. 13−17). Scanning electron
128 microscopy (SEM) images of this COF show a polyhedron-shaped morphology with the average
129 crystal size of ~500 nm (Supplementary Fig. 18). To determine the crystal structures of the three
130 catena-COFs, a combination of TEM techniques and PXRD analysis was employed. First, 3D
131 electron diffraction (ED)[37] datasets were collected to obtain the reconstructed 3D reciprocal
132 lattices (Supplementary Figs. 19−21). Catena-COF-805 crystallized in an *F* cubic lattice with a
133 unit cell parameter of $a$ = 56.8 Å, while -806 and -807 both crystallized in a *P* cubic lattice with
134 nearly identical unit cell parameters of $a$ = 28.4 Å and $a$ = 27.6 Å, respectively.

135 This information can also be deduced from the corresponding selected area electron diffraction
136 (SAED) patterns of the three catena-COFs (Fig. 3a−3d, Fig. 4a−4d and Supplementary Fig. 22).
137 The SAED patterns of the three catena-COFs are similar along each direction albeit minor
138 differences (Supplementary Fig. 22). After confirming that the interference from multiple
139 scattering can be eliminated (Supplementary Fig. 23), the *d*-spacing for $d_{400}$ of catena-COF-805
140 was calculated to be like that for $d_{200}$ of -806 and -807, and some extra reflections of odd-number
141 indices such as 113 series were only observed for catena-COF-805. These facts are in good

agreement with the two times larger lattice parameter *a* of catena-COF-805. Despite these differences, the SAED patterns of the three catena-COFs all showed the same $C_6$+$C_4$ symmetry which indicates related cubic lattices. This result is corroborated by the 3D ED data and is also in accordance with the targeted **bor-y** based structures, implying that the three catena-COFs have similar topologies with only minor structural differences.

Comparison of high-resolution TEM (HRTEM) images of the three catena-COFs (Fig. 3e−3h, Fig. 4e−4h and Supplementary Fig. 25) supported our analysis presented above. Despite the roughly similar images for the three catena-COFs along each direction, a significant difference can be observed along the [$1\bar{1}0$] direction (Figs. 3g and 4g, and Supplementary Fig. 25, c, g, k), highlighting the structural variations that cause the unit cell doubling of catena-COF-805 compared to -806 and -807. Specifically, an alternating arrangement of rows with differently sized bright spots is observed in all three HRTEM images along the [$1\bar{1}0$] for all catena-COFs. However, the bigger bright spots are aligned in a zigzag pattern as represented by yellow arrows in the micrograph of catena-COF-805 (Fig. 3g and Supplementary Fig. 25c), while for -806 and -807, these spots are aligned in a straight line (yellow line in Fig. 4g and Supplementary Fig. 25, g, k). When a Fourier filter was applied to the image of catena-COF-805 with some odd-number indices masked, the resulting HRTEM image became the same as that of -806 (Supplementary Fig. 26), addressing that these reflections of the odd-number indices in SAED pattern and the variations in HRTEM image along [$1\bar{1}0$] can be critical to differentiate the structures.

The datasets of each catena-COF were then integrated to be analysed for structure solution (Fig. 3 for catena-COF-805, Fig. 4 for -806 and Supplementary Fig. 27 for -807). For catena-COF-805, the reflection conditions observed from electron diffraction data (Fig. 3a–3d, Supplementary Fig. 19) can be summarized as: *hkl*: $h + k,\ h + l,\ k + l$ = 2n; 0*kl*: $k,l$ = 2n; *hhl*: $h + l$ = 2n; 00*l*: $l$ = 4n

(note that the weak abnormal reflections of 002 series were proved to come from multiple scattering, see Supplementary Fig. 23), which suggests $F4_132$ (No. 210) as the only possible space group. An initial structure model of interlocking polyhedra with **bor-y** topology was built in $F4_132$ with the unit cell of $a$ = 56.8 Å; however, projections of the model did not match with the HRTEM images (Supplementary Fig. 28). To account for these differences, a new model with a doubly interpenetrated **bor-y** topology (**bor-y-c***, Supplementary Fig. 29) was constructed. Comparison of HRTEM images (Fig. 3e−3h) with the projections of the interpenetrated model (Fig. 3i−3l) yielded a perfect match along all directions. It is worth noting that the HRTEM information along the $[1\bar{1}0]$ direction (Fig. 3g) aids in distinguishing unambiguously a non-interpenetrated from a doubly interpenetrated net (Supplementary Fig. 31). Accordingly, the overall reticular formula of catena-COF-805 was determined as $[(CuBF_4)_3(PDB)_6(TAPA)_4]_{imine}$, matching well with the empirical formula of $C_{228}H_{144}N_{28}Cu_3B_3F_{12}$ and the elemental analysis result (Methods and Supplementary Section 2). All these results demonstrate that catena-COF-805 has a doubly interpenetrated **bor-y** structure.

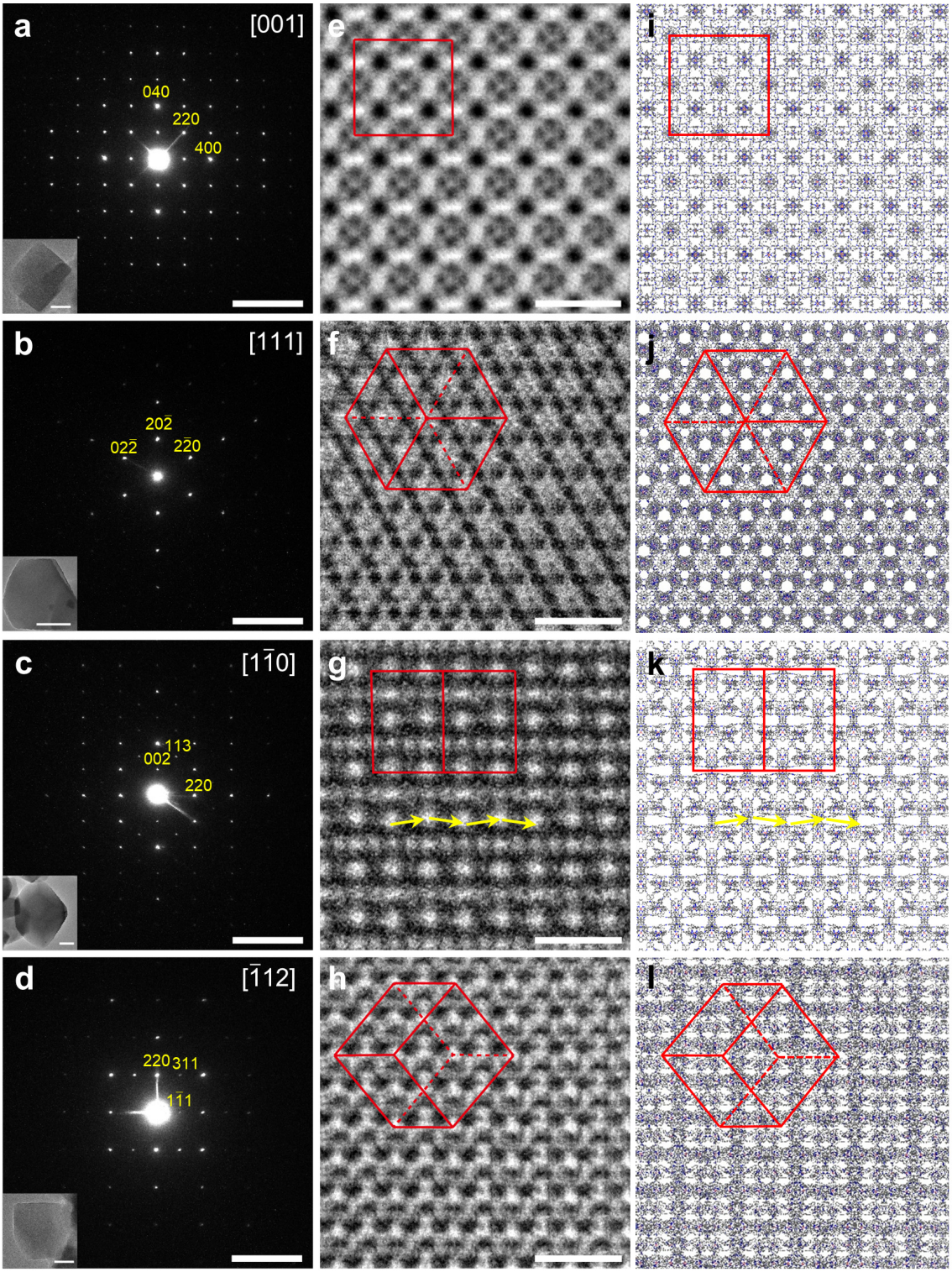


**Fig. 3 | TEM data and perspective illustrations of the crystal structure of catena-COF-805.** **a**–**d,** SAED patterns of catena-COF-805 from the [001], [111], [1$\bar{1}$0], and [$\bar{1}$12] incidences, respectively. Scale bar: 1 $nm^{-1}$. Insets: TEM images of the crystals used to collect data. Scale bar:

200 nm. **e**−**h,** HRTEM images of catena-COF-805 taken along the [001], [111], [1$\bar{1}$0], and [$\bar{1}$12] directions, respectively. Scale bar: 5 nm. **i**−**l,** The projections of the crystal structure of catena-COF-805 with a doubly interpenetrated **bor-y** topology along the [001], [111], [1$\bar{1}$0], and [$\bar{1}$12] directions, respectively. Atom color: C, gray; N, blue; Cu, pink. H atoms and $BF_4^-$ anions were omitted for clarity.

Catena-COF-806 and -807 have the same *P* lattice and similar unit cell parameters of $a$ = 28.4 Å and 27.6 Å, respectively. After elimination of interference from multiple scattering (Supplementary Fig. 24), the only reflection rule that can be derived from the diffraction patterns of catena-COF-806 (Fig. 4a−4d and Supplementary Fig. 20) and -807 (Supplementary Fig. 27a−27d, and Supplementary Fig. 21) is 00$l$: $l$ = 2n, which yields the possible cubic space groups of $P4_232$ (No. 208) and $P2_13$ (No. 198). $P2_13$ can be excluded by deducing the plane group symmetries from HRTEM images and calculating the ratio of vertices. For example, along the [1$\bar{1}$0] direction, the plane group $p1g1$ of $P2_13$ contains no mirror symmetry. However, the mirror symmetry is observed in the parallel alignment of arrays of bright spots in HRTEM images of catena-COF-806 and -807 (Fig. 4g and Supplementary Fig. 27g). Indeed, the plane group of *p2mm* can be deduced which is derived from space group $P4_232$, the only possible space group of catena-COF-806 and -807. This is in good agreement with the targeted **bor** type structure where the ratio of 3-connected to 4-connected vertices is 4:3 after the symmetrical operation of $P4_232$. Structural models of the catena-COF-806 and -807 were constructed with the same doubly interpenetrated **bor-y** topology (**bor-y-c***, Supplementary Fig. 29) and the projections of the structure models for both -806 (Fig. 4i−4l) and -807 (Supplementary Fig. 27i−27l) matched perfectly with the corresponding images from HRTEM micrographs (Fig. 4e−4h and Supplementary Fig. 27e−27h). The reticular formulas of catena-COF-806 and -807 were then determined as

206 $[(CuBF_4)_3(PDB)_6(TAPM)_4]_{imine}$ and $[(CuBF_4)_3(PDB)_6(TAPMol)_4]_{imine}$, respectively, which also
207 match well with the empirical formulas of $C_{232}H_{148}N_{24}Cu_3B_3F_{12}$ for catena-COF-806 and
208 $C_{232}H_{148}N_{24}O_4Cu_3B_3F_{12}$ for -807. These results were further confirmed by elemental analysis
209 (Method and Supplementary Section 2).

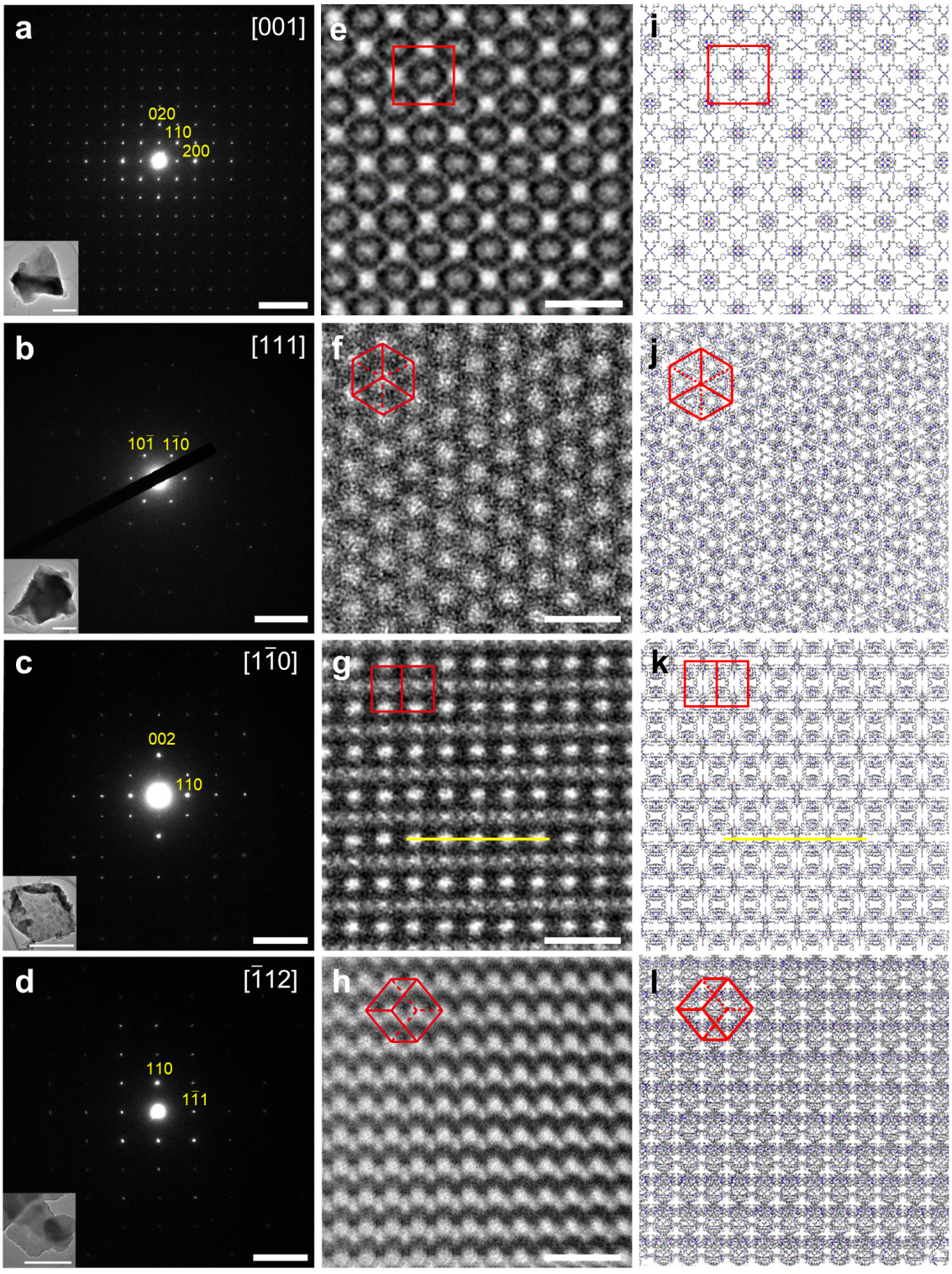


**Fig. 4 | TEM data and perspective illustrations of the crystal structure of catena-COF-806.** **a**–**d,** SAED patterns of catena-COF-806 from the [001], [111], [1$\bar{1}$0], and [$\bar{1}$12] incidences, respectively. Scale bar: 1 nm$^{-1}$. Insets: TEM images of the crystals used to collect data. Scale bar:

200 nm. **e**−**h,** HRTEM images of catena-COF-806 taken along the [001], [111], [1$\bar{1}$0], and [$\bar{1}$12] directions, respectively. Scale bar: 5 nm. **i**−**l,** The projections of the crystal structure of catena-COF-806 with a doubly interpenetrated **bor-y** topology along the [001], [111], [1$\bar{1}$0], and [$\bar{1}$12] directions, respectively. Atom color: C, gray; N, blue; Cu, pink. H atoms and $BF_4^-$ anions were omitted for clarity.

PXRD refinements were carried out to confirm the structure models. Pawley refinement was conducted with the PXRD pattern of activated catena-COF-805 in the space group $F4_132$ (No. 210), resulting in unit cell parameters of $a$ = 54.858(8) Å with $R$p = 0.63% and $wR$p = 1.62% (Fig. 5a). Similarly, the activated catena-COF-806 and -807 were both refined in the space group of $P4_232$, yielding unit cell parameters of $a$ = 27.854(4) Å for -806 with $R$p =0.69% and $wR$p = 1.24% (Fig. 5b), and $a$ = 26.1153(9) Å with $R$p = 0.45% and $wR$p = 1.27% for -807 (Supplementary Fig. 32a). The structure models were then finalized by geometry optimization (Fig. 5c, 5d, Supplementary Fig. 32b, and Supplementary Tables 1−3) and the simulated PXRD patterns from the structure models were found to be in good agreement with the experimentally obtained datasets (Supplementary Figs. 33−35).

Despite the same doubly interpenetrated **bor-y** topology, the structural difference in symmetry and unit cell size between catena-COF-805 and -806 or -807 can be attributed to the various polyhedra orientations when they were interlocked with each other. Specifically, each two polyhedra in catena-COF-805 are interlocked by twisting 90° (e.g., red and blue polyhedra, Fig. 5c), while they have identical orientation both in -806 and -807 (Fig. 5d and Supplementary Fig. 32b). When considering the difference in structure between the three catena-COFs, it is instructive to take a detailed look at geometric differences in their constituent polyhedral building units. While the identical phenanthroline linker was used in synthesizing all three catena-COFs, the orientations

of two respective phenanthroline units on opposite sides of the constituent polyhedra are approximately parallel to each other in the polyhedra of catena-COF-805 (Fig. 5e), but approximately orthogonal in the structures of catena-COF-806/807 (Fig. 5f, Supplementary Fig. 32). To accommodate the tetrahedral coordination of the Cu(I) template, two phenanthroline units of neighboring polyhedra need to assume an orthogonal orientation to each other. Consequently, a rotation of alternating polyhedra is observed for catena-COF-805, in contrast to lateral translation of neighboring polyhedra in catena-COF-806/807. The differences in the structures of polyhedra are caused by the different geometries of their respective tritopic building blocks. Specifically, the N atoms at the center of TAPA display a trigonal planar orientation of its aniline substituents (Fig. 5e). In contrast, these substituents are arranged in a trigonal pyramidal orientation in TAPM and TAPMol due to the tetrahedral geometry of their central C atoms (Fig. 5f and Supplementary Fig. 32. Detailed angular values are displayed in Supplementary Fig. 36).

Rietveld refinement and geometry optimization of crystal structures of catena-COF-806/807 (Supplementary Figs. 39, 40 and Table 1) yielded structures in which the C-H or C-OH bonds of TAPM and TAPMol centers point towards the inside of their respective polyhedra (Supplementary Fig. 37 and 38), thus yielding polyhedra with a concave structure (Supplementary Fig. 38). Together, these structural differences account for the different polyhedron sizes of ~35.5 Å, ~35.4 Å and ~33.7 Å for catena-COF-805, -806 and -807, respectively (Supplementary Fig. 37), which represents one of the largest organic polyhedra (> 30 Å)[15,16,38,39]. Taken together, these structural differences account for the variations observed in the HRTEM of the three catena-COFs (Supplementary Figs. 30, 31). It should be noted that due to the intrinsic flexibility of the interlocking polyhedra, all three catena-COFs show a dynamic response to solvents as confirmed by the observed variations in their PXRD patterns upon addition or removal of solvents (Supplementary Section 9).

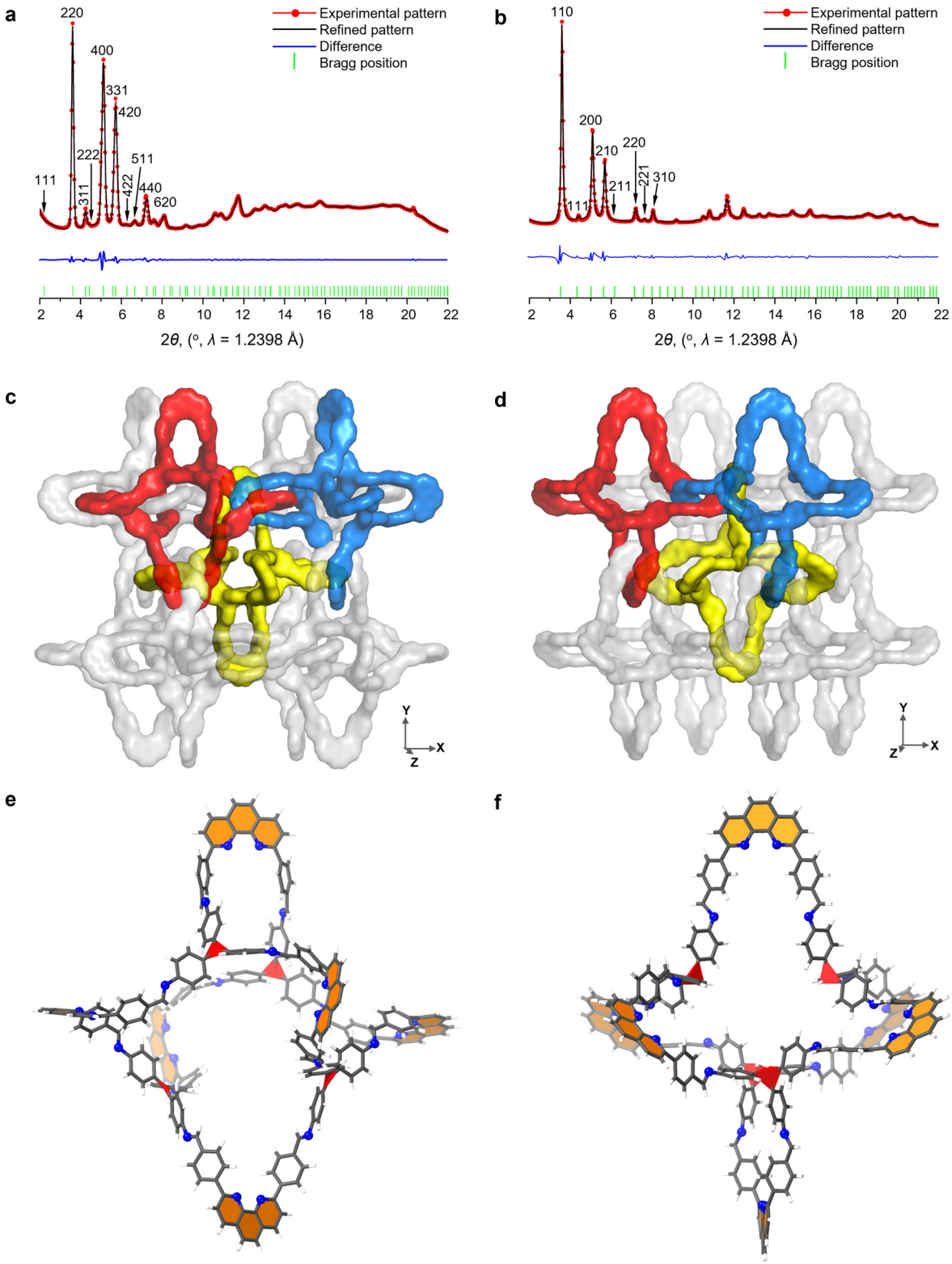


**Fig. 5 | PXRD refinement and crystal structures of 3D [∞]catenane COFs. a**, **b**, Pawley refinement of catena-COF-805 and -806, respectively. Experimental patterns, red; refined patterns,

black; difference patterns, blue; observed positions of Bragg reflections, green. **c**, **d**, The doubly interpenetrated **bor-y** frameworks of catena-COF-805 and -806, respectively, where their one subnet is represented by the catenated red, blue, and gray polyhedra, while the other subnet is differentiated by representing it in yellow. In each subnet, every two catenated polyhedra (highlighted in red and blue) adopt different orientations in catena-COF-805 while all polyhedra have the same orientations in catena-COF-806, which can be easily distinguished by the shape of the specific orientation of the polyhedra. **e**, **f**, The constituent polyhedron of catena-COF-805 and -806, respectively. The phenanthroline units (highlighted in orange) on opposite sides assume an approximately parallel orientation to each other in the polyhedron of catena-COF-805 (e), while they are oriented approximately orthogonal in that of catena-COF-806 (f). N atoms in the trifurcate center of TAPA approach a planar triangle geometry (shown as a red triangle) while C atoms in center of TAPM adopt a tetrahedron geometry (shown as a red tetrahedron). C atoms, gray; N atoms, blue; H atoms, white.

**Demetalation, flexibility and mechanical properties of catena-COFs.** Since the crystal structures of catena-COFs were confirmed as the discrete adamantane-like polyhedra catenated by virtue of the copper(I) ions templating, post-synthetic removal of the copper(I) ions was achieved up to 90% by addition of aqueous KCN to yield the corresponding demetalated organic frameworks in which the covalent polyhedra are held together by mechanical bonds (Supplementary Section 10). Although the non-crystalline structure of the demetalated catena-COFs (e.g., demetalated catena-COF-806) cannot be directly verified by the crystallographic methods, its interlocking form was studied and discussed by control experiments (Supplementary Scheme 1 and Fig. 48–49) and molecular dynamics simulation (Supplementary Fig. 53). We anticipated that the absence of copper(I) imparts a high degree of structural freedom onto the polyhedra. This was substantiated by the observed decrease in framework crystallinity upon

demetalation (Supplementary Fig. 51) and further by tetrahydrofuran (THF) vapor sorption measurements (Supplementary Section 11). Here, catena-COF-806 exhibited a Type I THF adsorption isotherm with characteristic micropore filling, while its demetalated derivative displayed a more linear THF isotherm profile (Supplementary Fig. 54). This indicates a structural expansion of demetalated catena-COF-806 and indeed a higher degree of flexibility as borne out in the fact that the saturated uptake is doubled upon demetallation.

The flexibility observed in the demetalated framework is manifested in the quasi-static and dynamic mechanical properties. The mechanical properties of both metalated and demetalated samples of catena-COF-806 were characterized by performing nanoindentation (Supplementary Section 12). The elastic modulus was found to decrease from 3.81 (± 0.60) GPa in metalated catena-COF-806 to 1.41 (± 0.37) GPa in the demetalated sample. The hardness decreases from 154.7 (± 27.7) MPa in the metalated catena-COF-806 to 55.8 (± 8.7) MPa after demetalation. All the measured values are within the expected range for weaving COFs[31]. The creep properties, measured as the change of the displacement under a constant load at room temperature, were studied to investigate the time-dependent plasticity of metalated and demetalated catena-COF-806. Maintaining compressive loads of 100 μN for 30 sec yielded a creep depth of ~80 nm for the demetalated sample, compared to ~10 nm for its metalated analogue, indicating that the demetalated catena-COF-806 is more mechanically flexible than the metalated sample.

## Conclusions

In this work, a series of [∞]catenane COFs which are formed through mechanical interlocking of discrete organic adamantane-like polyhedra were synthesized and structurally characterized. We wish to remark that obtaining [∞]catenane COFs crystals not only allows unambiguous visualization of poly[*n*]catenane networks but also affords new method to assess the degree of

catenation (*n*) by simply measuring the size of the crystals without sophisticated instrumental analysis, if one considers the crystal size obtained by SEM and the observed size of the unit cells (Supplementary Section 13). The previous record was held by an organic poly[*n*]catenane chain[21] with $n$ = 130, whereas $n$ in 3D catena-COFs was multiple orders of magnitude higher than the reported one, highlighting the prowess of reticular chemistry[40] in the design and synthesis of extended organic catenanes.

## Methods

**Synthesis of catena-COF-805.** A pressure tube was charged with Cu(I)-bis[4,4'-(1,10-phenanthroline-2,9-diyl)dibenzaldehyde]tetrafluoroborate ($[Cu(PDB)_2]BF_4$, 8.0 mg, 0.008 mmol), tris(4-aminophenyl)amine (TAPA, 3.3 mg, 0.011 mmol), and *p*-Br-aniline (27.5 mg, 20 equiv.) as a modulator. The mixture of 0.25 mL of 1,4-dioxane, 0.25 mL mesitylene and 0.05 mL of 6 M aqueous acetic acid was added. Then the tube was sealed and heated at 150°C for 72 h, yielding a reddish-brown solid at the bottom of the tube which was isolated as catena-COF-805. The as-synthesized catena-COF-805 was washed with *N*,*N*-dimethylformamide (DMF) and tetrahydrofuran (THF), and dried at room temperature for 12 h and at 120°C for 12 h. This material is insoluble in water and in common organic solvents such as methanol, acetone, THF, DMF, and dimethylsulfoxide. Yield: 8.1 mg, 75.7%. Elemental analysis (EA) results: calcd. for $C_{228}H_{144}N_{28}Cu_3B_3F_{12}\cdot 20H_2O$: C 67.00%; H 4.50%; N 9.59%. Found: C 66.36%; H 4.22%; N 9.11%.

**Synthesis of catena-catena-COF-806.** A pressure tube was charged with $[Cu(PDB)_2]BF_4$ (8.0 mg, 0.008 mmol) and tris(4-aminophenyl)methane (TAPM, 5.0 mg, 0.017 mmol). The mixture of 0.5 mL of 1,4-dioxane, 20 μL aniline (24.4 equiv.) and 0.1 mL of aqueous acetic acid (6 M) was added and the tube was sealed. The reaction was heated at 120°C for 72 h, yielding a reddish-brown solid as catena-COF-806 at the bottom of the tube. The solid was isolated by centrifugation and washed

with DMF and THF, and then dried at room temperature for 12 h and at 120°C for 12 h. Similarly, this product is insoluble in water and in common organic solvents as mentioned for catena-COF-805. Yield: 7.6 mg, 71.0 %. EA results: calcd. for $C_{232}H_{148}N_{24}Cu_3B_3F_{12}\cdot 25H_2O$: C 68.13%; H 4.50%; N 7.91%. Found: C 68.93%; H 4.47%; N 8.09%.

**Synthesis of catena-COF-807.** A pressure tube was charged with $[Cu(PDB)_2]BF_4$ (8.0 mg, 0.008 mmol) and tris(4-aminophenyl)methanol (TAPMol, 3.4 mg, 0.011 mmol). The mixture of 0.25 mL of 1,4-dioxane, 0.25 mL mesitylene, 0.1 mL of aqueous acetic acid (6 M) was added and the tube was sealed. The reaction was heated at 85°C for 72 h, yielding a reddish-brown solid as catena-COF-807 at the bottom of the tube. The crude product was isolated by centrifugation and washed with DMF and THF, and then dried at room temperature for 12 h and at 120°C for 12 h. Similarly, this product is also insoluble in water and in common organic solvents as mentioned for catena-COF-805 and -806. Yield: 6.9 mg, 63.9%. EA results: calcd. for $C_{232}H_{148}N_{24}O_4Cu_3B_3F_{12}\cdot 25H_2O$: C 69.17%; H 4.74%; N 8.01%. Found: C 69.58%; H 4.71%; N 7.93%. Note that all the obtained catena-COFs are air stable.

**Transmission electron microscopy (TEM).** Catena-COF samples for TEM analysis were dispersed in ethanol by ultrasonication. A droplet of the suspension was transferred onto a carbon coated copper grid. All datasets were obtained using a JEM-2100Plus microscope at 200 kV with a TVIPS (XF416) camera for high signal-to-noise ratio data acquisition. Due to the beam-sensitivity of the samples, three-dimensional electron diffraction (3D ED) datasets were collected using fast method where the sample holder was tilted continuously and stopped every 5° for sample tracking. The obtained datasets were processed and reconstructed by the *EDT-process* program[37]. High-resolution TEM (HRTEM) images were obtained under low dose conditions. Before taking images, the crystals were aligned to the desired orientations quickly under a depressed illumination

condition. With a careful control of the electron dose and short exposure time, multiple images were taken and then integrated into one image to reduce the blur caused by sample drift.

**Powder X-ray diffraction (PXRD).** The synchrotron PXRD datasets were collected at Beamline 7.3.3 of Advanced Light Source (ALS) in the Lawrence Berkeley National Laboratory (LBNL), with $\lambda$ = 1.2398 Å in the capillary mode.

**Data and materials availability:** Crystallographic data for the structures reported in this Article have been deposited at the Cambridge Crystallographic Data Centre, under deposition numbers CCDC 2216102 (catena-COF-805), 2216103 (catena-COF-806) and 2216104 (catena-COF-807). Copies of the data can be obtained free of charge via https://www.ccdc.cam.ac.uk/structures/. All data are available in the main text or the Supplementary Materials.

**Acknowledgments:** This research was partly supported by King Abdulaziz City for Science and Technology (Center of Excellence for Nanomaterials and Clean Energy Applications), and mechanical property measurements funded by the Defense Advanced Research Projects Agency (DARPA) under contract HR001-119-S-0048. This research used resources of the Advanced Light Source (beamline 7.3.3) at Lawrence Berkeley National Laboratory, which is a DOE Office of Science user facility under contract DE-AC02-05CH11231. Y.Z., O.T. acknowledge the support of the Center for High-resolution Electron Microscopy (C*ℏ*EM), ShanghaiTech University (EM02161943) and Shanghai Science and Technology Plan (21DZ2260400). We thank Dr. C. Zhu for assistance in acquiring synchrotron PXRD data on beamline 7.3.3 of the Advanced Light Source, Drs. A. Lund and H. Celik of the School of Chemical Sciences at University of California-Berkeley NMR facility for assistance with SSNMR data acquisition, Dr. Z. Wang in Cornell High Energy Synchrotron Source and Drs. T. Matsumoto and A. Yamano in Rigaku Co., Japan for the

initial trials on acquiring SXRD and PXRD data. D.M.P. thanks Prof. Vladislav A. Blatov at the Samara Center for Theoretical Materials Science for providing the ToposPro software.

**Author contributions:** C.S.D., T.M., O.M.Y. conceived the idea. T.M., O.M.Y. led the project and interpreted the results. T.M. conducted the syntheses, structure analyses and characterizations for all samples and interpreted the data. Y.Z., O.T. collected and analyzed the TEM data, and supported the comparison of TEM and PXRD results. J.K., R.O.R. collected and analyzed nanoindentation data. F.G. and P.P.S. finalized PXRD refinement. H.L. and Y.Z. supported SEM measurements. N.H. conducted THF sorption experiment. Y.L. and N.J.D. supported linker synthesis. D.M.P. helped in literature and topological analysis of the organic polyhedra and catenation. T.M., C.S.D., O.M.Y. wrote the manuscript and all authors reviewed it.

**Competing interests:** The authors declare no competing interests.

## Figure legends/captions (for main text figures):

**Fig. 1 | Synthetic strategy and design of the 3D [∞]catenane COFs.** Catena-COF-805, -806 and -807 were synthesized by imine-formation reactions between tetrahedral $[Cu(PDB)_2]BF_4$ and tritopic TAPA, TAPM or TAPMol, respectively (a), forming extended structures of interlocking organic polyhedra with Cu(I) templating and $BF_4^-$ as counter anions (b). Two colours of red and blue were used to illustrate interlocking between each two polyhedra.

**Fig. 2 | Perspectives of the crystal structure of catena-COF-805.** The discrete polyhedra are represented by various colors. **a**, A fragment containing three interlocking organic adamantane-like polyhedra in catena-COF-805. **b**, In the 3D [∞]catenane framework of catena-COF-805, each adamantane-like polyhedron is interlocked with six adjacent polyhedra through the Cu(I) templates, where each PDB serves as one of the six corners of a polyhedron, with the $BF_4^-$ occupying the void spaces in and between the polyhedra for charge balance. Cu(I) ions and $BF_4^-$ anions are omitted

for clarity. **c**, The overall crystal structure of the extended framework constructed entirely of interlocking covalent polyhedra.

**Fig. 3 | TEM data and perspective illustrations of the crystal structure of catena-COF-805.** **a**–**d,** SAED patterns of catena-COF-805 from the [001], [111], [1$\bar{1}$0], and [$\bar{1}$12] incidences, respectively. Scale bar: 1 $nm^{-1}$. Insets: TEM images of the crystals used to collect data. Scale bar: 200 nm. **e**–**h,** HRTEM images of catena-COF-805 taken along the [001], [111], [1$\bar{1}$0], and [$\bar{1}$12] directions, respectively. Scale bar: 5 nm. **i**–**l,** The projections of the crystal structure of catena-COF-805 with a doubly interpenetrated **bor-y** topology along the [001], [111], [1$\bar{1}$0], and [$\bar{1}$12] directions, respectively. Atom colour: C, grey; N, blue; Cu, pink. H atoms and $BF_4^-$ anions were omitted for clarity.

**Fig. 4 | TEM data and perspective illustrations of the crystal structure of catena-COF-806.** **a**–**d,** SAED patterns of catena-COF-806 from the [001], [111], [1$\bar{1}$0], and [$\bar{1}$12] incidences, respectively. Scale bar: 1 $nm^{-1}$. Insets: TEM images of the crystals used to collect data. Scale bar: 200 nm. **e**–**h,** HRTEM images of catena-COF-806 taken along the [001], [111], [1$\bar{1}$0], and [$\bar{1}$12] directions, respectively. Scale bar: 5 nm. **i**–**l,** The projections of the crystal structure of catena-COF-806 with a doubly interpenetrated **bor-y** topology along the [001], [111], [1$\bar{1}$0], and [$\bar{1}$12] directions, respectively. Atom colour: C, grey; N, blue; Cu, pink. H atoms and $BF_4^-$ anions were omitted for clarity.

**Fig. 5 | PXRD refinement and crystal structures of 3D [∞]catenane COFs. a**, **b**, Pawley refinement of catena-COF-805 and -806, respectively. Experimental patterns, red; refined patterns, black; difference patterns, blue; observed positions of Bragg reflections, green. **c**, **d**, The doubly interpenetrated **bor-y** frameworks of catena-COF-805 and -806, respectively, where their one subnet is represented by the catenated red, blue, and gray polyhedra, while the other subnet is

differentiated by representing it in yellow. In each subnet, every two catenated polyhedra (highlighted in red and blue) adopt different orientations in catena-COF-805 while all polyhedra have the same orientations in catena-COF-806, which can be easily distinguished by the shape of the specific orientation of the polyhedra. **e**, **f**, The constituent polyhedron of catena-COF-805 and -806, respectively. The phenanthroline units (highlighted in orange) on opposite sides assume an approximately parallel orientation to each other in the polyhedron of catena-COF-805 (e), while they are oriented approximately orthogonal in that of catena-COF-806 (f). N atoms in the trifurcate center of TAPA approach a planar triangle geometry (shown as a red triangle) while C atoms in center of TAPM adopt a tetrahedron geometry (shown as a red tetrahedron). C atoms, grey; N atoms, blue; H atoms, white.

## References


1. Wasserman, E. The preparation of interlocking rings: a catenane. *J. Am. Chem. Soc.* **82**, 4433–4434 (1960).

2. Schill, G. & Lüttringhaus, A. The preparation of catena compounds by directed synthesis. *Angew. Chem. Int. Ed. Engl.* **3**, 546–547 (1964).

3. Dietrich-Buchecker, C. O., Sauvage, J.-P. & Kintzinger, J. P. Une nouvelle famille de molecules: les metallo-catenanes. *Tetrahedron Lett.* **24**, 5095–5098 (1983).

4. Ashton, P. R., Goodnow, T. T., Kaifer, A. E., Reddington, M. V., Slawin, A. M. Z., Spencer, N., Stoddart, J. F., Vicent, C. & Williams, D. J. A [2] catenane made to order. *Angew. Chem. Int. Ed. Engl.* **28**, 1396–1399 (1989).

5. Forgan, R. S., Sauvage, J.-P. & Stoddart, J. F. Chemical topology: complex molecular knots, links, and entanglements. *Chem. Rev.* **111**, 5434–5464 (2011).

6. Gil-Ramírez, G., Leigh, D. A. & Stephens, A. J. Catenanes: fifty years of molecular links. *Angew. Chem. Int. Ed.* **54**, 6110–6150 (2015).

7. Sauvage, J.-P. et.al. *Molecular machines and motors* (Springer, Berlin, 2001).

8. Browne, W. R. & Feringa, B. L. Making molecular machines work. *Nature Nanotech.* **1**, 25–35 (2006).

9. Kay, E. R., Leigh, D. A. & Zerbetto, F. Synthetic molecular motors and mechanical machines. *Angew. Chem. Int. Ed.* **46**, 72–191 (2007).

10. Stoddart, J. F. Mechanically interlocked molecules (MIMs)—molecular shuttles, switches, and machines. *Angew. Chem. Int. Ed.* **56**, 11094–11125 (2017).

11. Iino, R., Kinbara, K. & Bryant, Z. Introduction: molecular motors. *Chem. Rev.* **120**, 1–4 (2020).

12. Wikoff, W. R., Liljas, L., Duda, R. L., Tsurta, H., Hendrix, R. W. & Johnson, J. E. Topologically linked protein rings in the bacteriophage HK97 capsid. *Science* **289**, 2129–2133 (2000).

13. Fujita, M., Fujita, N., Ogura, K. & Yamaguchi, K. Spontaneous assembly of ten components into two interlocked, identical coordination cages. *Nature* **400**, 52–55 (1999).

14. Hasell, T., Wu, X., Jones, J. T. A., Bacsa, J., Steiner, A., Mitra, T., Trewin, A., Adams, D. J. & Cooper, A. I. Triply interlocked covalent organic cages. *Nat. Chem.* **2**, 750–755 (2010).

15. Zhang, G., Presly, O., White, F., Oppel, I. M. & Mastalerz, M. A shape-persistent quadruply interlocked giant cage catenane with two distinct pores in the solid state. *Angew. Chem. Int. Ed.* **53**, 5126–5130 (2014).

16. Benke, B. P., Kirschbaum, T., Graf, J., Mastalerz, M. Dimeric and trimeric catenation of giant chiral [8+12] imine cubes driven by weak supramolecular interactions. 10.26434/chemrxiv.14394266.v1.

17. Harrison, I. T. & Harrison, S. Synthesis of a stable complex of a macrocycle and a threaded chain. *J. Am. Chem. Soc.* **89**, 5723–5724 (1967).

18. Anelli, P. L., Spencer, N. & Stoddart, J. F. A molecular shuttle. *J. Am. Chem. Soc.* **113**, 5131–5133 (1991).

19. Leigh, D. A., Wong, J. K. Y., Dehez, F. & Zerbetto, F. Unidirectional rotation in a mechanically interlocked molecular rotor. *Nature* **424**, 174–179 (2003).

20. Niu, Z. & Gibson, H. W. Polycatenanes. *Chem. Rev.* **109**, 6024–6046 (2009).

21. Wu, Q., Rauscher, P. M., Lang, X., Wojtecki, R. J., de Pablo, J. J. Hore, M. J. A. & Rowan, S. J. Poly[*n*]catenanes: synthesis of molecular interlocked chains. *Science* **358**, 1434–1439 (2017).

22. Raphael, E., Gay, C. & de Gennes, P. G. Progressive construction of an "Olympic" gel. *J. Stat. Phys.* **89**, 111–118 (1997).

23. Fischer, J., Lang, M. & Sommer, J. U. The formation and structure of Olympic gels. *J. Chem. Phys.* **143**, 243114 (2015).

24. Jin, C.-M., Lu, H., Wu, L.-Y. & Huang, J. A new infinite inorganic [*n*]catenane from silver and bis(2-methylimidazoyl)methane ligand. *Chem. Commun.* 5039–5041 (2006).

25. Loots, L. & Barbour, L. J. An infinite catenane self-assembled by π···π interactions. *Chem. Commun.* **49**, 671–673 (2013).

26. Thorp-Greenwood, F. L., Kulak, A. N. & Hardie, M. J. An infinite chainmail of M6L6 metallacycles featuring multiple Borromean links. *Nat. Chem.* **7**, 526–531 (2015).

27. Kuang, X., Wu, X., Yu, R., Donahue, J. P., Huang, J. & Lu, C.-Z. Assembly of a metal–organic framework by sextuple intercatenation of discrete adamantane-like cages. *Nat. Chem.* **2**, 461–465 (2010).

28. Heine, J., Schmedt auf der Günne, J. & Dehnen, S. Formation of a strandlike polycatenane of icosahedral cages for reversible one-dimensional encapsulation of guests. *J. Am. Chem. Soc.* **133**, 10018–10021 (2011).

29. Jiang, L., Ju, P., Meng, X.-R., Kuang, X.-J. & Lu, T.-B. Constructions of two polycatenanes and one polypseudo-rotaxane by discrete tetrahedral cages and stool-like building units. *Sci. Rep.* **2**, 668 (2012).

30. Shen, Y., Zhu, H.-B., Hu, J. & Zhao, Y. Construction of a metal–organic framework by octuple intercatenation of discrete icosahedral coordination cages. *CrystEngComm* **17**, 2080–2082 (2015).

31. Chen, L., Chen, Q., Wu, M., Jiang, F. & Hong, M. Controllable coordination-driven self-assembly: from discrete metallocages to infinite cage-based frameworks. *Acc. Chem. Res.* **48**, 201–210 (2015).

32. Wu, X., Xu, Z.-X., Wang, F. & Zhang, J. Catenation of homochiral metal–organic nanocages or nanotubes. *Inorg. Chem.* **55**, 5095–5097 (2016).

33. Cheng, L., Liang, C., Liu, W., Wang, Y., Chen, B., Zhang, H., Wang, Y., Chai, Z. & Wang, S. Three-dimensional polycatenation of a uranium-based metal–organic cage: structural complexity and radiation detection. *J. Am. Chem. Soc.* **142**, 16218–16222 (2020).

34. O'Keeffe, M. Peskov, M. A., Ramsden, S. J. & Yaghi, O. M. The reticular chemistry structure resource (RCSR) database of, and symbols for, crystal nets. *Acc. Chem. Res.* **41**, 1782–1789 (2008).

35. Liu, Y., Ma, Y., Zhao, Y., Sun, X., Gándara, F., Furukawa, H., Liu, Z., Zhu, H., Zhu, C., Suenaga, K., Oleynikov, P., Alshammari, A. S., Zhang, X., Terasaki, O. & Yaghi, O. M. Weaving of organic threads into a crystalline covalent organic framework. *Science* **351**, 365–369 (2016).

36. Ma, T., Kapustin, E. A., Yin, S. X., Liang, L., Zhou, Z., Niu, J., Li, L.-H., Wang, Y., Su, J., Li, J., Wang, X., Wang, W. D., Wang, W., Sun, J. & Yaghi, O. M. Single-crystal x-ray diffraction structures of covalent organic frameworks. *Science* **361**, 48–52 (2018).

37. Gemmi, M. & Oleynikov, P. Scanning reciprocal space for solving unknown structures: energy filtered diffraction tomography and rotation diffraction tomography methods. *Z. Kristallogr.* **228**, 51–58 (2013).

38. Skowronek, P., Warżajtis, B., Rychlewska, U. & Gawroński, J. Self-assembly of a covalent organic cage with exceptionally large and symmetrical interior cavity: the role of entropy of symmetry. *Chem. Commun.* **49**, 2524–2526 (2013).

39. Ivanova, S., Köster, E., Holstein, J. J., Keller, N., Clever, G. H., Bein, T. & Beuerle, F. Isoreticular crystallization of highly porous cubic covalent organic cage compounds. *Angew. Chem. Int. Ed.* **60**, 17455–17463 (2021).

40. Yaghi, O. M., Kalmutzki, M. J. & Diercks, C. S. *Introduction to reticular chemistry: metal-organic frameworks and covalent organic frameworks.* (Wiley-VCH, Weinheim, Germany, 2019).

## Table of Content

## Materials and Instrumentation

### Materials

Tris(4-aminophenyl)amine (TAPA) (purity ≥ 98.0%) and tris(4-aminophenyl)methane (TAPM) (purity ≥ 97.0%) were purchased from Tokyo Chemical Industry Co. Tris(4-aminophenyl)methanol (TAPMol) (purity ≥ 98.0%), aniline (AR, ≥ 99.5%), 1,4-dioxane (AR, ≥ 99.5%), glacial acetic acid (AR, ≥ 99.5%), *N*,*N*-dimethylformamide (DMF) (AR, ≥ 99.9%) were purchased from Sigma-Aldrich Co. Mesitylene (AR, ≥ 98.0%), *p*-Br-aniline (AR, ≥ 98.0%) were purchased from Alfa Aesar Co. Tetrahydrofuran (THF) (AR, ≥ 99.9%) was purchased from Fisher Chemical Co. All regents and solvents were used without further purification unless otherwise specified. Cu(I)-bis[4,4'-(1,10-phenanthroline-2,9-diyl)dibenzaldehyde]tetrafluoroborate ($[Cu(PDB)_2]BF_4$) was prepared according to the reported procedures[1].

### Instrumentation

**Powder x-ray diffraction (PXRD).** The laboratory PXRD datasets were collected on a Bruker D8 Advance diffractometer with Cu K$\alpha$ radiation of wavelength ($\lambda$) = 1.5418 Å at 40 kV and 40 mA in the reflection mode. The step size was 0.02° with an exposure time of 5 s per step. The synchrotron PXRD datasets were collected at Beamline 7.3.3 of Advanced Light Source (ALS) in the Lawrence Berkeley National Laboratory (LBNL), with $\lambda$ = 1.2398 Å in the capillary mode.

**Transmission electron microscopy (TEM).** Catena-COF samples for TEM analysis were dispersed in ethanol by ultrasonication. A droplet of the suspension was transferred onto a carbon coated copper grid. All datasets were obtained using a JEM-2100Plus microscope at 200 kV with a TVIPS (XF416) camera for high signal-to-noise ratio data acquisition. Due to the beam-sensitivity of the samples, three-dimensional electron diffraction (3D ED) datasets were collected using fast method where the sample holder was tilted continuously and stopped every 5° for sample tracking. The obtained datasets were processed and reconstructed by the *EDT-process* program[2]. High-resolution TEM (HRTEM) images were obtained under low dose conditions. Before taking images, the crystals were aligned to the desired orientations quickly under a depressed illumination condition. With a careful control of the electron dose and short exposure time, multiple images were taken and then integrated into one image to reduce the blur caused by sample drift.

**Solid-state nuclear magnetic resonance (SSNMR) spectroscopy.** All the SSNMR experiments were performed with magic angle spinning (MAS) on a Bruker Avance II 500 MHz wide-bore SSNMR spectrometer at a magnetic field of 9.4 T. $^{13}C$ MAS NMR data were acquired at the Larmor frequency ($\nu_0$) of 100.6 MHz. The $^{13}C$ chemical shifts were referenced to tetramethylsilane (TMS) at 0 ppm ($\delta_{iso}$). All the $^{13}C$ experiments were carried out on a standard 4 mm double-resonance probe with the sample spinning rate of 12 kHz. $^{13}C$ cross-polarization (CP) MAS experiments were carried out with a $^1H$ $\pi/2$ pulse length of 3.2 μs, a contact time of 3 ms, a pulse delay of 3 s, and a two-pulse phase modulation (TPPM) decoupling frequency of 78.1 kHz. Two-

dimensional (2D) $^{1}H$-$^{13}C$ heteronuclear correlation (HETCOR) spectra were recorded using cross polarization (CP) with frequency switched Lee-Goldberg homonuclear decoupling[3,4] during the $^{1}H$ evolution period, and a homonuclear decoupling field strength of 80 kHz was used. In order to probe direct connectivity, a $^{1}H$-$^{13}C$ contact time of 100 μs was used with a $^{13}C$ field strength of 40 kHz, and a $^{1}H$ rf field strength of 75 kHz ramped from 50–100%. $^{1}H$ heteronuclear decoupling was applied during detection at a field strength of 50 kHz.

**THF vapor sorption.** THF vapor sorption isotherms were collected at 283 K using a BEL Japan BELSORP-aqua[3] vapor adsorption apparatus with a water circulator bath. The water bath with circulator was used for temperature control at 283 K. Anhydrous THF was degassed through five freeze-pump-thaw cycles and used as vapor source for the measurements. Ultra-high-purity helium (Praxair, 99.999% purity) was used for free space corrections. The catena-COF samples were activated under dynamic vacuum at 120 °C for 12 h before the measurements.

**Nanoindentation.** Nanoindentation tests were conducted with a Hysitron TI-950 Triboindenter. A Berkovich tip (TI-0039-1, 50 nm tip radius) was used to indent the catena-COF particle after scanning the area to localize the tip position. The sample preparation and other experimental details are described in Section 12.

**Other characterization methods.** The elemental analyses were carried out on a Perkin Elmer CHNS 2400 Series II Analyzer. The Fourier transform infrared (FT-IR) spectra were recorded with a Bruker Alpha FT-IR spectrometer. The thermogravimetric (TG) curves were recorded on a TA Instrument Q-500 thermal analyzer under $N_2$. The scanning electron microscopy (SEM) images were obtained on a Hitachi S-5000 field-emission scanning electron microscope with the accelerating voltage of 10.0 kV. Inductively coupled plasma atomic emission spectroscopy (ICP-AES) analyses, which were used to determine the copper component in COFs (Section 10), were conducted on an Agilent 7500ce instrument using the helium collision gas mode. The catena-COF samples were dissolved in OPTIMA grade nitric acid to form stock solutions, which were then diluted to 1:10 (*v*/*v*) with ultrapure $H_2O$ for analyses.

## Section 1. Topology Analysis

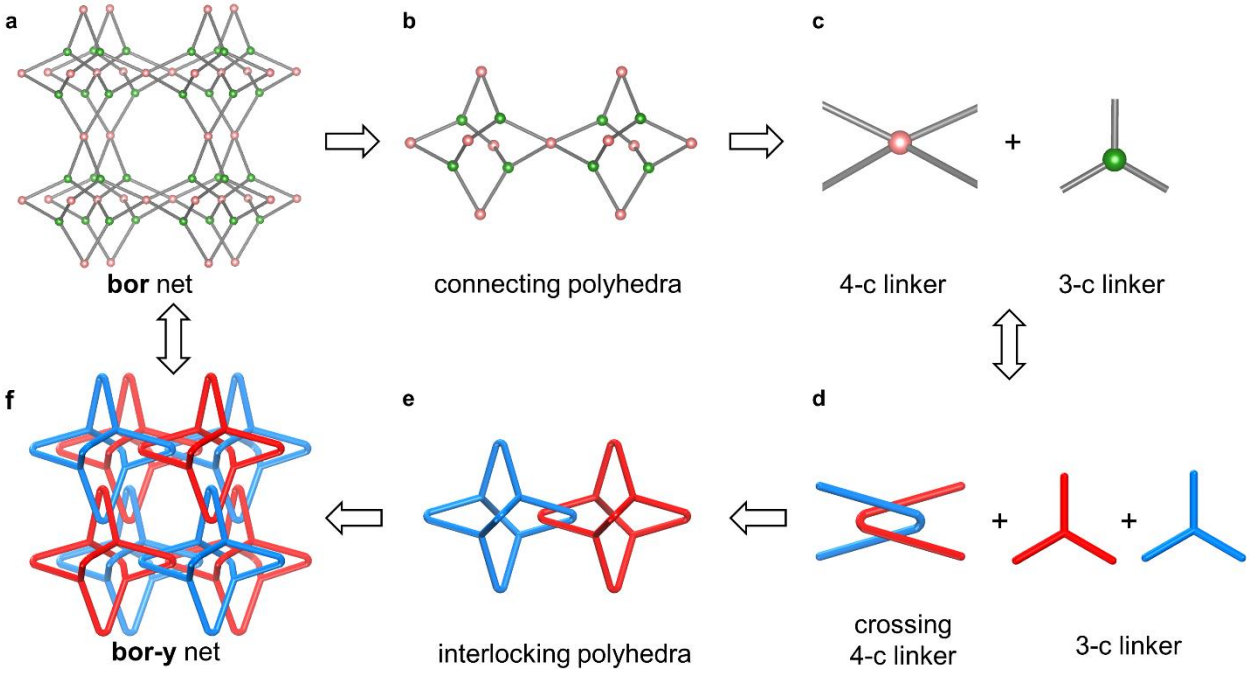


**Supplementary Fig. 1 | Strategy for construction of 3D [∞]catenane frameworks with underlying bor (bor-y) topology.** The bor net (a) is composed of corner sharing adamantane-like polyhedra (b), which can further be dissected into their fundamental 4-c tetrahedral and 3-c triangular building units (c). The 4-c tetrahedra need to be translated to the crossing points (d) that link the interlocking polyhedra (e) to yield the targeted interlocking **bor-y** net (f). Note that if the center of each polyhedron was simplified as a node, a **pcu** topology can be obtained. All the topologies discussed here can be found in RCSR database[5,6].

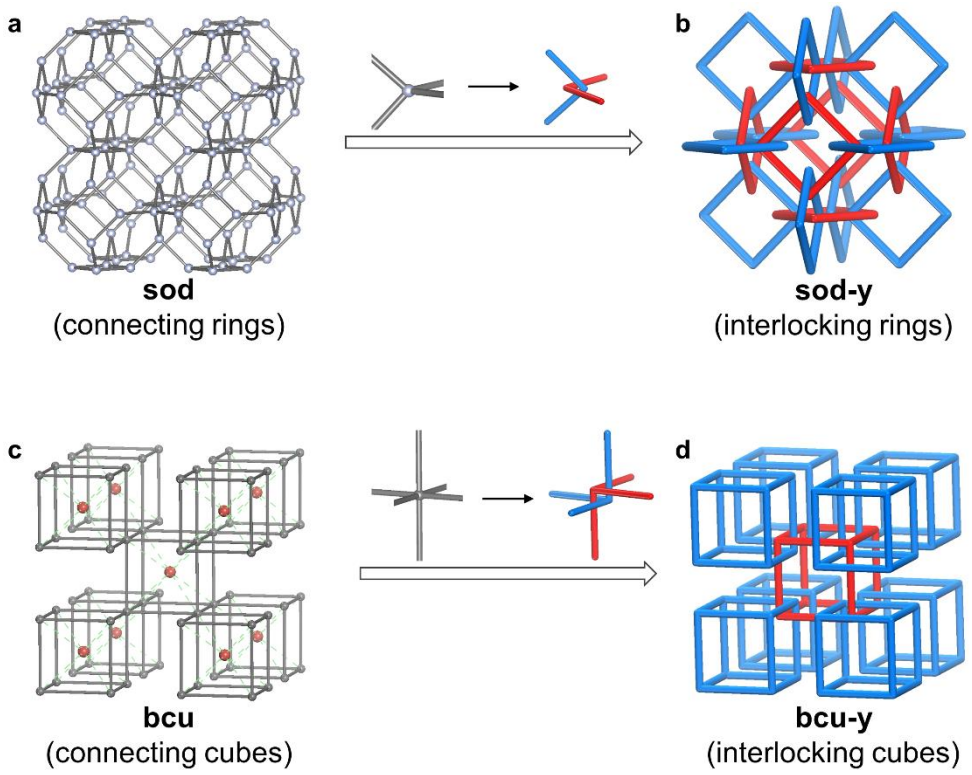


**Supplementary Fig. 2 | The examples of potential topologies which can be deconstructed into connecting rings/polyhedra and further translated to its interlocking motifs. a**, **sod** net. **b**, **sod-y** net. **c**, **bcu** net. **d**, **bcu-y** net.

Similar to the translation between **bor** and **bor-y** nets shown in Supplementary Fig. 1, the **sod** net which is composed of conner sharing rings can be translated into its underlying motif **sod-y** of interlocking rings, by replacing the connecting points with the crossing linkers (a to b). Besides, the original **bcu** topology (the net of linking red balls in c) can be expanded into a form consisting of cubes (the net of gray cubes in c). The connecting cubes can be translated into its underlying motif **bcu-y** as interlocking cubes, with replacing each orthogonal corner with crossing linkers (c to d). It should be noted that the crossing linkers should possess the same geometry with the connecting points and have to be linked with the other building units in the desirable distances and angles by covalent bonds to form intact and closed covalent rings/polyhedra. All the topologies discussed here can be found in RCSR database[5,6]. This reticulation method can be developed into a general strategy for the design and synthesis of 2D/3D [∞]catenane COFs.

It is worth mentioning that the woven COFs, which were composed of entangled 1D organic threads to form crystalline extended lattices were recently developed[1], where the rational design for the crossing points in the interlacing threads (i.e., points of registry) was also one of the key issues to enrich the molecular weaving materials[7,8].

## Section 2. Crystallization of Catena-COFs

**Crystallization of catena-COF-805.** A pressure tube was charged with Cu(I)-bis[4,4'-(1,10-phenanthroline-2,9-diyl)dibenzaldehyde]tetrafluoroborate ($[Cu(PDB)_2]BF_4$, 8.0 mg, 0.008 mmol), tris(4-aminophenyl)amine (TAPA, 3.3 mg, 0.011 mmol), and *p*-Br-aniline (27.5 mg, 20 equiv.) as a modulator. The mixture of 0.25 mL of 1,4-dioxane, 0.25 mL mesitylene and 0.05 mL of 6 M aqueous acetic acid was added. Then the tube was sealed and heated at 150°C for 72 h, yielding a reddish-brown solid at the bottom of the tube which was isolated as catena-COF-805. The as-synthesized catena-COF-805 was washed with *N*,*N*-dimethylformamide (DMF) and tetrahydrofuran (THF), and dried at room temperature for 12 h and at 120°C for 12 h. This material is insoluble in water and in common organic solvents such as methanol, acetone, THF, DMF, and dimethylsulfoxide. Yield: 8.1 mg, 75.7%. Elemental analysis (EA) results: calcd. for $C_{228}H_{144}N_{28}Cu_3B_3F_{12}\cdot 20H_2O$: C 67.00%; H 4.50%; N 9.59%. Found: C 66.36%; H 4.22%; N 9.11%.

**Crystallization of catena-catena-COF-806.** A pressure tube was charged with $[Cu(PDB)_2]BF_4$ (8.0 mg, 0.008 mmol) and tris(4-aminophenyl)methane (TAPM, 5.0 mg, 0.017 mmol). The mixture of 0.5 mL of 1,4-dioxane, 20 μL aniline (24.4 equiv.) and 0.1 mL of aqueous acetic acid (6 M) was added and the tube was sealed. The reaction was heated at 120°C for 72 h, yielding a reddish-brown solid as catena-COF-806 at the bottom of the tube. The solid was isolated by centrifugation and washed with DMF and THF, and then dried at room temperature for 12 h and at 120°C for 12 h. Similarly, this product is insoluble in water and in common organic solvents as mentioned for catena-COF-805. Yield: 7.6 mg, 71.0 %. EA results: calcd. for $C_{232}H_{148}N_{24}Cu_3B_3F_{12}\cdot 25H_2O$: C 68.13%; H 4.50%; N 7.91%. Found: C 68.93%; H 4.47%; N 8.09%.

**Crystallization of catena-COF-807.** A pressure tube was charged with $[Cu(PDB)_2]BF_4$ (8.0 mg, 0.008 mmol) and tris(4-aminophenyl)methanol (TAPMol, 3.4 mg, 0.011 mmol). The mixture of 0.25 mL of 1,4-dioxane, 0.25 mL mesitylene, 0.1 mL of aqueous acetic acid (6 M) was added and the tube was sealed. The reaction was heated at 85°C for 72 h, yielding a reddish-brown solid as catena-COF-807 at the bottom of the tube. The crude product was isolated by centrifugation and washed with DMF and THF, and then dried at room temperature for 12 h and at 120°C for 12 h. Similarly, this product is also insoluble in water and in common organic solvents as mentioned for catena-COF-805 and -806. Yield: 6.9 mg, 63.9%. EA results: calcd. for $C_{232}H_{148}N_{24}O_4Cu_3B_3F_{12}\cdot 25H_2O$: C 69.17%; H 4.74%; N 8.01%. Found: C 69.58%; H 4.71%; N 7.93%.

## Section 3. Thermogravimetric Analysis (TGA)

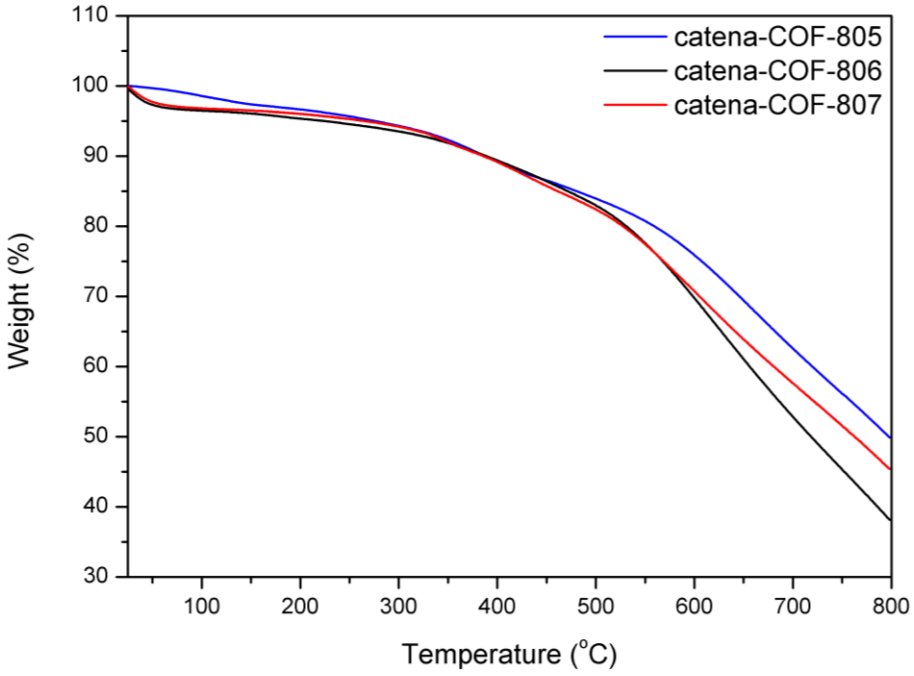


**Supplementary Fig. 3 | TGA curves of catena-COF-805 (blue), -806 (black) and -807 (red).** The decomposition temperatures for three catena-COFs are similarly to reach ~500°C, which is comparable with previously observed decomposition temperatures for imine COFs.

## Section 4. Fourier Transform Infrared (FT-IR) Spectroscopic Analysis

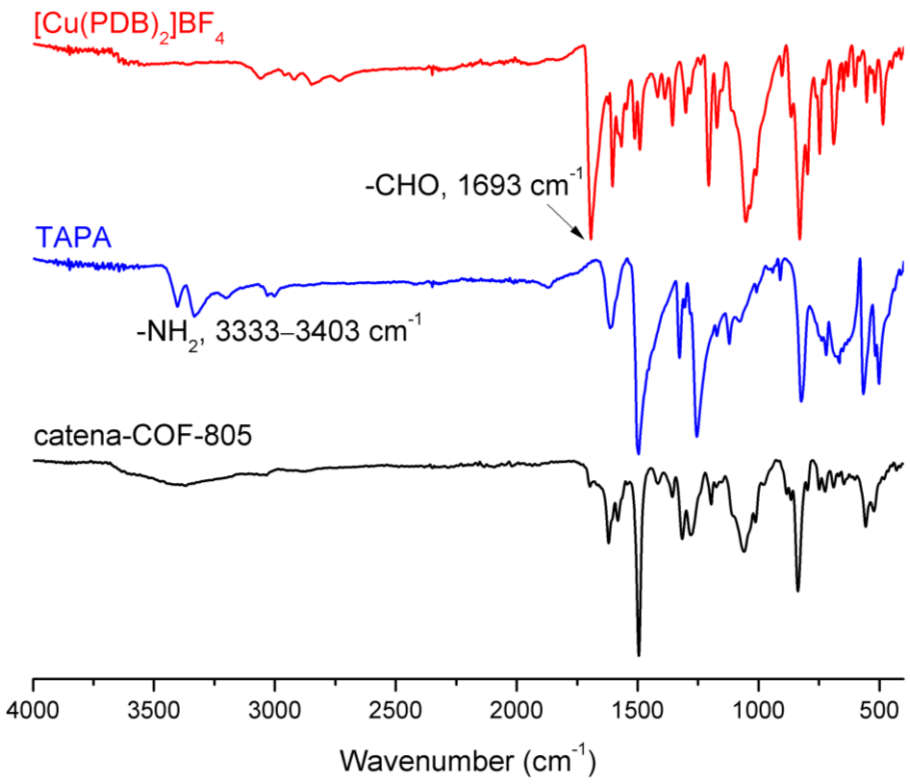


**Supplementary Fig. 4 | FT-IR spectra of $[Cu(PDB)_2]BF_4$ (red), TAPA (blue) and catena-COF-805 (black).** As labeled in figure, the signals of –CHO (~1693 $cm^{-1}$) and $–NH_2$ (3333–3403 $cm^{-1}$) in linkers ($[Cu(PDB)_2]BF_4$ and TAPA) were largely decreased in the spectrum of catena-COF-805, implying that the imine condensation reaction occurred between linkers as expected.

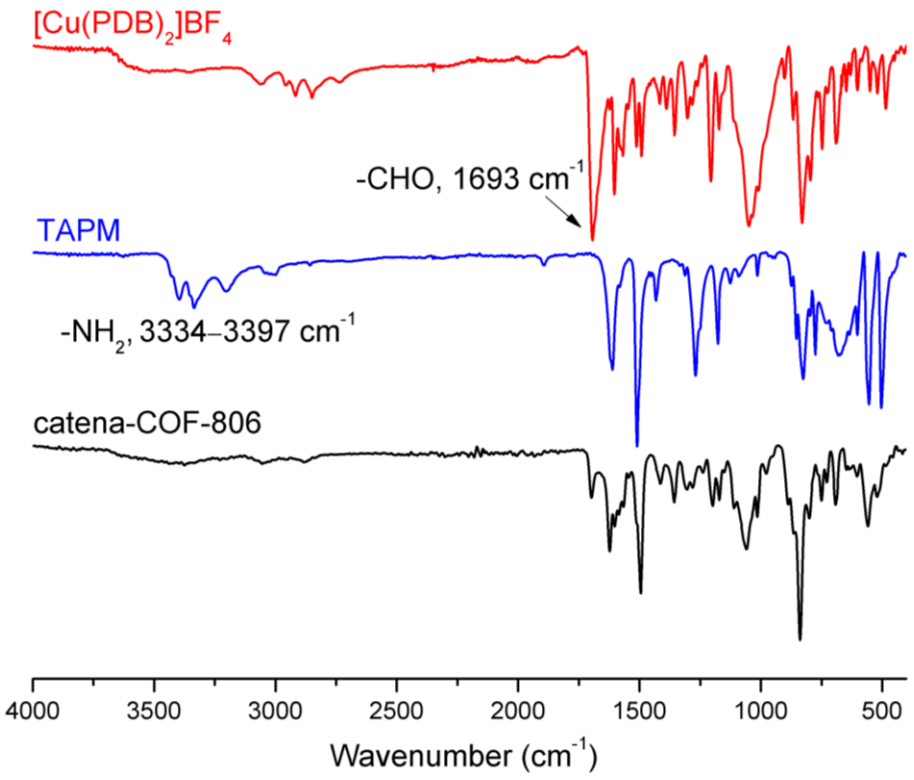


**Supplementary Fig. 5 | FT-IR spectra of $[Cu(PDB)_2]BF_4$ (red), TAPM (blue) and catena-COF-806 (black).** As labeled in figure, the signals of –CHO (~1693 $cm^{-1}$) and $–NH_2$ (3334–3397 $cm^{-1}$) in linkers ($[Cu(PDB)_2]BF_4$ and TAPM) were largely decreased in the spectrum of catena-COF-806, implying that the imine condensation reaction occurred between linkers as expected.

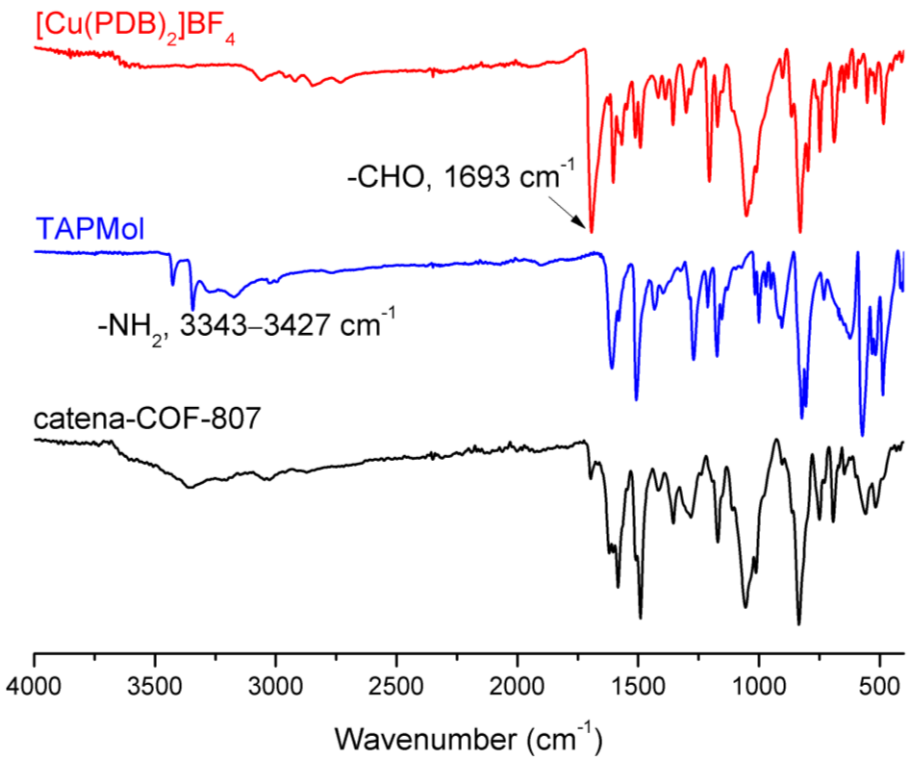


**Supplementary Fig. 6 | FT-IR spectra of $[Cu(PDB)_2]BF_4$ (red), TAPMol (blue) and catena-COF-807 (black).** As labeled in figure, the signals of –CHO (~1693 $cm^{-1}$) and $–NH_2$ (3343–3427 $cm^{-1}$) in linkers ($[Cu(PDB)_2]BF_4$ and TAPMol) were largely decreased in the spectrum of catena-COF-807, implying that the imine condensation reaction occurred between linkers as expected.

## Section 5. Solid-State Nuclear Magnetic Resonance (SSNMR) Spectroscopic Analysis

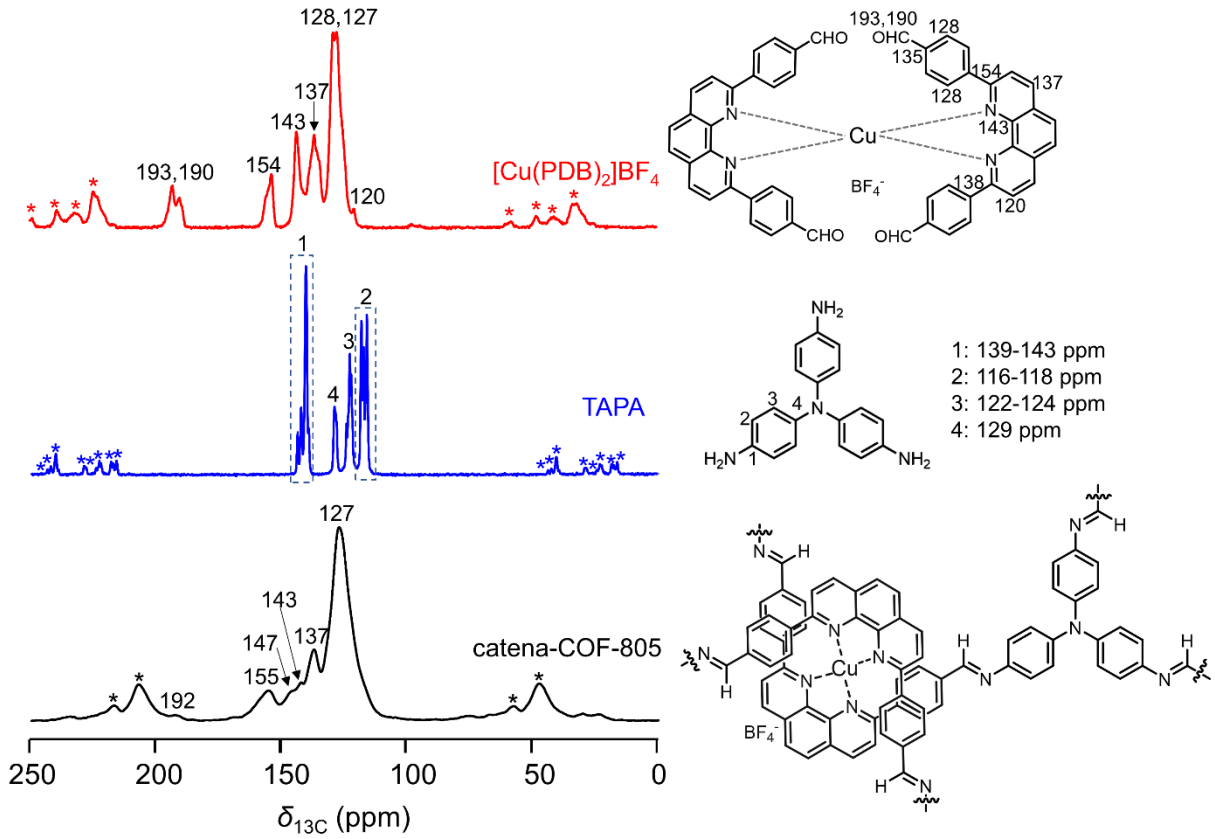


**Supplementary Fig. 7 | $^{13}$C CP/MAS NMR spectra of [Cu(PDB)$_2$]BF$_4$ (red), TAPA (blue) and catena-COF-805 (black).** The $^{13}$C CP/MAS NMR signals have been assigned as shown in chemical structures. Asterisks denote spinning sidebands. Comparison of the three spectra confirmed that catena-COF-805 featured characteristic signals of both linkers ([Cu(PDB)$_2$]BF$_4$ and TAPA). The $^{13}$C signals related to the functional groups of linkers such as –CHO (190–193 ppm, assigned to C in –CHO) and –NH$_2$ (116–118 ppm, assigned to the C adjacent to C–NH$_2$) decreased largely in the spectrum of catena-COF-805. All the information implied that the imine condensation reaction occurred between two linkers to produce COF. The new formation of imine bonds was directly evidenced by a 2D $^{1}$H-$^{13}$C HETCOR experiment as shown in Supplementary Fig. 10.

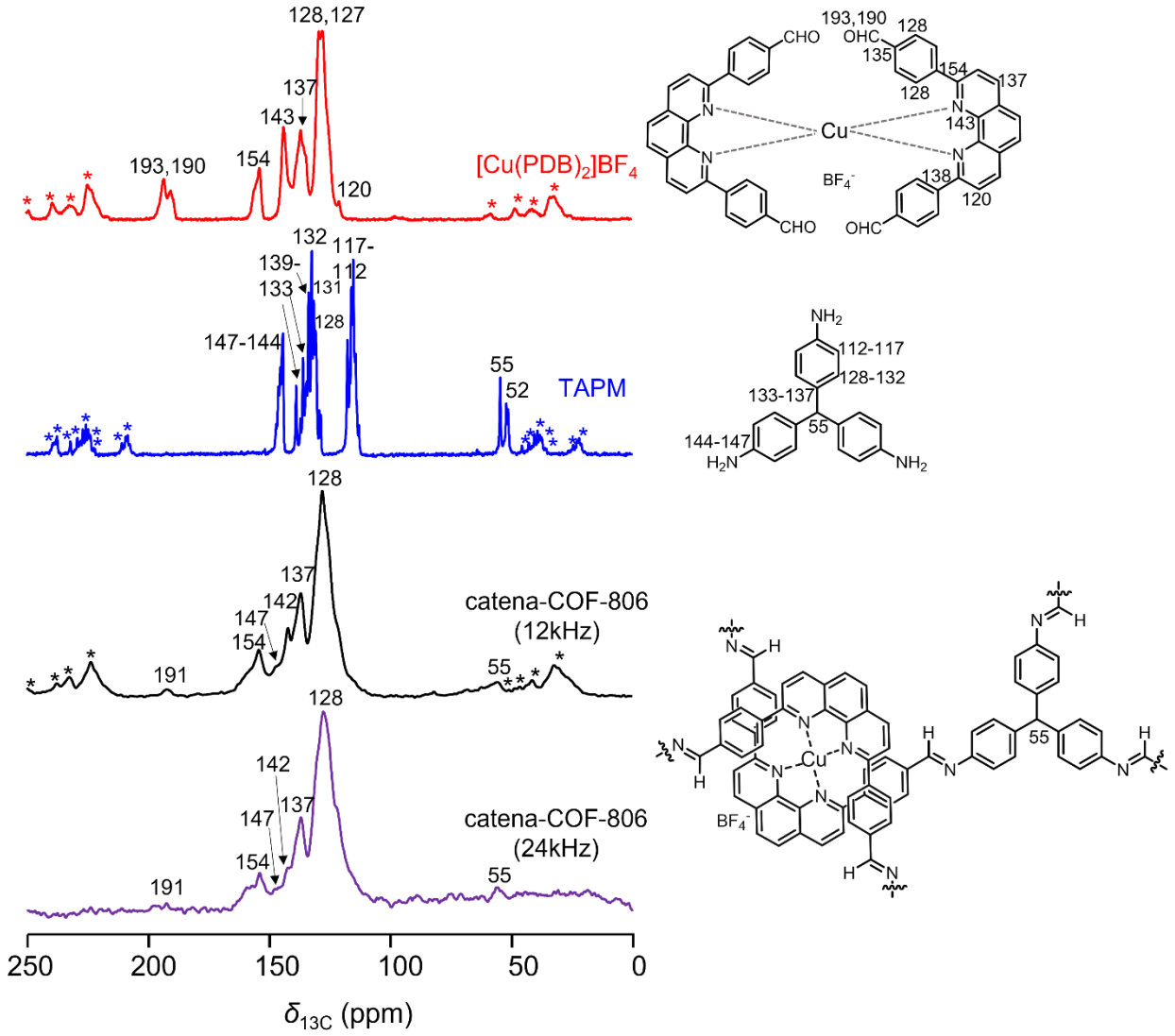


**Supplementary Fig. 8 | $^{13}$C CP/MAS NMR spectra of [Cu(PDB)$_2$]BF$_4$ (red), TAPM (blue) and catena-COF-806 (black and purple, collected with different spinning rates of 12kHz and 24kHz, respectively).** The $^{13}$C CP/MAS NMR signals have been assigned as shown in chemical structures. Asterisks denote spinning sidebands. The characterized signals of the linkers ([Cu(PDB)$_2$]BF$_4$ and TAPM) can be found in the spectrum of catena-COF-806; for example, the signal of ~55 ppm corresponding to the quaternary C in TAPM can be observed in the spectrum of catena-COF-806. Similar to catena-COF-805, the signals related to the functional groups such as –CHO (190–193 ppm, were assigned to C in –CHO) and –NH$_2$ (112–117 ppm, assigned to the C adjacent to C–NH$_2$) in linkers decreased largely in the spectrum of catena-COF-806. All the information implied that the imine condensation reaction occurred between two linkers to yield COF. The new formation of imine bonds was directly evidenced by a 2D $^{1}$H-$^{13}$C HETCOR experiment as shown in Supplementary Fig. 11. Note that in the spectrum of catena-COF-806 collected with the spinning rate of 12kHz, some spinning sidebands on the right side were contained in the signals of quaternary C atom at ~55 ppm, comparing with the spinning sidebands

on the left side. To address this issue, a higher spinning rate (24 kHz) was adopted to acquire an extra spectrum for this sample (purple) in a 1 mm sample rotor with the adjusted instrumentation parameters. Indeed, the peak at ~55 ppm is the signal of quaternary C but not the side band.

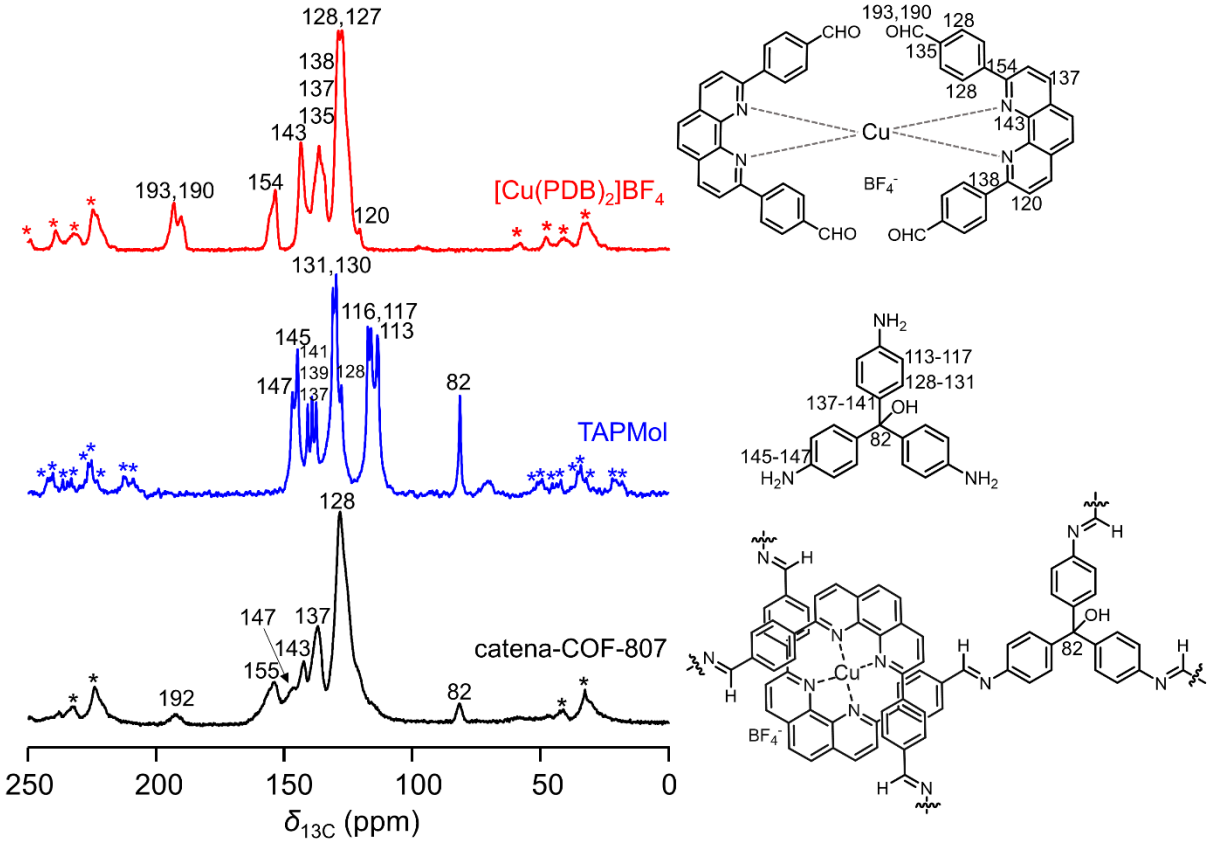


**Supplementary Fig. 9 | $^{13}$C CP/MAS spectra of [Cu(PDB)$_2$]BF$_4$ (red), TAPMol (blue) and catena-COF-807 (black).** The $^{13}$C CP/MAS NMR signals have been assigned as shown in chemical structures. Asterisks denote spinning sidebands. The characterized signals of linkers ([Cu(PDB)$_2$]BF$_4$ and TAPMol) can be found in the spectrum of catena-COF-807; for example, the signal of ~82 ppm corresponding to the quaternary C in TAPMol can be observed in the spectrum of catena-COF-807. Similar to catena-COF-805 and -806, the signals related to the functional groups such as –CHO (190–193 ppm, assigned to C in –CHO) and –NH$_2$ (113–117 ppm, assigned to the C adjacent to C–NH$_2$) in linkers decreased largely in the spectrum of catena-COF-807. All the information implied that the imine condensation reaction occurred between two linkers to produce COF. The new formation of imine bonds was directly evidenced by a 2D $^{1}$H-$^{13}$C HETCOR experiment as shown in Supplementary Fig. 12.

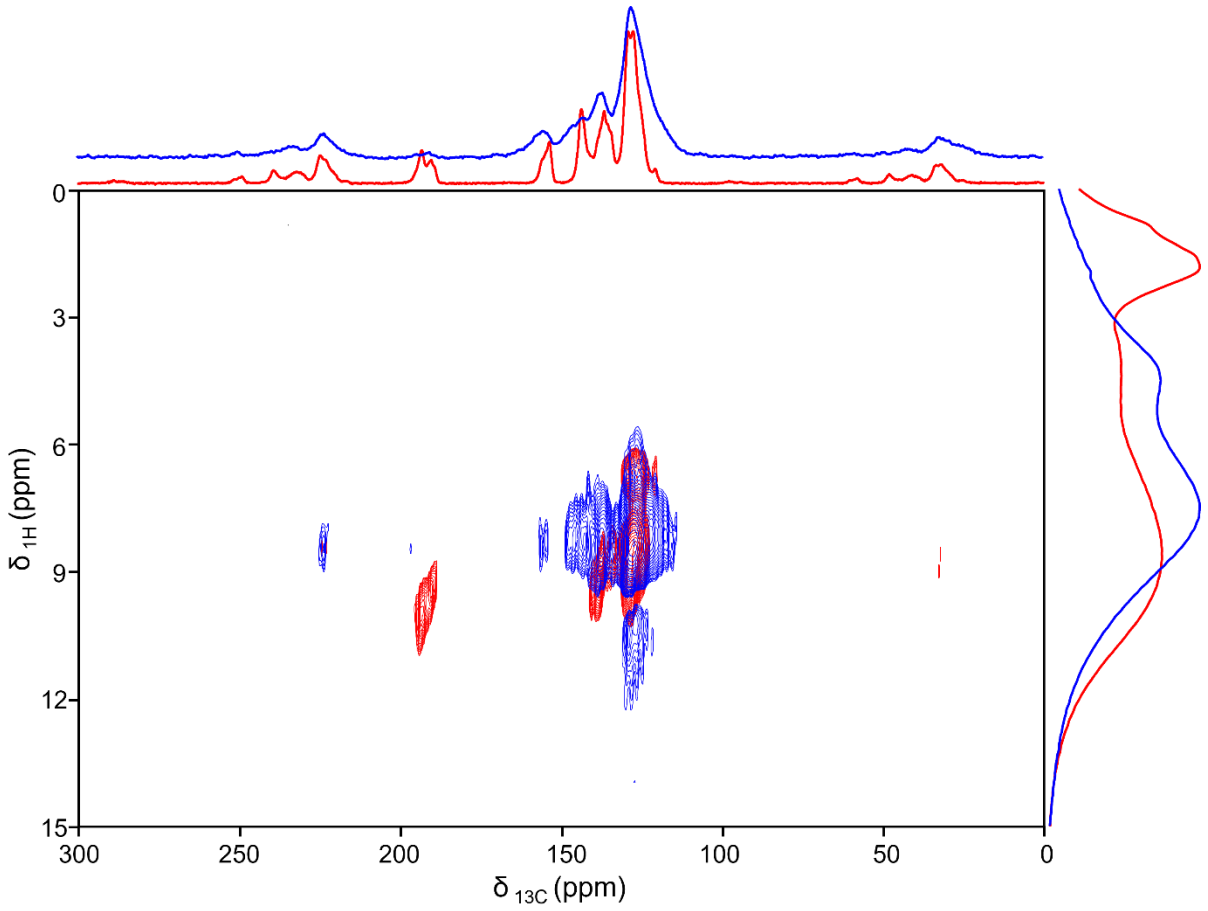


**Supplementary Fig. 10 | The overlaid $^{1}$H-$^{13}$C HETCOR spectra of [Cu(PDB)$_2$]BF$_4$ (red) and catena-COF-805 (blue).** The 1D $^{13}$C CP/MAS and $^{1}$H spectra are displayed on top and right of the 2D spectra, respectively, to demonstrate the different assignment and correlations of the two samples. In 1D $^{13}$C CP/MAS spectra, it is unambiguous to distinguish the newly formed imine bonds (HC=N, expected at 154−156 ppm) in catena-COF-805 with the C=N bonds (~155 ppm) from the [Cu(PDB)$_2$]BF$_4$ linker. In 2D HETCOR spectra of catena-COF-805 (blue), the cluster of peaks appears at $^{13}$C chemical shift of 154–156 ppm which shows a correlation with a $^{1}$H chemical shift of ~8 ppm assigned to the imine groups (HC=N), demonstrating the new formation of the imine linkage in COF. There is no correlation signal of same species in the 2D HETCOR spectrum of [Cu(PDB)$_2$]BF$_4$ (red), since the C=N bonds here contain no proton. Besides, the correlation signal corresponding to chemical shifts of $^{13}$C at 190–193 ppm and $^{1}$H at ~10 ppm is assigned to the C and H of aldehyde groups in [Cu(PDB)$_2$]BF$_4$ (red). A similar but diminished signal can also be observed in the spectrum of catena-COF-805 (blue), which means that aldehyde has been consumed largely and only a small amount was left as terminal group at the surface of the COF.

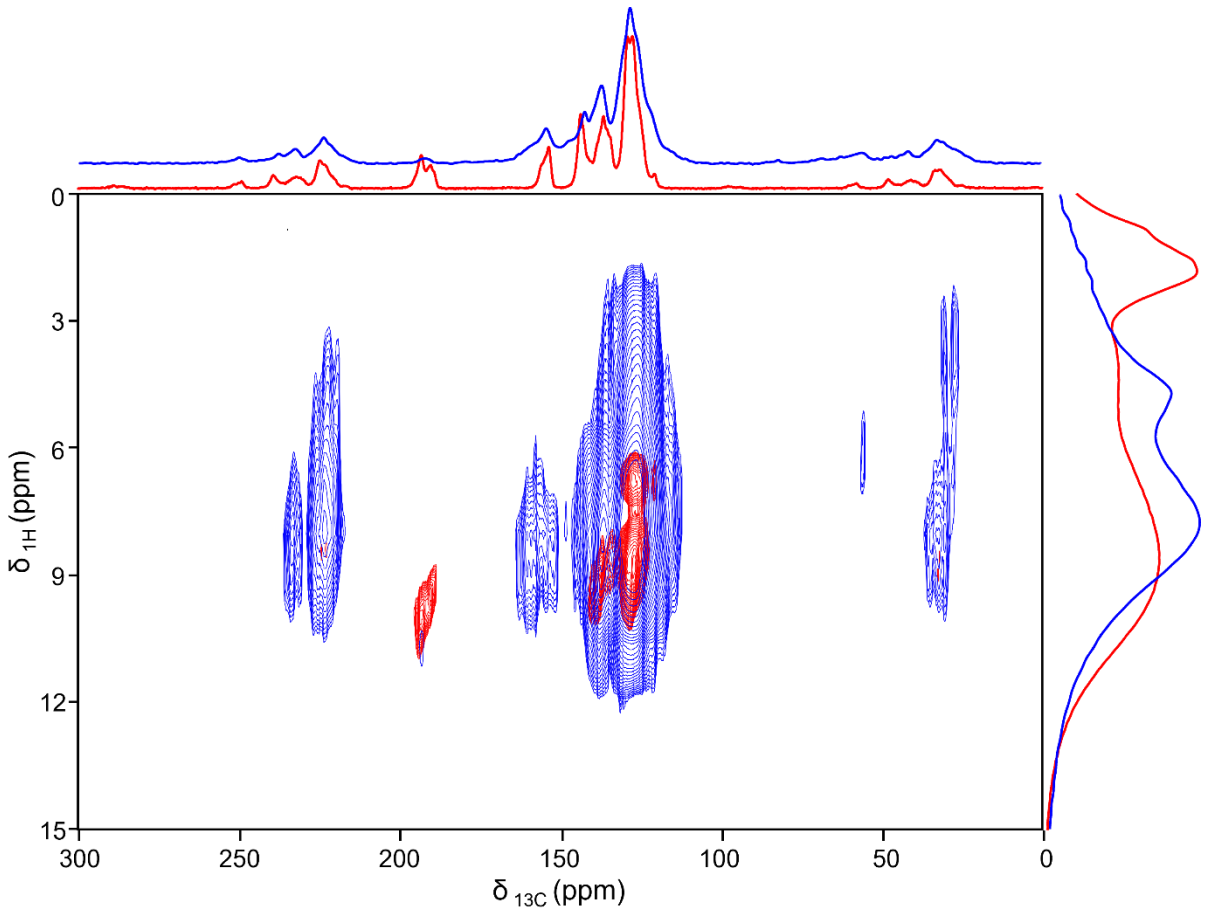


**Supplementary Fig. 11 | The overlaid $^{1}$H-$^{13}$C HETCOR spectra for [Cu(PDB)$_2$]BF$_4$ (red) and catena-COF-806 (blue).** The 1D $^{13}$C CP/MAS and $^{1}$H spectra are displayed on top and right of the 2D spectra, respectively, to demonstrate the different assignment and correlations of the two samples. Similar to the case of catena-COF-805, in 1D $^{13}$C CP/MAS spectra, it is unambiguous to distinguish the newly formed imine bonds (HC=N, expected at 154−156 ppm) in catena-COF-806 with the C=N bonds (~155 ppm) from the [Cu(PDB)$_2$]BF$_4$ linker. In 2D HETCOR spectrum of catena-COF-806 (blue), the cluster of peaks appears at $^{13}$C chemical shift of 154–156 ppm which shows a correlation with a $^{1}$H chemical shift of 8–9 ppm is assigned to the imine groups (HC=N), demonstrating the new formation of the imine linkage in COF. There is no correlation signal of the same species in the 2D HETCOR spectra of [Cu(PDB)$_2$]BF$_4$ (red), since the C=N bonds here contain no proton. Besides, the correlation signal corresponding to chemical shifts of $^{13}$C at 192–193 ppm and $^{1}$H at ~10 ppm is assigned to the C and H of aldehyde groups in [Cu(PDB)$_2$]BF$_4$ (red). A similar but intensely diminished signal can also be observed in the spectrum of catena-COF-806 (blue), which means that aldehyde groups have been consumed largely and only a small amount was left as terminal group at the surface of the COF.

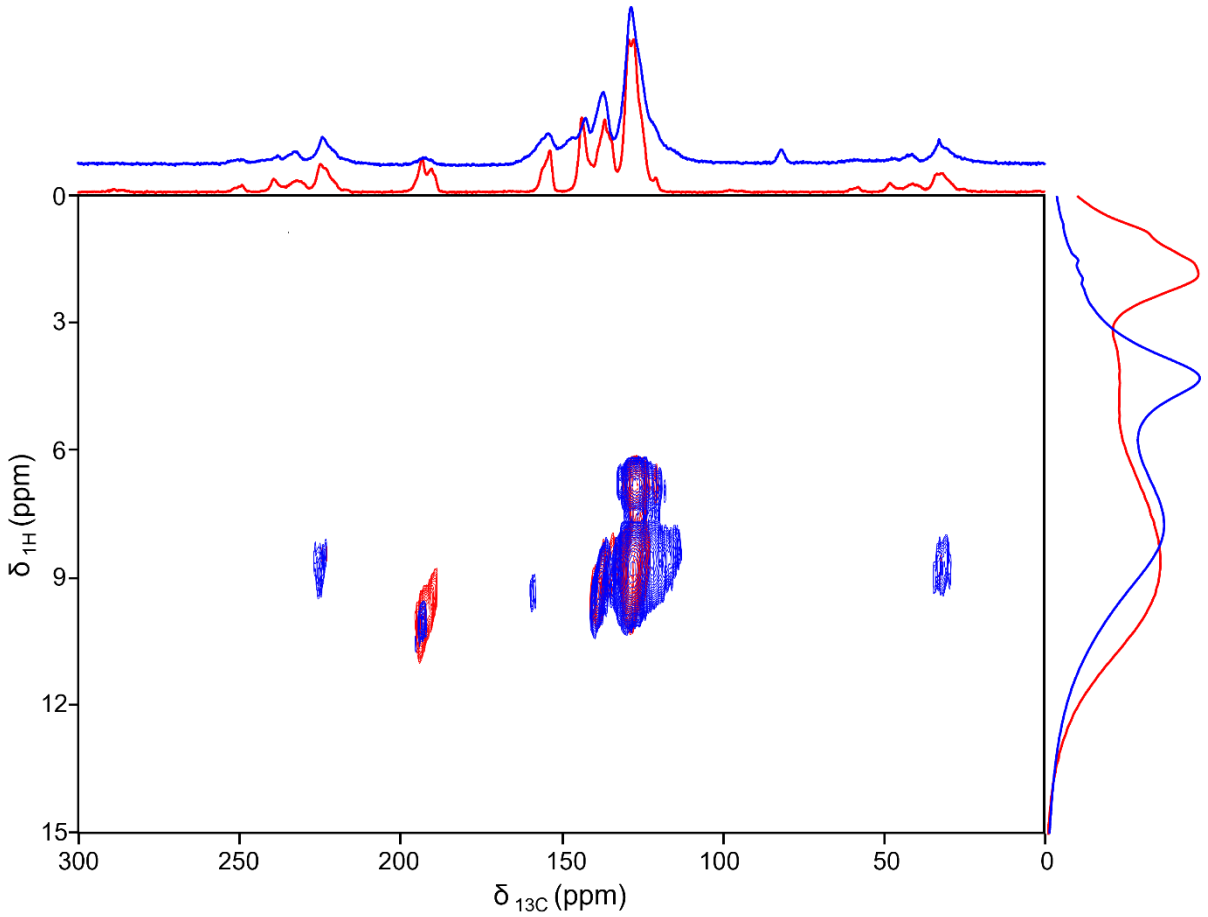


**Supplementary Fig. 12 | The overlaid $^{1}$H-$^{13}$C HETCOR spectra for [Cu(PDB)$_2$]BF$_4$ (red) and catena-COF-807 (blue).** The 1D $^{13}$C CP/MAS and $^{1}$H spectra are displayed on top and right of the 2D spectra, respectively, to demonstrate the different assignment and correlations of the two samples. Similar to the cases of catena-COF-805 and -806, in 1D $^{13}$C CP/MAS spectra, it is unambiguous to distinguish the newly formed imine bonds (HC=N, expected at 154−156 ppm) in catena-COF-807 with the C=N bonds (~155 ppm) from the [Cu(PDB)$_2$]BF$_4$ linker. In 2D HETCOR spectrum of catena-COF-807 (blue), the cluster of peaks appears at $^{13}$C chemical shift of 154–156 ppm which shows a correlation with a $^{1}$H chemical shift of ~9 ppm assigned to the imine groups (HC=N), demonstrating the new formation of the imine linkage in COF. There is no correlation signal of same species in the 2D HETCOR spectra of [Cu(PDB)$_2$]BF$_4$ (red), since the C=N bonds here contain no proton. Besides, the correlation signal corresponding to chemical shifts of $^{13}$C at 192–193 ppm and $^{1}$H at ~10 ppm is assigned to the C and H of aldehyde groups in [Cu(PDB)$_2$]BF$_4$ (red). A similar but diminished signal can also be observed in the spectrum of catena-COF-807 (blue), which means that aldehyde groups have been consumed largely and only a small amount was left as terminal group at the surface of the COF.

**Section 6. Phase Analysis by Powder X-ray Diffraction (PXRD)**

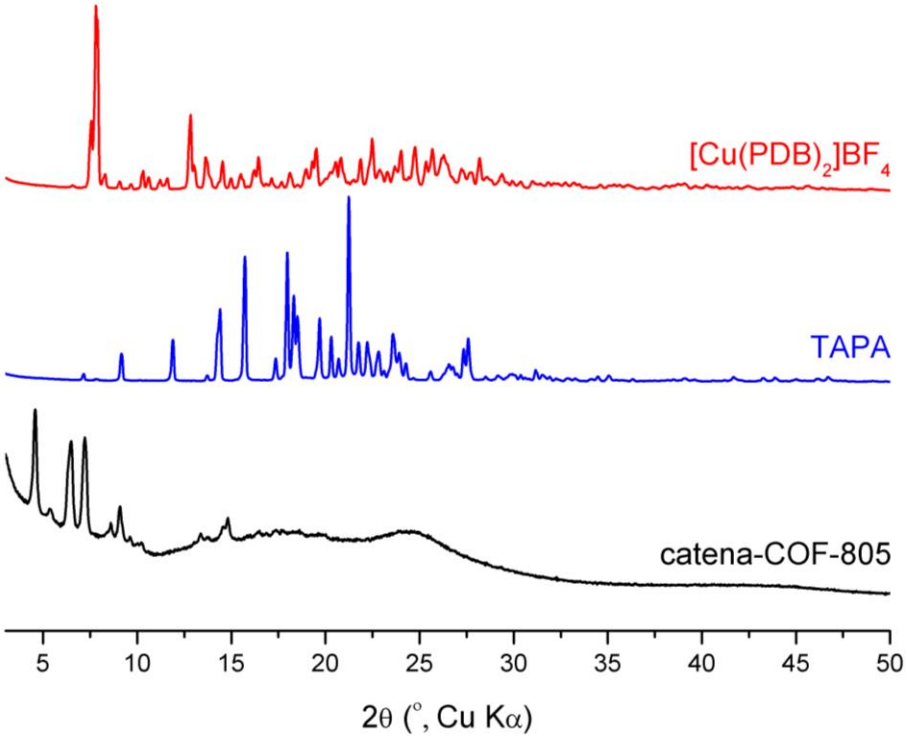


**Supplementary Fig. 13 | PXRD patterns of $[Cu(PDB)_2]BF_4$ (red), TAPA (blue) and catena-COF-805 (black).** The datasets were collected at the Bruker D8 Advance diffractometer as mentioned in Instrumentation. The intensity values along the Y–axis were normalized for comparison. The PXRD pattern of catena-COF-805 is different from those of linkers, indicating that a new crystalline phase has been formed.

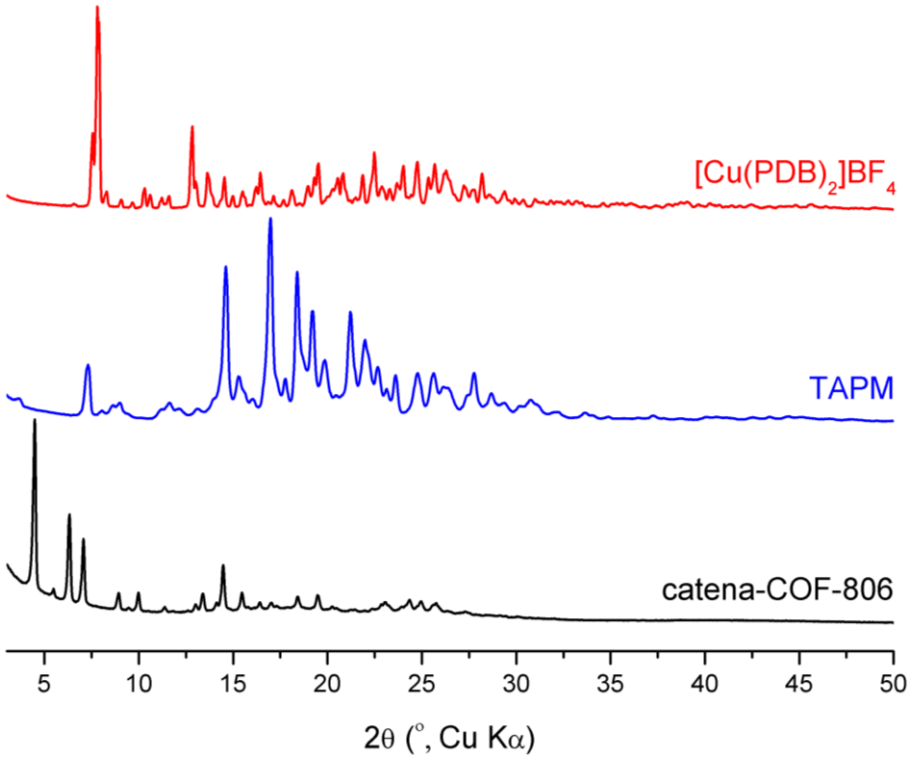


**Supplementary Fig. 14 | PXRD patterns of $[Cu(PDB)_2]BF_4$ (red), TAPM (blue) and catena-COF-806 (black).** The datasets were collected at Bruker D8 Advance diffractometer as described in Instrumentation. The intensity values along the Y−axis were normalized for comparison. The PXRD pattern of catena-COF-806 is different from those of linkers, indicating that a new crystalline phase has been formed.

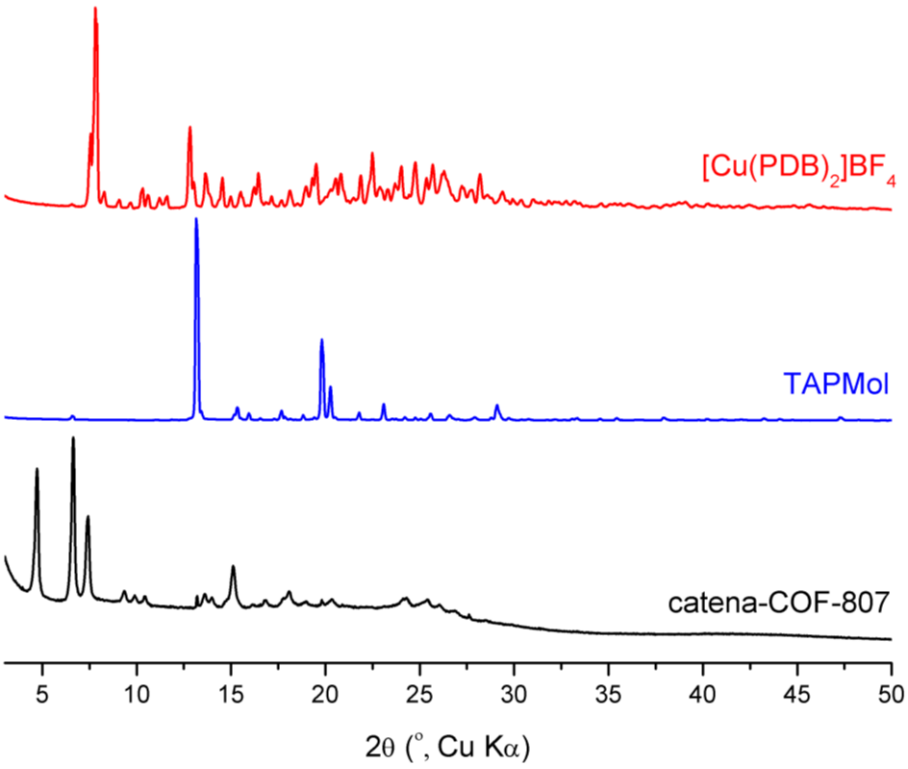


**Supplementary Fig. 15 | PXRD patterns of $[Cu(PDB)_2]BF_4$ (red), TAPMol (blue) and catena-COF-807 (black).** The datasets were collected at Bruker D8 Advance diffractometer as described in Instrumentation. The intensity values along the Y–axis were normalized for comparison. The PXRD pattern of catena-COF-807 is different from those of linkers, indicating that a new crystalline phase has been formed.

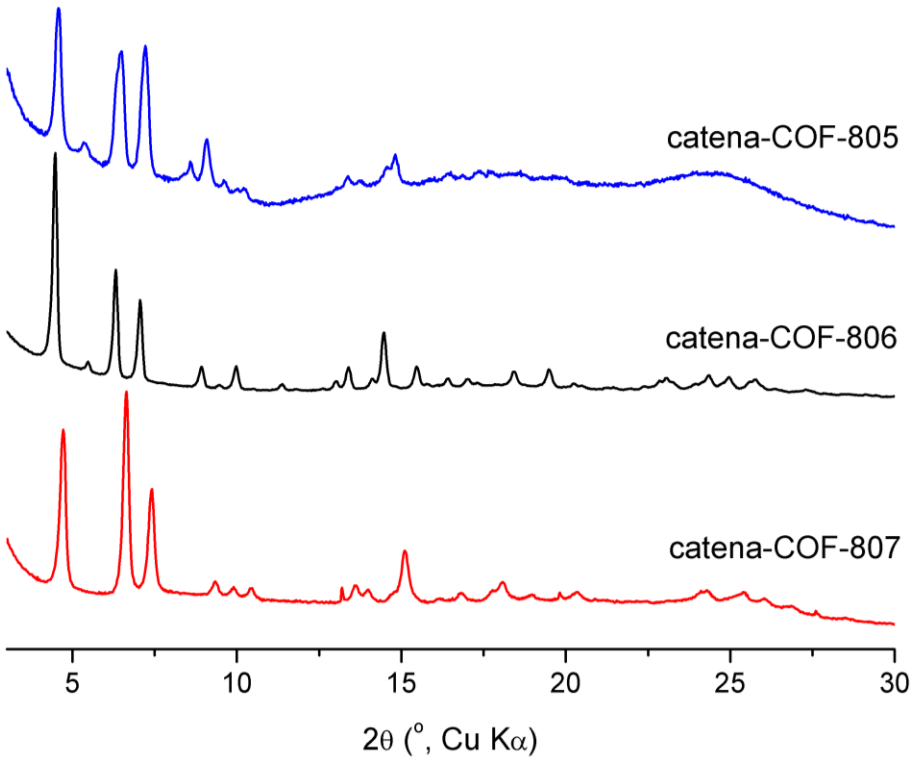


**Supplementary Fig. 16 | Comparison of PXRD patterns of catena-COF-805 (blue), -806 (black) and -807 (red) collected with laboratory diffractometer.** The datasets were collected at Bruker D8 Advance diffractometer as described in Instrumentation. The intensity values along the Y–axis were normalized for comparison. PXRD patterns of three catena-COFs are very similar regarding reflection positions but slightly different on the relative intensity, implying that they have similar basic structures with minor variations.

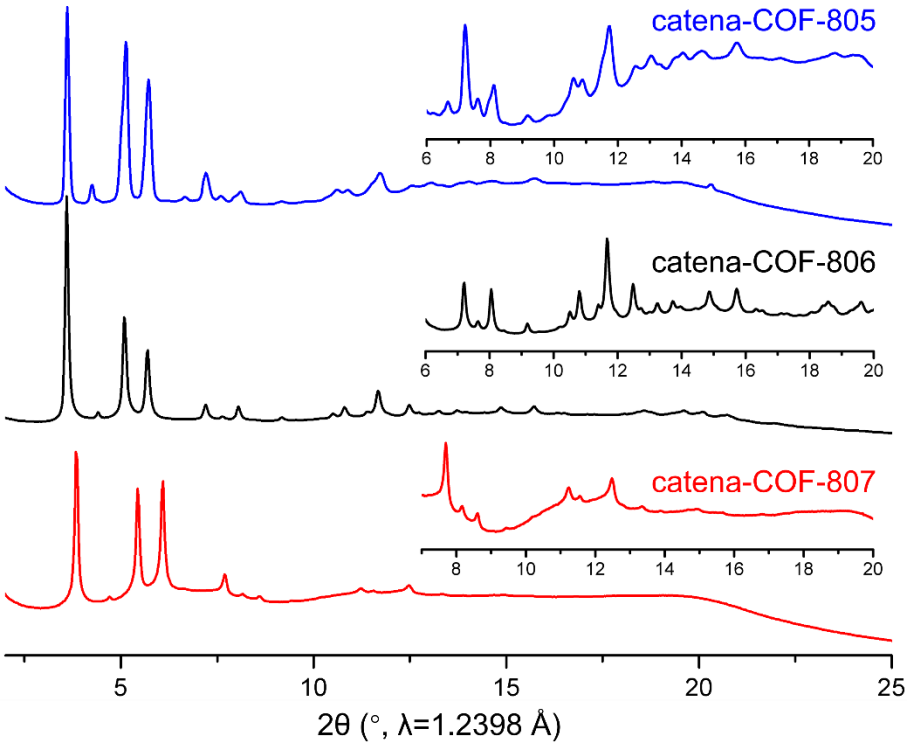


**Supplementary Fig. 17 | Comparison of PXRD patterns of catena-COF-805 (blue), -806 (black) and -807 (red) collected with synchrotron beam.** Insets: the magnified range of PXRD patterns. These patterns were collected with the synchrotron beam with $\lambda$ = 1.2398 Å as described in Instrumentation. The intensity values along the Y–axis were normalized for comparison. It is shown that PXRD patterns of three catena-COFs are very similar regarding reflection positions but slightly different on the relative intensity, implying that they have similar basic structures with minor variations.

## Section 7. Scanning Electron Microscopy (SEM)

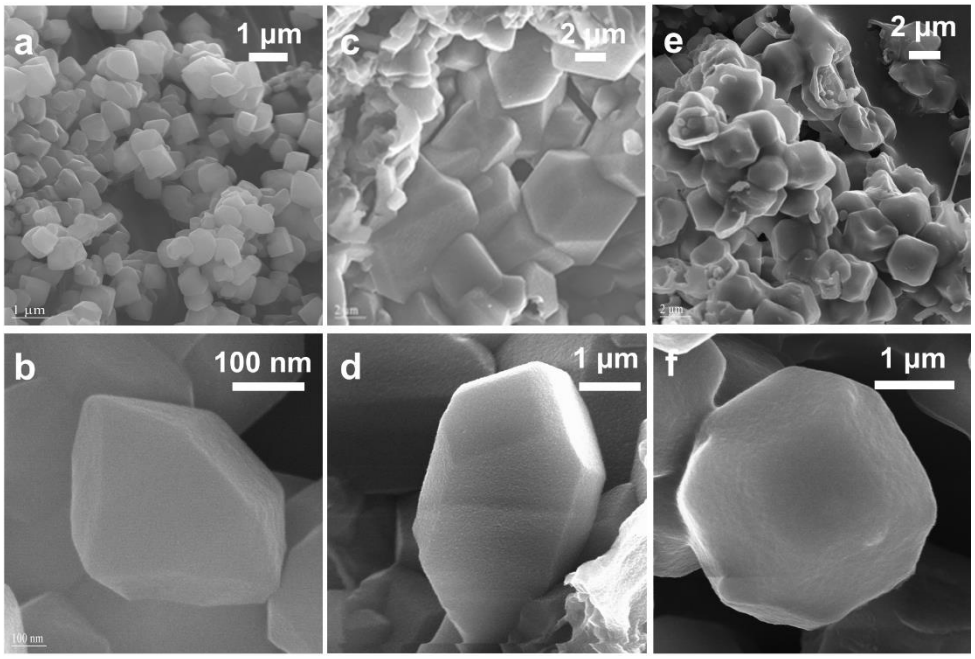


**Supplementary Fig. 18 | SEM images of catena-COF-805 (a,b), catena-COF-806 (c,d) and catena-COF-807 (e,f).** All three COF crystals have polyhedron-shaped morphology with the average crystal sizes of ~500 nm for catena-COF-805, ~5 μm for -806 and ~3 μm for -807, respectively.

**Section 8. Structure Analysis by Transmission Electron Microscopy (TEM)**

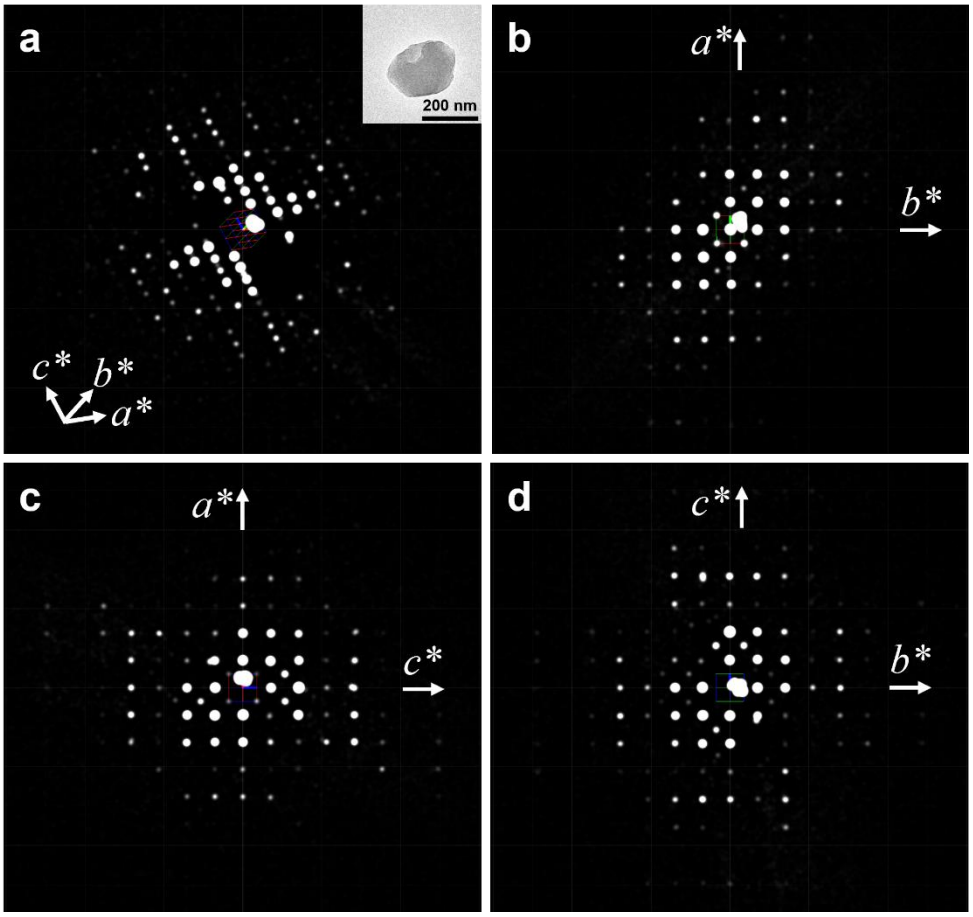


**Supplementary Fig. 19 | Three-dimensional electron diffraction (3D ED) data of catena-COF-805. a**, The reconstructed 3D reciprocal lattice of catena-COF-805 with unit cell parameter of $a$ = 56.8 Å adopting $F$ cubic symmetry. Inset: TEM image of the crystal used to collect data. **b**–**d**, Projection views of the 3D ED data along $c^*$, $b^*$, and $a^*$, respectively.

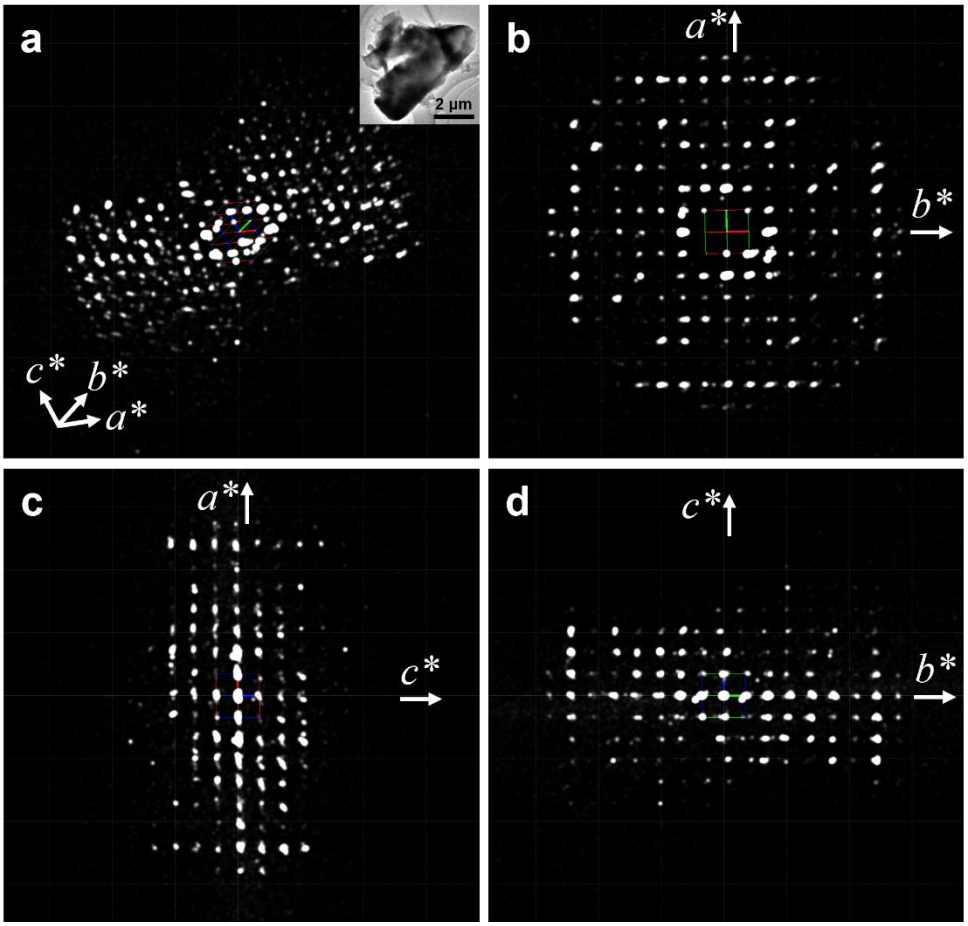


**Supplementary Fig. 20 | 3D ED data of catena-COF-806. a**, The reconstructed 3D reciprocal lattice of catena-COF-806 with unit cell parameter of $a$ = 28.4 Å adopting *P* cubic symmetry. Inset: TEM image of the crystal used to collect data. **b**–**d**, Projection views of the 3D ED data along $c^*$, $b^*$, and $a^*$, respectively.

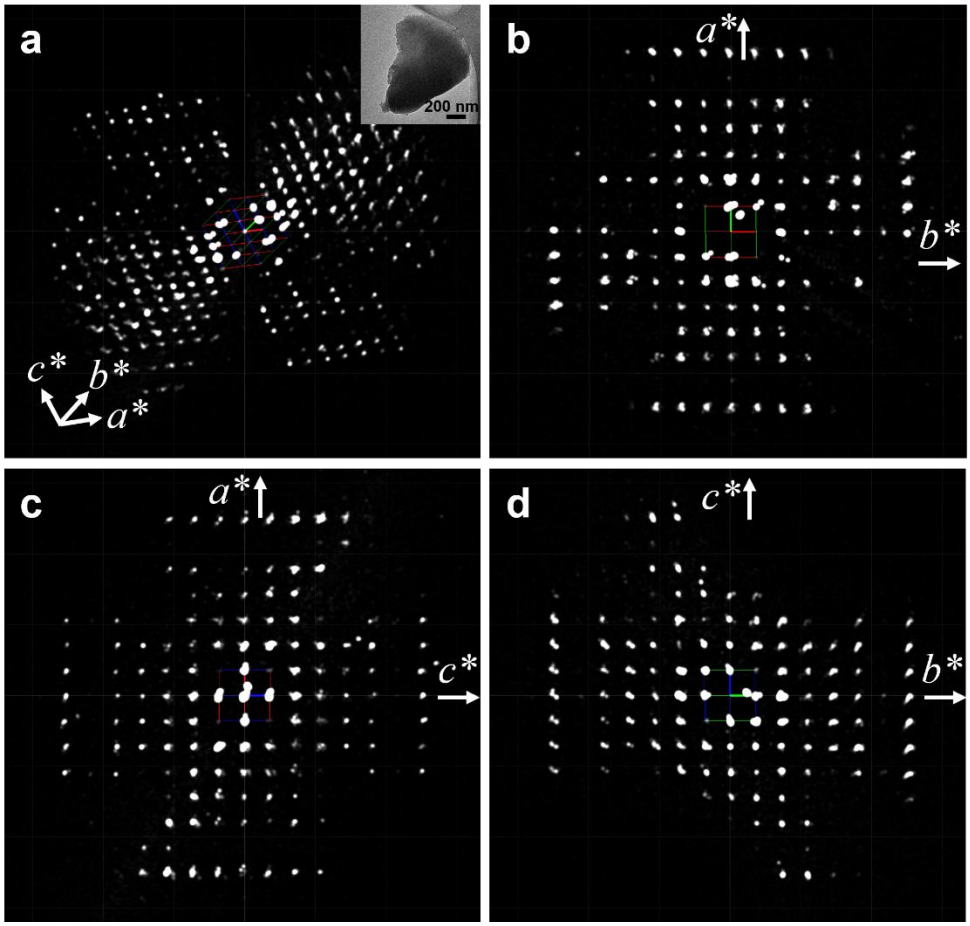


**Supplementary Fig. 21 | 3D ED data of catena-COF-807. a**, The reconstructed 3D reciprocal lattice of catena-COF-807 with unit cell parameter of $a$ = 27.6 Å adopting $P$ cubic symmetry. Inset: TEM image of the crystal used to collect data. **b**–**d**, Projection views of the 3D ED data along $c$*, $b$*, and $a$*, respectively.

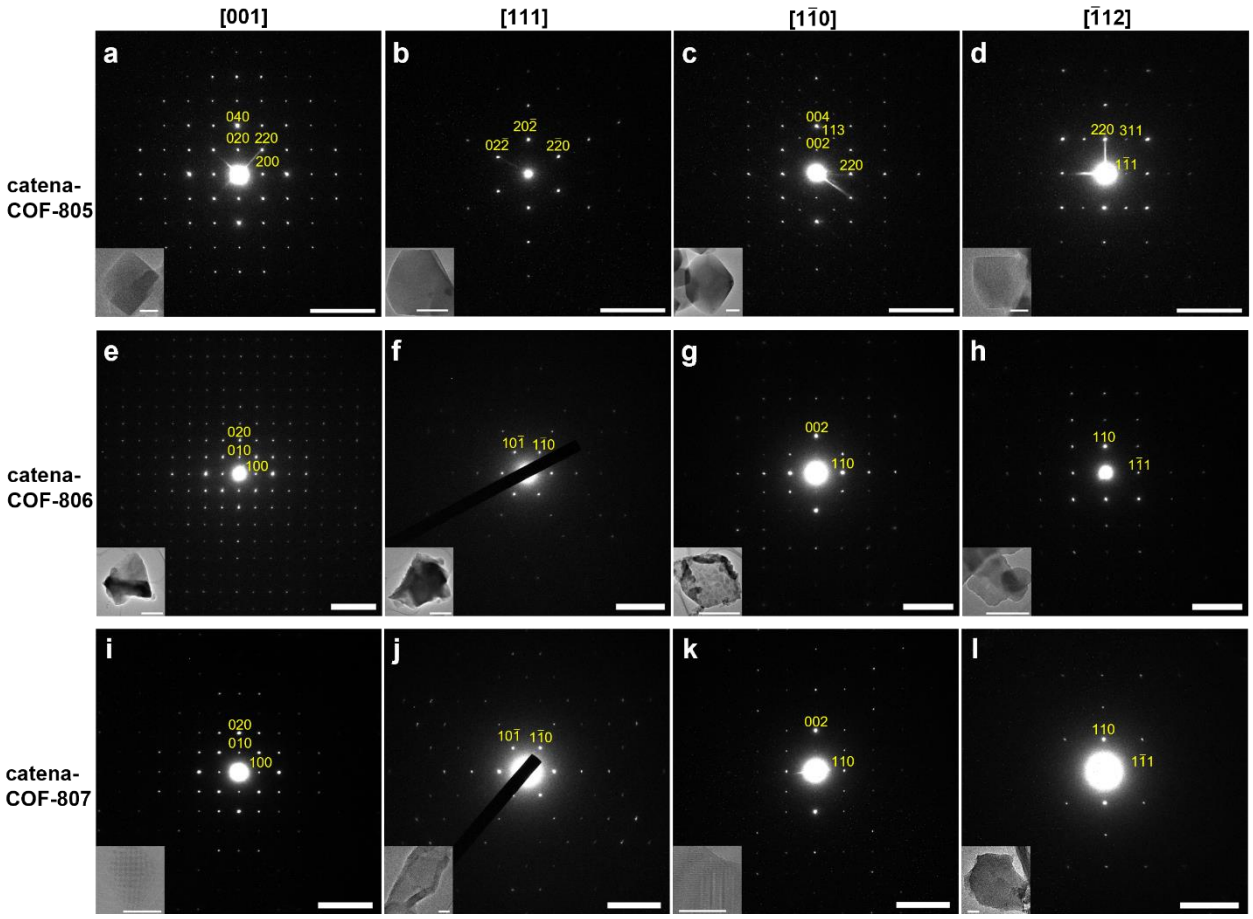


**Supplementary Fig. 22 | Comparison of selected area electron diffraction (SAED) patterns of three catena-COFs along different directions ([001], [111], [1$\bar{1}$0] and [$\bar{1}$12]). a–d**, SAED patterns of catena-COF-805. **e–h**, SAED patterns of catena-COF-806. **i–l**, SAED patterns of catena-COF-807. Scale bar for all the patterns: 1 $nm^{-1}$. Insets: TEM images of crystals which were used to collect corresponding SAED patterns. Scale bar for these TEM images: a–d, 200 nm; e–h, 1 μm; i–l, 100 nm. These patterns and images are the same as the corresponding ones in Fig. 2 for catena-COF-805, Fig. 3 for -806 and Supplementary Fig. 27 for -807. Here they are listed for comparison between different COFs.

Along [1$\bar{1}$0] incidence (c, g, and k), the extra reflections of odd-number indices (e.g., 113, 115, 331 series, etc.) can only be observed for catena-COF-805 but are absent for -806 and -807, which confirmed further that lattice parameter *a* of catena-COF-805 is roughly twice those of -806 and -807. It should be noted that weak abnormal reflections of 002 series are observed in the [001] and [1$\bar{1}$0] patterns of catena-COF-805 (a and c) which were proved to come from multiple scattering (Supplementary Fig. 23). Similarly, the weak abnormal reflections of 001 series in the [001] and [1$\bar{1}$0] patterns of catena-COF-806 (e and g) and -807 (i and k) were also demonstrated to be yielded from the multiple scattering (Supplementary Fig. 24).

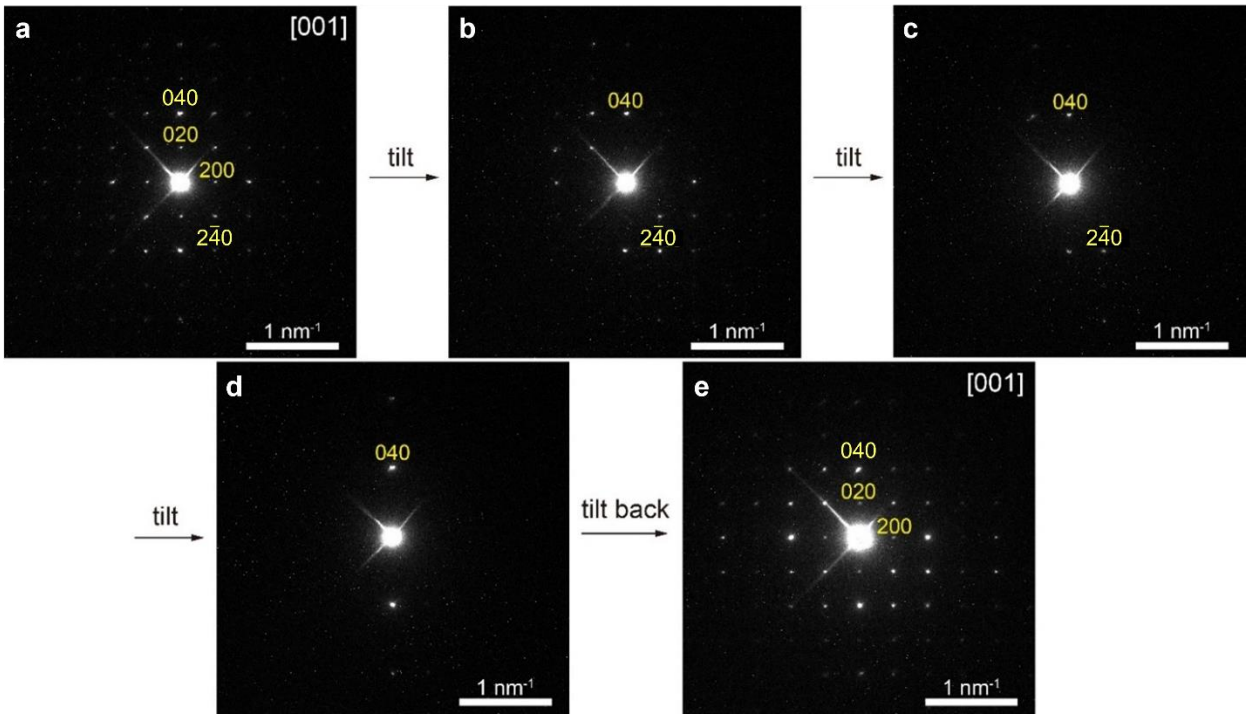


**Supplementary Fig. 23 | The evidence to differential real diffractions and abnormal reflections in SAED pattern of catena-COF-805. a**, The weak reflection of 020 series (200, 0$\bar{2}$0, $\bar{2}$00, etc.) can be observed in the SAED of catena-COF-805 along [001] direction. **b**–**d**, When the crystal was deviated away from its zone axis ([001] direction) with the sample holder tilted step by step, these weak reflections of 020 series disappeared while the reflections of 040 series can be retained. This experiment confirmed that the abnormal reflections of 020 series came from the multiple scattering while 040 series are the real reflections, supporting the reflection condition of 00*l*: *l* = 4n. Besides, these reflections from multiple scattering cannot be observed in 3D ED data. **e**, The sample holder was then tilted back and the reflections of 020 series appeared again after the crystal was back to its zone axis along [001], verifying that the absence of diffraction in B–D was not caused by beam damage but by eliminating the multiple scattering.

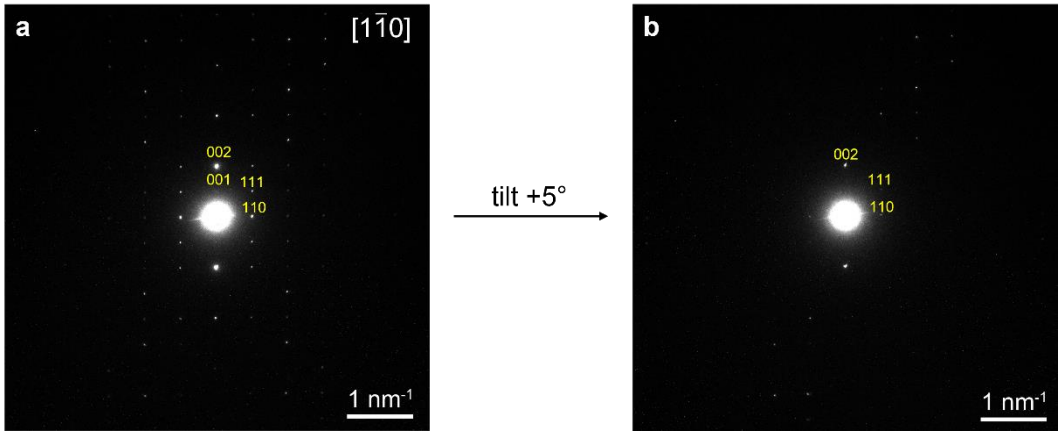


**Supplementary Fig. 24 | The evidence to differential real diffractions and abnormal reflections in SAED pattern of catena-COF-806. a**, Similar to the case observed in SAED pattern of catena-COF-805 along [001] direction, very weak reflections of 001 series can be observed in the SAED pattern of catena-COF-806 along [1$\bar{1}$0]. **b**, These weak reflections can be eliminated through the sample holder tilting as well, proving that they also resulted from multiple scattering. This is in accordance with the fact that these reflections cannot be observed in 3D ED data.

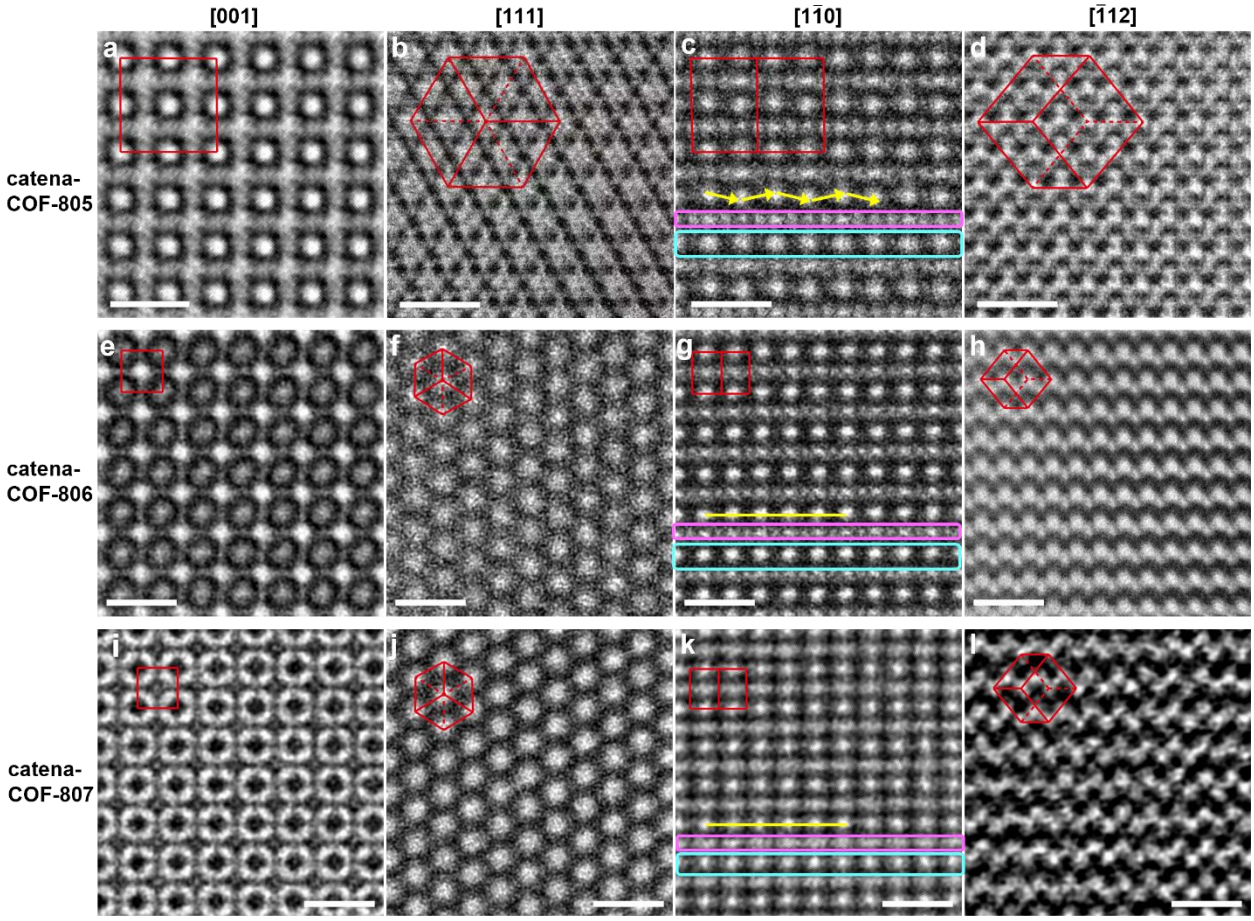


**Supplementary Fig. 25 | Comparison of HRTEM images of three catena-COFs along different directions ([001], [111], [1$\bar{1}$0] and [$\bar{1}$12]). a**–**d**, HRTEM images of catena-COF-805. **e**–**h**, HRTEM images of catena-COF-806. **i**–**l**, HRTEM images of catena-COF-807. Scale bar for all images: 5 nm. These images are the same as the corresponding ones in Fig. 3 for catena-COF-805, Fig. 4 for catena-COF-806 and Supplementary Fig. 27 for catena-COF-807. Here they are listed for comparison between different COFs.

Despite that the similar images can be intuitively observed for different catena-COFs along each direction, it is worth noting that there are still subtle nuances. For example, along [1$\bar{1}$0] direction, different-sized bright spots arrays are arranging alternately row by row (e.g., small bright spots array in pink box and big bright spots array in cyan boxes). However, the big bright spots (in cyan boxes) in image of catena-COF-805 (c) align as zigzag pattern along yellow arrows, while those big bright spots (in cyan boxes) in images of catena-COF-806 (g) and -807 (k) align straightly along yellow lines. These differences can be assigned to as structure variations in Supplementary Fig. 31.

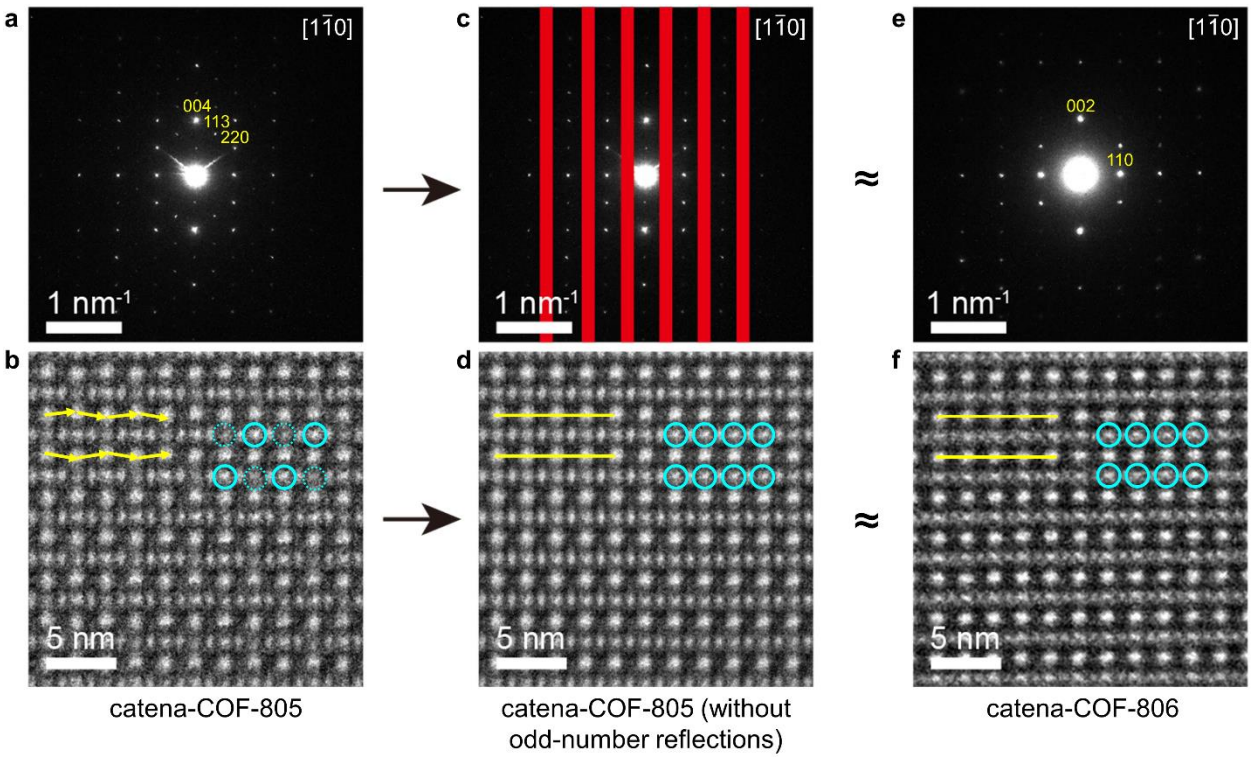


**Supplementary Fig. 26 | Comparison of experimental SAED patterns and HRTEM images with Fourier filter results. a**, **b**, Experimental SAED pattern and HRTEM image of catena-COF-805 along the [1$\bar{1}$0] direction. **c**, The reflections of odd-number indices (e.g., 113, 115, 331 series, etc.) were masked (as shown along red-bars) from the Fourier diffractogram of catena-COF-805 along the [1$\bar{1}$0] direction. **d**, The resulted image of applying inverse Fourier transform to the pattern **c** where the contribution from reflections of odd-number indices were eliminated. **e**, **f**, Experimental SAED pattern and HRTEM image of catena-COF-806 along the [1$\bar{1}$0] direction.

It can be seen that the Fourier diffractogram of catena-COF-805 without odd-number reflections (c) is very similar to the experimental SAED pattern of catena-COF-806. Besides, the image produced by Fourier filter (d) is nearly the same as the HRTEM of catena-COF-806 (f). Specifically, the big bright spots align in zigzag form as shown by yellow arrow in HRTEM of catena-COF-805 (b) as mentioned in Supplementary Fig. 25, however, these bright spots are arranged along a straight line in the Fourier filter image (d) and in the HRTEM of catena-COF-806 (f). Those small bright spots as cyan-circled exhibit different brightness as distinguished by dashed and solid circles in the HRTEM of catena-COF-805 (b), while they have equal brightness in the processed image of catena-COF-805 (d) and HRTEM image of catena-COF-806 (f). All the information revealed that these isoreticular catena-COFs have similar topology but with minor structure differences. These differences in catena-COF-805 should be the reason to produce the reflections of extra odd-number reflections (e.g., 113 series) and *F* lattice. The details of structure difference are discussed in main text and in Supplementary Fig. 31.

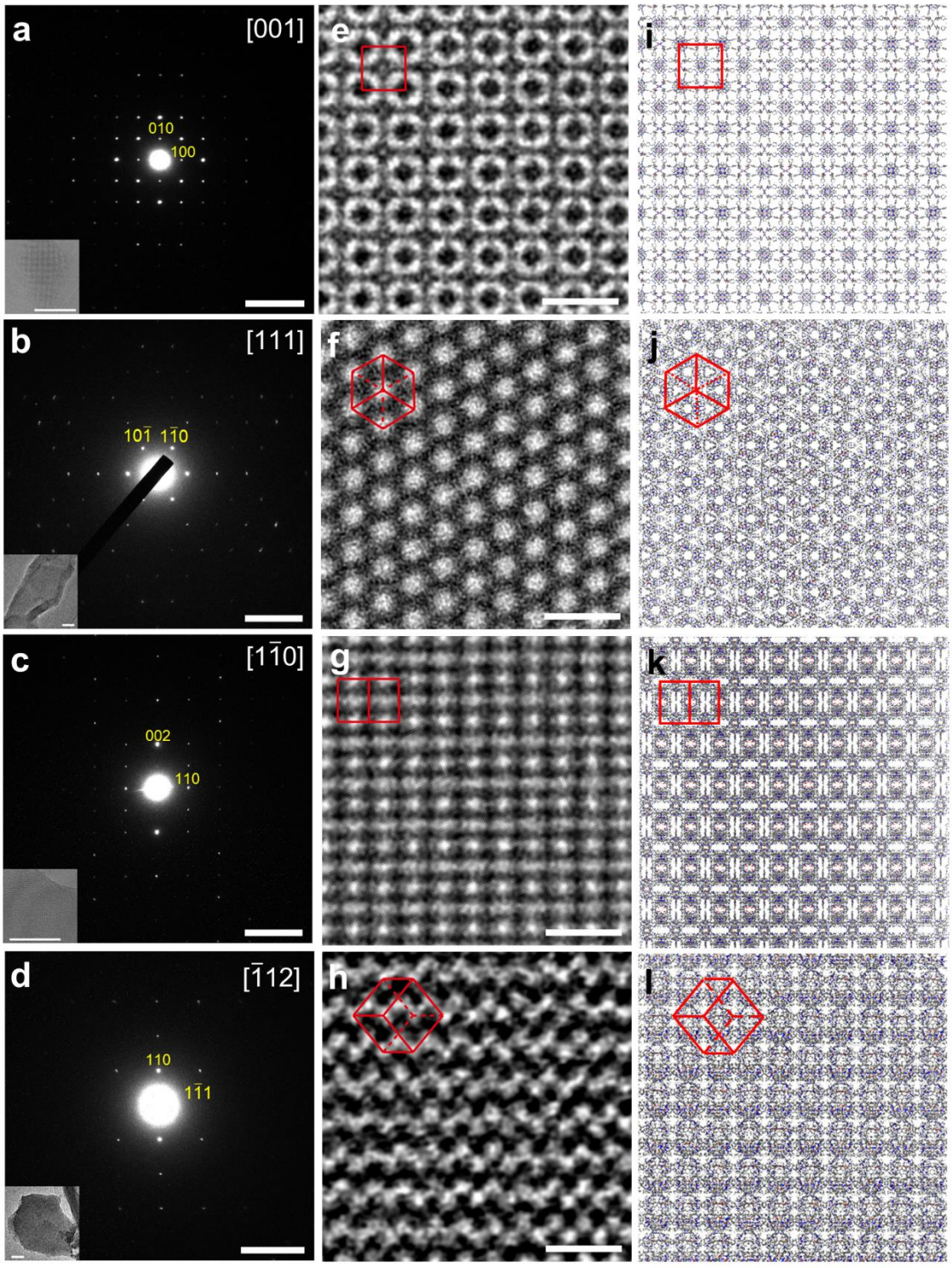


**Supplementary Fig. 27 | TEM data and perspective illustrations of the crystal structure of catena-COF-807. a**–**d**, SAED patterns of catena-COF-807 from the [001], [111], [1$\bar{1}$0], and [$\bar{1}$12] incidences, respectively. Scale bar: 1 $nm^{-1}$. Insets: TEM images of the crystals used to collect data. Scale bar: 100 nm. **e**–**h**, HRTEM images taken along the [001], [111], [1$\bar{1}$0], and [$\bar{1}$12] directions

of catena-COF-807, respectively. Scale bar: 5 nm. **i**–**l**, The projections of the crystal structure of catena-COF-807 with a doubly interpenetrated **bor-y** topology along the [001], [111], [$1\bar{1}0$], and [$\bar{1}12$] directions, respectively. Atom color: C, gray; N, blue; Cu, pink. H atoms and $BF_4^-$ anions were omitted for clarity.

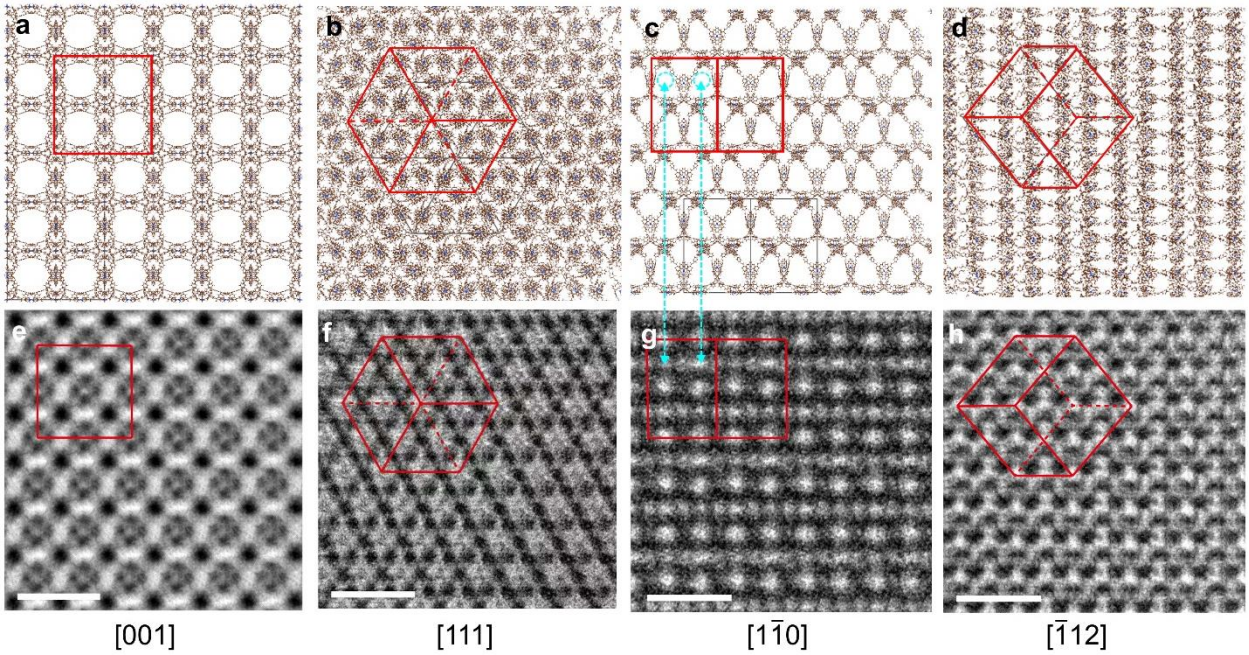


**Supplementary Fig. 28 | The projections of non-interpenetrated bor-y structure model of catena-COF-805 (a–d) comparing with the experimental HRTEM images (e–h) along [001], [111], [1$\bar{1}$0], and [$\bar{1}$12] directions, respectively.** Scale bar: 5 nm. Atom color: C, brown; N, light blue; O, red; Cu, blue. H, light pink. $BF_4$ anions were omitted for clarity. It shows large differences between the projections of structure model and experimental images, especially along [1$\bar{1}$0] direction (highlighted by cyan arrows and dashed circles in C and G). These results suggested that catena-COF-805 should not have non-interpenetrated **bor-y** structure. The further analysis confirmed that catena-COF-805 possesses a doubly interpenetrated **bor-y** structure (**bor-y-c***), see in main text and Supplementary Fig. 31.

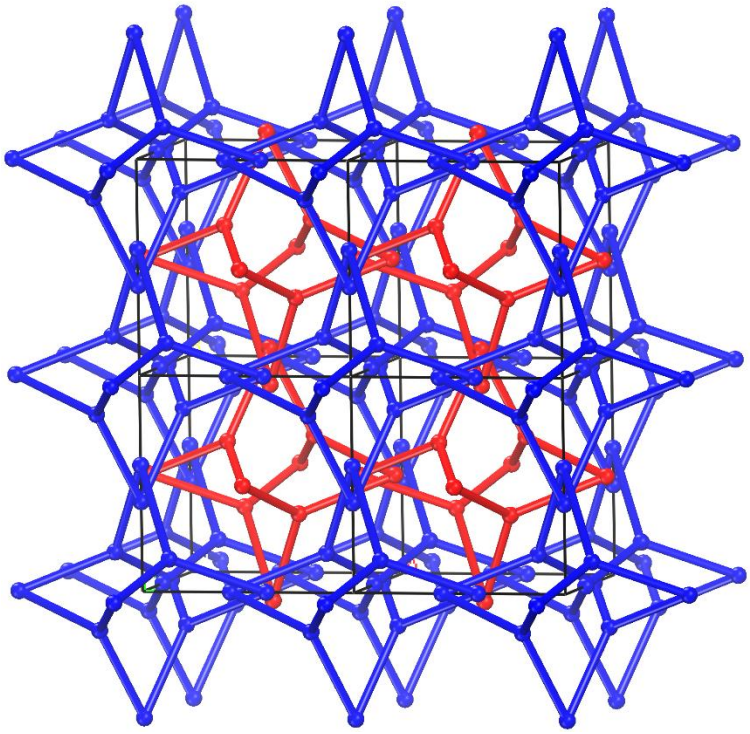

**Supplementary Fig. 29 | Topology of doubly interpenetrated bor-y (bor-y-c*). bor-y-c*** has the same pattern of interpenetration observed for **bor-c*** but underlying. In **bor-y-c*** net, two subnets of **bor-y** are related by inversion.

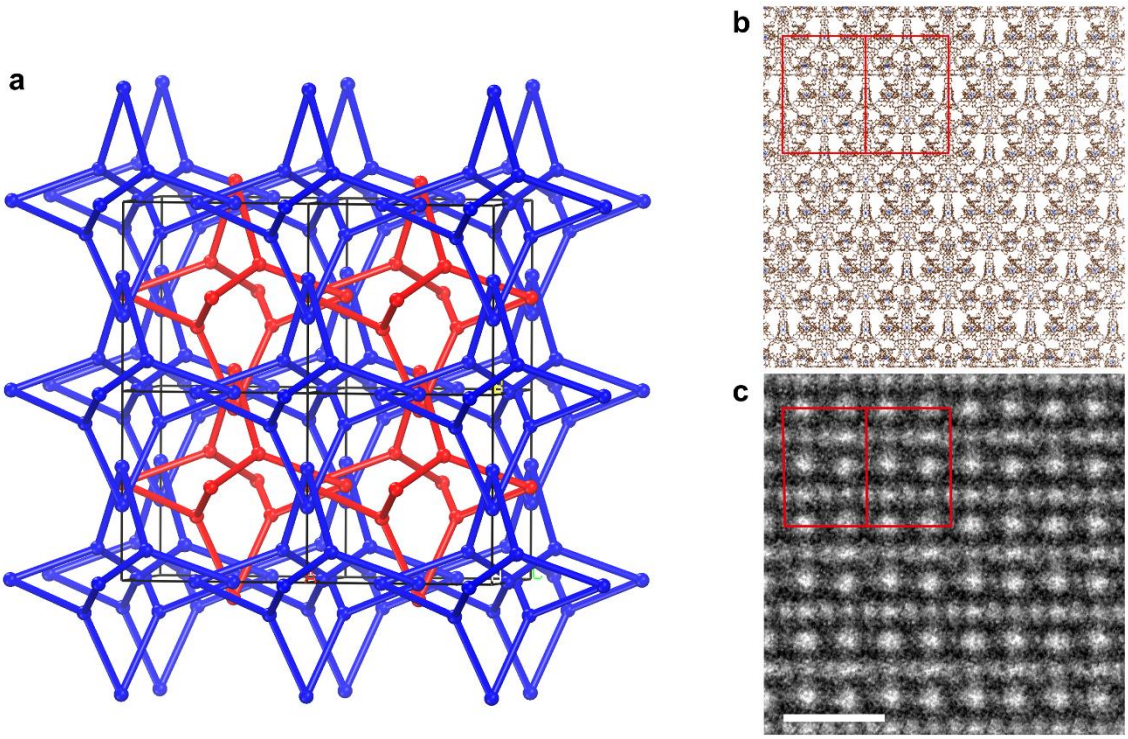


**Supplementary Fig. 30 | Topology of bor-y-c (a), projection of bor-y-c model for catena-COF-805 along [1$\bar{1}$0] (b) and experimental HRTEM image along [1$\bar{1}$0] (c).** Different from **bor-y-c***, **bor-y-c** is composed of two interpenetrated **bor-y** subnets which are related by translation (a). The **bor-y-c** model for catena-COF-805 was built (b) but it was found to mismatch with the HRTEM results especially along [1$\bar{1}$0] direction (c).

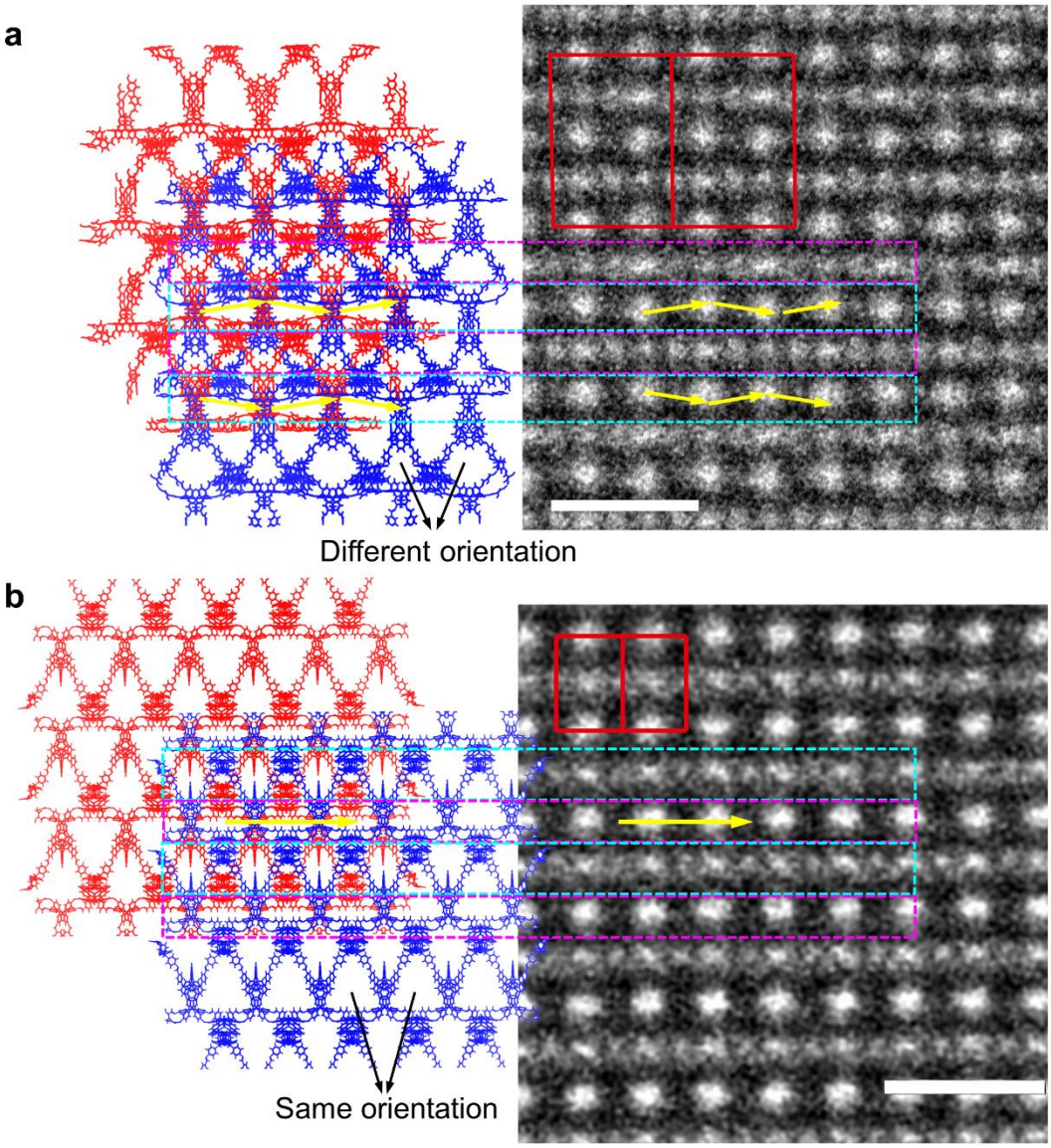


**Supplementary Fig. 31 | Representation of 2-fold interpenetrated bor-y subnets (red and blue) in catena-COF-805 (a) and in catena-COF-806 (b) viewed from [1$\bar{1}$0] direction comparing with their respective HRTEM images taken along [1$\bar{1}$0] direction.** Scale bar in HRTEM images: 5 nm. It can be seen that the interpenetrated parts (the overlaid red and blue subnets) in structures matched exactly with the HRTEM images while the non-interpenetrated parts (the individual red or blue network without overlay) cannot match both in catena-COF-805 and -806. Besides, the different alignments of bright spots (zigzag *vs.* straight, i.e., yellow arrows *vs.* straight arrow) observed in two HRTEM images of the respective catena-COFs were caused by the structural differences of the orientation of the interlocking polyhedra (twisted in catena-COF-805 and identical in -806). These structure models were further validated by PXRD refinement (Section 9).

## Section 9. PXRD Refinement, Simulation, Structure Details and Framework Flexibility

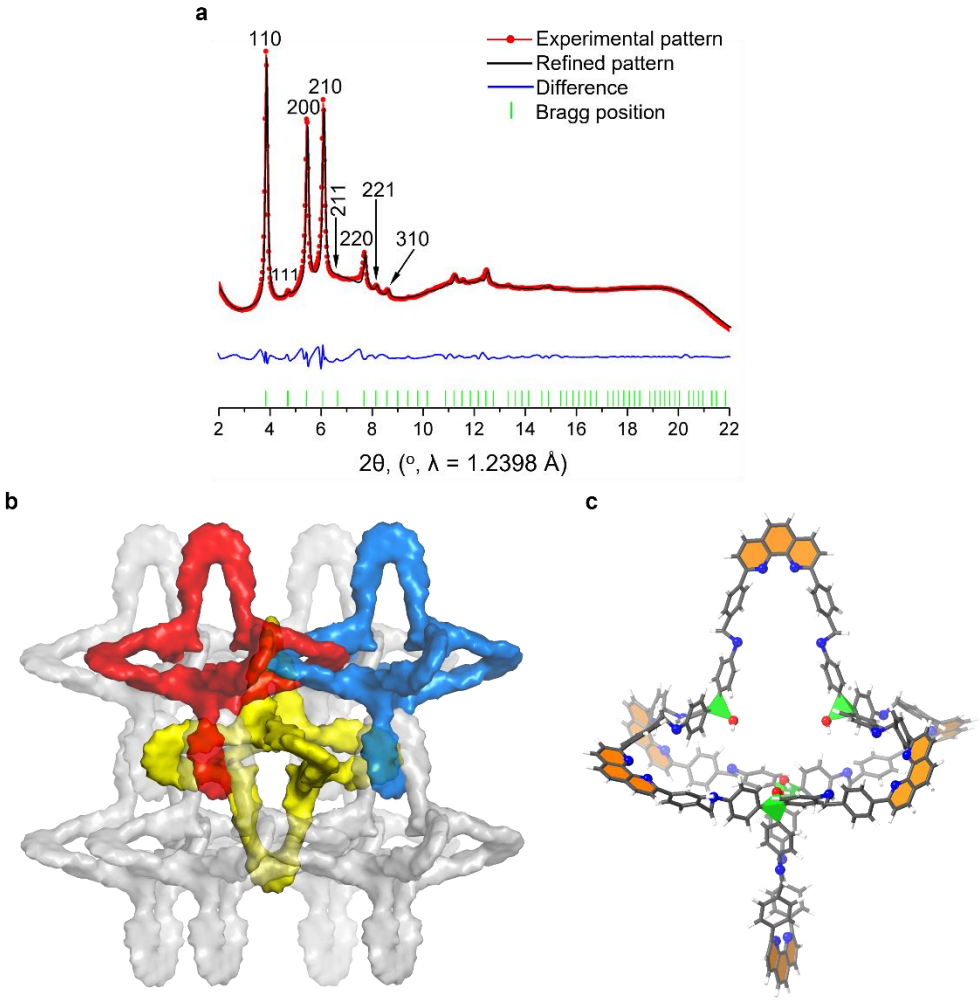


**Supplementary Fig. 32 | Pawley refinement (a), doubly interpenetrated bor-y structure (b), and constituent polyhedron (c) of catena-COF-807.** Experimental pattern, red; refined pattern, black; difference pattern, blue; and observed positions of Bragg reflections, green. The refined unit cell parameter of catena-COF-807 is $a$ = 26.1153(9) Å in space group of $P4_23_2$ with $R$p = 0.45% and $wR$p = 1.27%. The structure model was then finalized by geometry optimization, and the simulated PXRD pattern from the structure model was found to be in good agreement with the experimentally obtained data (Supplementary Fig. 35). Similar to catena-COF-806, the interlocking polyhedra within one subnet of catena-COF-807, which are represented by red, blue and grey, all display the same orientation. The second subnet is represented by one yellow polyhedron to facilitate differentiating. Similar to the constituent polyhedron in catena-COF-806 (Fig. 5f), the phenanthroline units (highlighted in orange) on opposite sides of the polyhedron units of catena-COF-807 are oriented approximately orthogonal to each other, with the C atom in center of TAPMol adopting a tetrahedral geometry (shown as green tetrahedra). C atoms, gray; N atoms, blue; O atoms, red; H atoms, white.

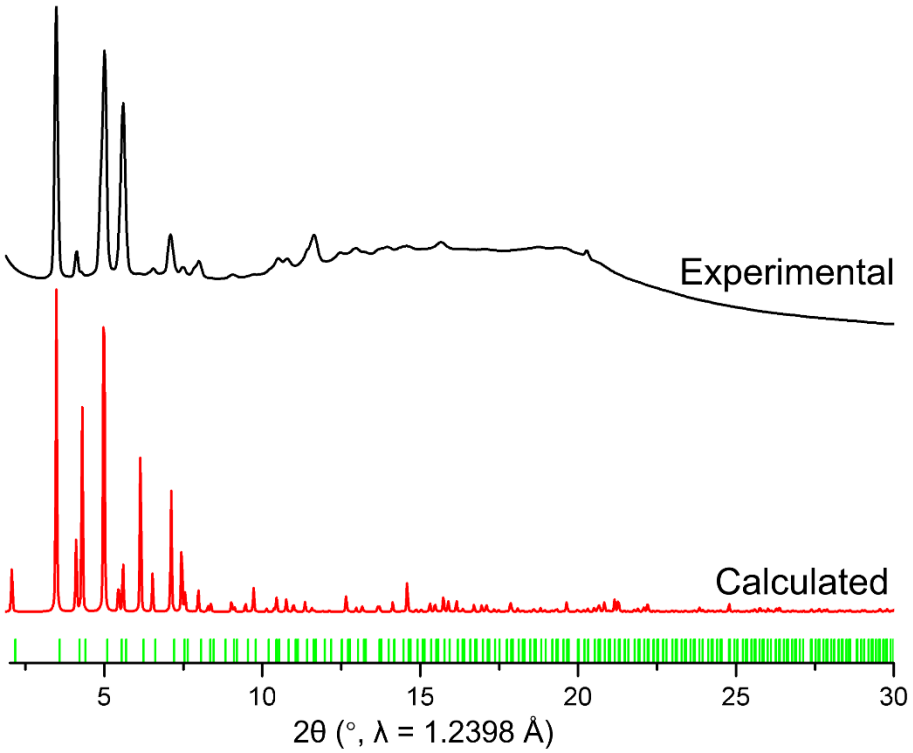


**Supplementary Fig. 33 | Comparison of calculated PXRD pattern (red) with the experimental pattern (black) of catena-COF-805.** The observed positions of Bragg reflections are shown in green vertical bars. The calculated and experimental patterns match well to demonstrate the rationality of the structure model, except several reflections exhibiting different relative intensity (e.g., reflections at ~4.4°, ~6.2°, etc.). The discrepancy can be ascribed to the influences from the disordered $BF_4^-$ anions and residual guest molecules such as water which cannot be fully removed from the sample. The influence of disordered counter ions to the relative intensity of PXRD can also be observed for zeolites[9]. EA results supported the existence of water molecules in the sample (Section 2). The influence of guest molecules can further be verified by the study of framework flexibility, where different PXRD intensities can be observed for the activated and solvated COF samples (Supplementary Fig. 36).

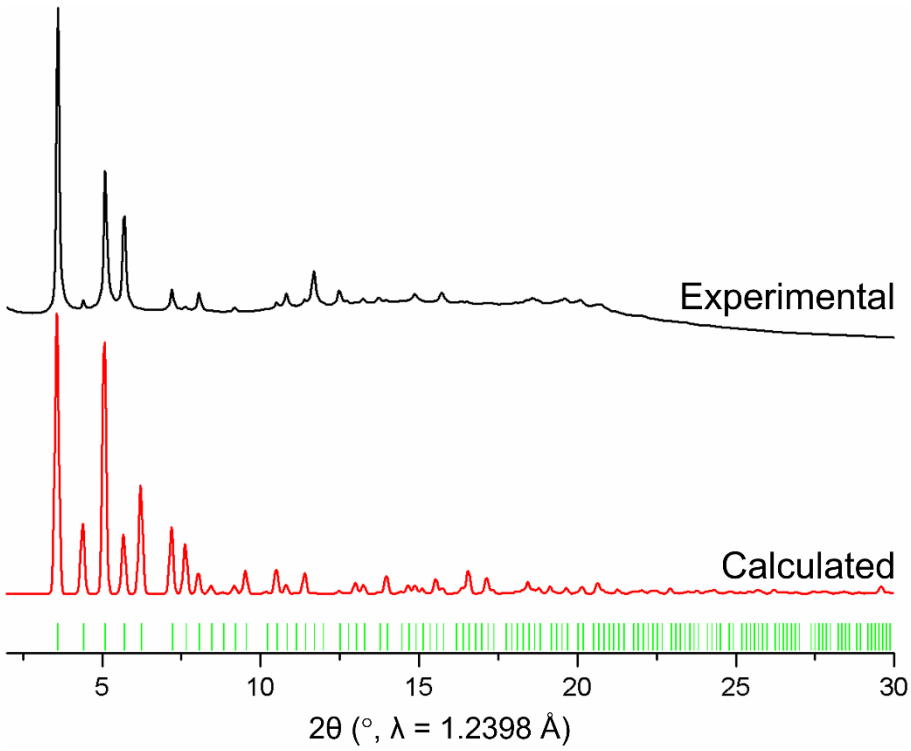


**Supplementary Fig. 34 | Comparison of calculated PXRD pattern (red) with the experimental pattern (black) of catena-COF-806.** The observed positions of Bragg reflections are shown in green vertical bars. The calculated and experimental patterns match well to demonstrate the rationality of the structure model, except several reflections exhibiting different relative intensity (e.g., reflections at ~4.4°, ~6.2° etc.). These differences can be ascribed to the same influences of disorders as observed for catena-COF-805.

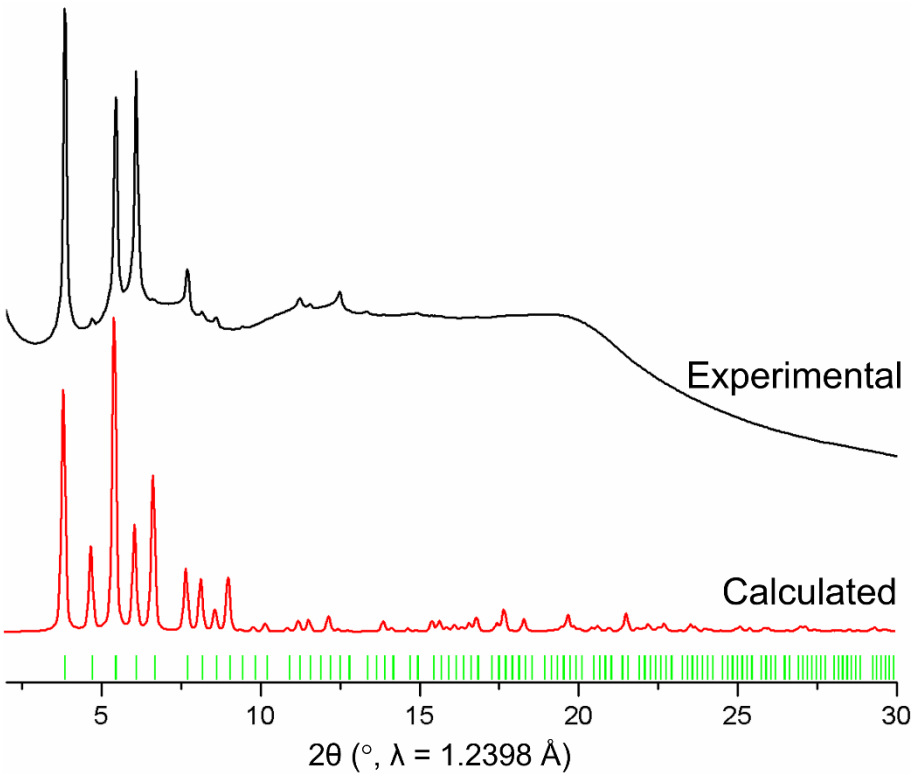


**Supplementary Fig. 35 | Comparison of calculated PXRD pattern (red) with the experimental pattern (black) of catena-COF-807.** The observed positions of Bragg reflections are shown in green vertical bars. The calculated and experimental patterns match well to demonstrate the rationality of the structure model, except several reflections exhibiting different relative intensity (reflections at ~4.4°, ~6.2° etc.). These differences can be ascribed to the same influences of disorders as observed for catena-COF-805 and -806.

Structure Details

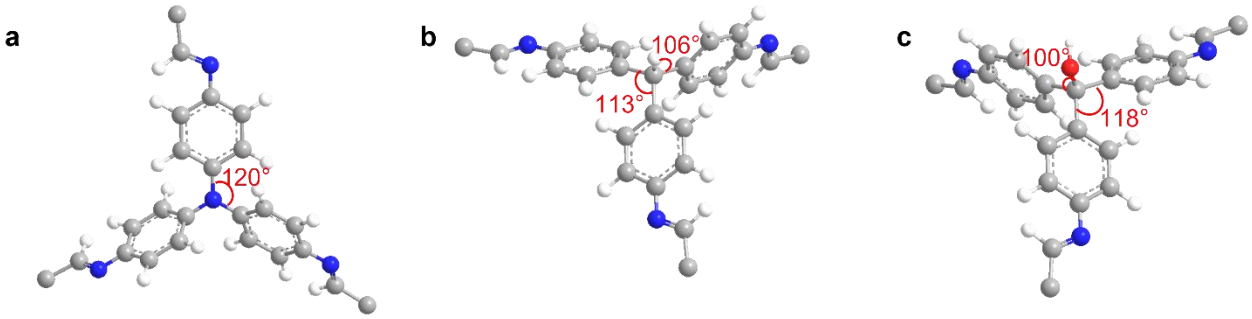


**Supplementary Fig. 36 | The local structures of three catena-COFs and angular details as labeled. a**, The three (Ph)C–N–C(Ph) angles of the tritopic center in catena-COF-805 were all measured as ~120°. **b**, The (Ph)C–C(H)–C(Ph) angles in catena-COF-806 is 113° and (Ph)C–C–H angle is 106°. **c**, Similar to catena-COF-806, those angles in catena-COF-807 have been measured and the (Ph)C–C(OH)–C(Ph) angle was found to be 118°, and the (Ph)C–C–O angle to be 100°.

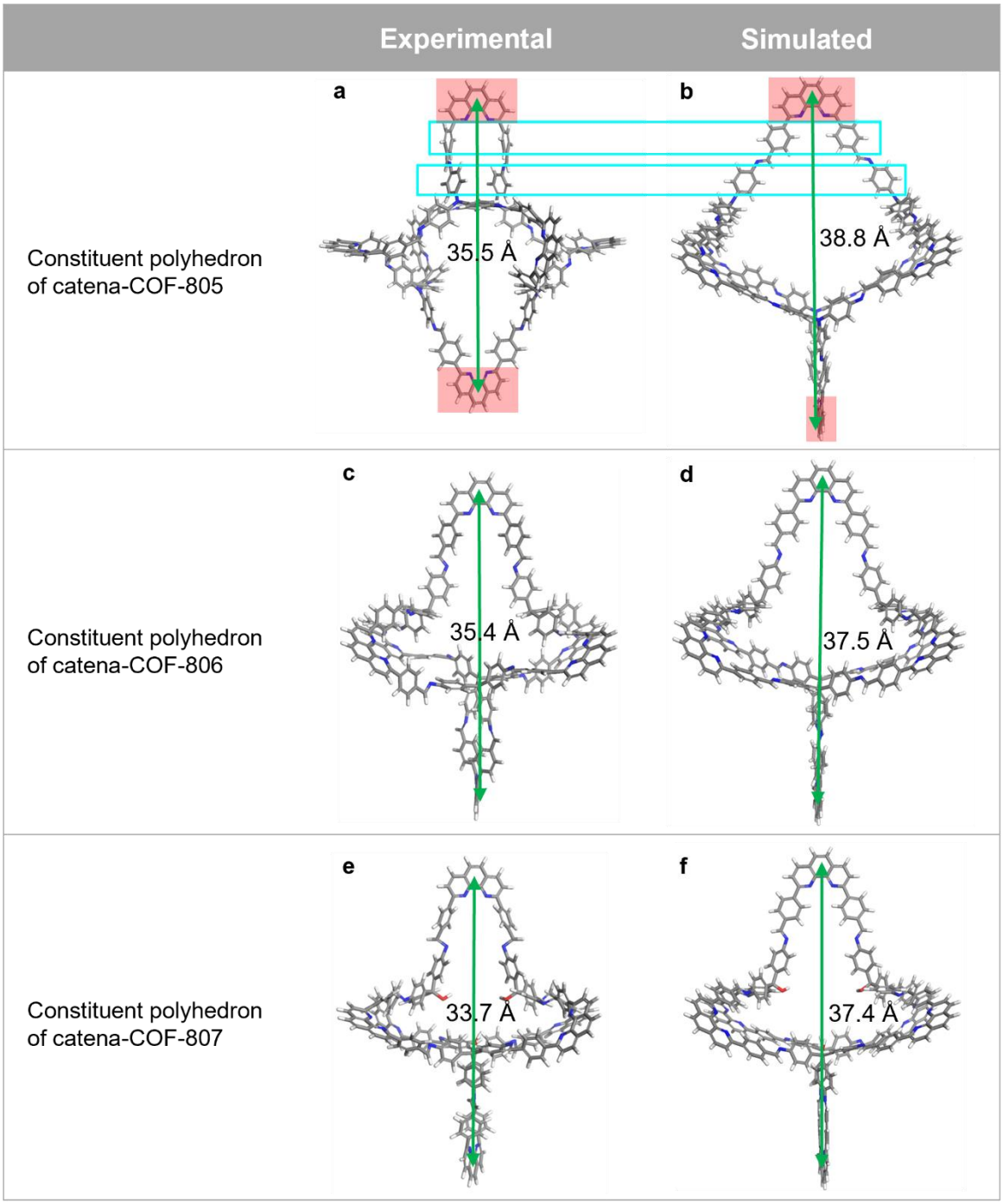


**Supplementary Fig. 37 | The experimentally observed constituent polyhedra of the three catena-COFs (left) compared to the geometry optimized individual polyhedra (right).**

To better understand the constituent polyhedral structures of three catena-COFs and the influence of central atoms (N, CH or COH) in tritopic linkers on the conformers, geometry optimization was carried out for a single polyhedron of each catena-COF to simulate its lowest-energy conformation (*i.e.*, the idealized structure). The calculation was conducted with Forcite Module by using force field of universal in Materials Studio and the results were compared to the

experimental structure models of the polyhedra in the catena-COF crystal structures. As reported in main text, the N atoms at the center of TAPA display a trigonal planar orientation of its aniline substituents (Fig. 5e). In contrast, these substituents are arranged in a trigonal pyramidal orientation in TAPM and TAPMol due to the tetrahedral geometry of their central C atoms. In detail, the three C–N–C angles of the tritopic center in catena-COF-805 were all measured as 120° (Supplementary Fig. 36a and 37a), which is exactly the same as they were calculated in the idealized structure (Supplementary Fig. 37b). The (Ph)C–C(H)–C(Ph) angles in TAPM center of catena-COF-806 is 112.6° and (Ph)C–C–H angle is 106.1° according to the experimental structure model (Supplementary Fig. 36b and 37c), which close to they are in the idealized structure model (113.5° and 105.1°, respectively, Supplementary Fig. 37d). Similar to catena-COF-806, those angles in center of TAPMol of catena-COF-807 have been measured and the (Ph)C–C(OH)–C(Ph) angle was found to be 117.5°, and the (Ph)C–C–O angle to be 100.4° in the experimental structure model (Supplementary Fig. 36c and 37e), corresponding to the 113.4° and 110.1°, respectively, in its idealized structure model (Supplementary Fig. 37f). The experiment models of catena-COF-805 and -806 polyhedra are in good agreement with the idealized structure models regarding geometry of tritopic center. The difference between experimental and idealized models of catena-COF-807 might be caused by the guest molecules which have interactions with -OH in the TAPMol center, resulting in a small distortion of experimental structure. Without considering the influence of guest molecules, the experiment models of catena-COFs basically matched with the idealized models, implying that the difference between tritopic centers of 805 and 806/807 is the key factor for forming three isoreticular structures.

Additionally, the other conformational differences were observed between the experimental and idealized structure models: **1) The orientation of phenanthroline units.** As we discussed in main text, in the experimental structures, the phenanthroline parts on opposite sides of the constituent polyhedron of catena-COF-805 oriented approximately parallel to each other, while they oriented approximately orthogonal in catena-COF-806/807. However, in the simulated structures, they oriented approximately orthogonal in all three polyhedra. Constituent polyhedra of -806 and -807 are in good agreement with the idealized structure models (orthogonal phenanthroline units) but the structure of the -805 differs from the idealized model. **2) The orientation of benzene rings connected to the phenanthroline unit.** In the three simulated polyhedra, the benzene rings connected to the phenanthroline units align in parallel to the plane of the phenanthroline core. In contrast, torsion angles are observed in all experimental structures. **3) The torsion angles of imine bonds.** In the geometry optimized structures, the angles approach 180°. However, they are 173°, 156° and 164° in the experimental structures of catena-COF-805, -806, -807, respectively. **4) The benzene rings in the triangular linkers.** To accommodate the torsion angles of imine bonds, the benzene rings in the triangular linkers lie in the same plane as the PDB linker in the simulated polyhedra; however, they were distorted in the experimental structures. 5) All these variations mentioned above resulted in **different polyhedron sizes** between experimental and simulated models. The maximum dimensions of the polyhedra in experimental models of catena-COF-805,

-806 and -807 reached ~35.5 Å, ~35.4 Å and ~33.7 Å, respectively, while the simulated sizes are ~38.8 Å, ~37.5 Å and ~37.4 Å, respectively.

At the same time, we tried to synthesize monomeric organic molecular cages by linking 4,4'-(1,10-phenanthroline-2,9-diyl)dibenzaldehyde) (PDB) with tritopic tris-(4-aminophenyl)amine (TAPA), tris-(4-aminophenyl)methane (TAPM), and tris-(4-aminophenyl)methanol (TAPMol). While we have not been able to isolate the monomeric [6+4] cages with the same geometry of constituent polyhedra in catena-COFs, we surprisingly obtained some other variants such as molecular rings and 3-stranded [3+3] cages.

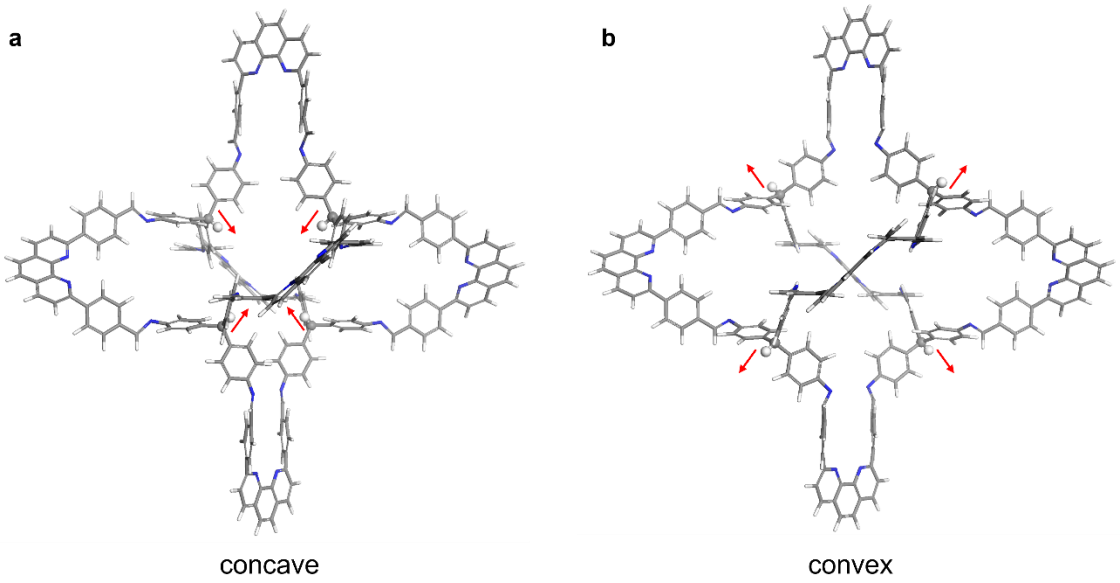


**Supplementary Fig. 38 | Possible polyhedra conformers of catena-COF-806. a,** the concave conformer where C-H bonds orient towards the inside of the polyhedra. **b,** the convex conformer where C-H bonds orient towards the outside of the polyhedra. Based on the results of Rietveld refinement (Supplementary Fig. 39 and 40) and geometry optimization (Supplementary Table 1), all polyhedra in catena-COF-806 were found to be concave.

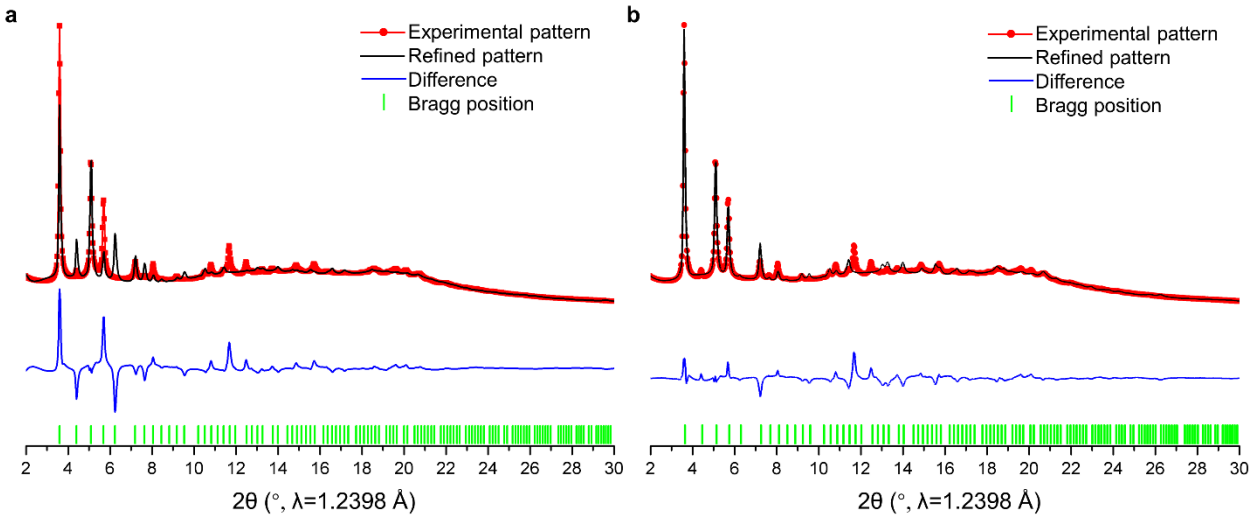


**Supplementary Fig. 39 | Rietveld refinement of catena-COF-806 (a) without refining the preferred orientation and (b) with refining the preferred orientation.** Experimental patterns, red; refined patterns, black; difference patterns, blue; observed positions of Bragg reflections, green.

The refinement was accomplished by using the Reflex module in Materials Studio. A Pearson VII function with asymmetry correction and a 20-polynomial order background were employed for profile refinement. Constraints were used during the structural refinement by creating rigid bodies in the $Cu(PDB)_2$, TAPM, and $BF_4^-$ moieties, and finally a Rietveld-Toraya preferred orientation factor was introduced, reaching the final residual values of *R*p = 2.58%, *wR*p = 4.34%. In contrast, the refinement without refining the preferred orientation resulted larger residual values of *R*p = 3.94%, *wR*p = 8.23%. It is reasonable to use a preferred orientation factor since catena-COF-806 has somewhat larger crystal size (~5 μm) and particle aggregation (Supplementary Fig. 18). For comparison, a hypothetical all-convex structure of catena-COF-806 was also refined with resulting higher *R* values (Supplementary Fig. 40).

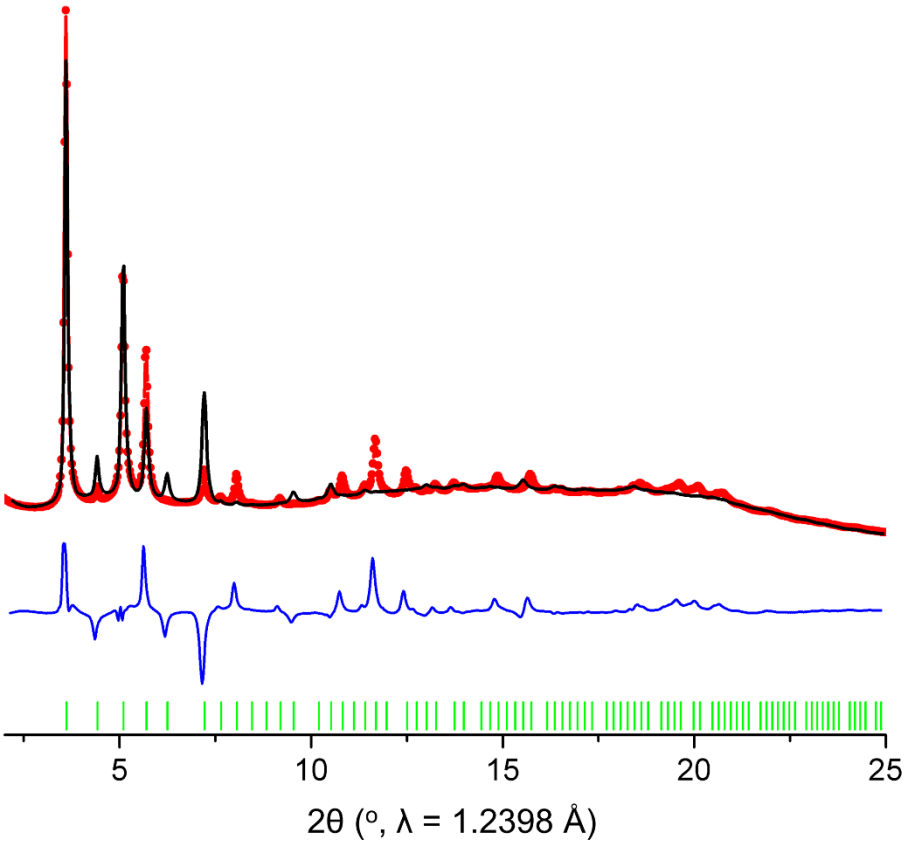


**Supplementary Fig. 40 | Rietveld refinement for a hypothetical all-convex conformer of catena-COF-806.** Experimental pattern, red; refined pattern, black; difference pattern, blue; observed positions of Bragg reflections, green. With using the same constraints and a Rietveld-Toraya preferred orientation factor, the resulted *R* values of *R*p = 3.4%, *wR*p = 6.78% were higher than those for the all-concave conformer (*R*p =2.58%, *wR*p =4.34%, Supplementary Fig. 39). The all-concave conformer structure was further supported by geometry optimization (Supplementary Table 1).

**Supplementary Table 1 | Calculated energies of the all-concave and all-convex conformers of catena-COF-806.**

| Item | *all-convex* conformer | *all-concave* conformer |
|---|---|---|
| Total energy (kcal/mol) | 3866.0 | 6068.2 |
| Valence energy(diag. terms) (kcal/mol) | 3000.4 | 2140.7 |
| Bond (kcal/mol) | 1765.0 | 425.2 |
| Angle (kcal/mol) | 691.8 | 890.5 |
| Torsion (kcal/mol) | 535.4 | 801.5 |
| Inversion (kcal/mol) | 8.1 | 23.6 |
| Non-bond energy (kcal/mol) | 865.6 | 3927.5 |
| van der Waals (kcal/mol) | 872.9 | 3934.7 |
| Long range correction (kcal/mol) | 7.4 | -7.2 |
| Electrostatic (kcal/mol) | 0.0 | 0.0 |

Geometry optimization was conducted for two catena-COF-806 conformers (all-convex and all-convex) with Forcite Module by using universal force field in Materials Studio. The results show that all-concave conformer possesses a lower energy of 3866.0 kcal/mol while the all-convex one possesses a higher energy of 6068.2 kcal/mol (Supplementary Table 1), which means that all-concave structure is energy-preferential structure. This is also accordance with the Rietveld refinement results (Supplementary Figs. 39 and 40).

**Supplementary Table 2 | Fractional atomic coordinates for catena-COF-805.**

| Catena-COF-805 | | | |
|---|---|---|---|
| Space group $F4_132$, $a$ = 54.8588 Å | | | |
| Atom | *x* | *y* | *z* |
| C | 0.73376 | 0.83155 | 0.93417 |
| C | 0.51991 | 0.76573 | 1.0522 |
| C | 0.51329 | 0.78892 | 1.06039 |
| C | 0.49432 | 0.79157 | 1.07727 |
| C | 0.48388 | 0.7707 | 1.08781 |
| C | 0.49101 | 0.74754 | 1.08009 |
| C | 0.50811 | 0.74496 | 1.06123 |
| C | 0.98931 | 0.72131 | 0.45124 |
| C | 0.98681 | 0.69953 | 0.43795 |
| C | 0.98889 | 0.67703 | 0.44991 |
| C | 0.9966 | 0.69835 | 0.48755 |
| C | 0.9941 | 0.67623 | 0.47492 |
| C | 0.99722 | 0.65413 | 0.4875 |
| C | 0.58384 | 0.73821 | 0.74482 |
| C | 0.56169 | 0.72623 | 0.73979 |
| C | 0.5398 | 0.73815 | 0.7451 |
| C | 0.56042 | 0.70265 | 0.72974 |
| C | 0.53759 | 0.69138 | 0.72612 |
| C | 0.51616 | 0.70404 | 0.73226 |
| C | 0.49231 | 0.80463 | 0.76235 |
| C | 0.48289 | 0.80452 | 0.73869 |
| C | 0.67951 | 0.74933 | 0.41901 |
| C | 0.43945 | 0.79133 | 0.51557 |
| C | 0.43365 | 0.80689 | 0.49606 |
| C | 0.43204 | 0.79713 | 0.47244 |
| C | 0.43795 | 0.7726 | 0.46826 |
| N | 0.99308 | 0.71991 | 0.47572 |
| N | 0.51815 | 0.72692 | 0.74103 |
| N | 0.163 | 0.43239 | 0.78918 |
| C | 0.15694 | 0.36788 | 0.83153 |
| C | 0.15362 | 0.36665 | 0.80617 |
| C | 0.15561 | 0.38766 | 0.79186 |
| C | 0.16085 | 0.41024 | 0.80285 |
| C | 0.16397 | 0.41145 | 0.82811 |
| C | 0.16233 | 0.39045 | 0.8423 |
| C | 0.41013 | 0.44556 | 0.06314 |
| C | 0.38844 | 0.43229 | 0.0602 |
| C | 0.36603 | 0.44413 | 0.06023 |
| C | 0.36467 | 0.4694 | 0.06297 |
| C | 0.38629 | 0.48302 | 0.06514 |
| C | 0.4089 | 0.47108 | 0.06533 |

| | | | |
|---|---|---|---|
| N | 0.3408 | 0.52015 | -0.06429 |
| H | 0.74571 | 0.83007 | 0.91723 |
| H | 0.53501 | 0.76362 | 1.03808 |
| H | 0.52333 | 0.80569 | 1.05334 |
| H | 0.46954 | 0.77265 | 1.10271 |
| H | 0.48295 | 0.73064 | 1.0891 |
| H | 0.98312 | 0.7002 | 0.41751 |
| H | 0.98633 | 0.65935 | 0.43929 |
| H | 0.99526 | 0.63607 | 0.47741 |
| H | 0.60191 | 0.72889 | 0.74052 |
| H | 0.57786 | 0.69263 | 0.72452 |
| H | 0.53662 | 0.67216 | 0.71828 |
| H | 0.4951 | 0.79944 | 0.72266 |
| H | 0.43922 | 0.79856 | 0.53505 |
| H | 0.42593 | 0.80915 | 0.45663 |
| H | 0.43674 | 0.76474 | 0.44906 |
| H | 0.14928 | 0.34845 | 0.79712 |
| H | 0.15299 | 0.38648 | 0.77128 |
| H | 0.16788 | 0.4297 | 0.83723 |
| H | 0.16537 | 0.39153 | 0.86283 |
| H | 0.38912 | 0.41166 | 0.05777 |
| H | 0.34865 | 0.43296 | 0.05799 |
| H | 0.38541 | 0.50372 | 0.06673 |
| H | 0.42643 | 0.48206 | 0.06726 |
| H | 0.42086 | 0.8427 | 0.4845 |
| O | 1.02046 | 1.16708 | 0.64909 |
| N | 0.5975 | 0.5975 | 0.5975 |
| N | 0.56716 | 0.56716 | 0.06716 |
| F | 0.38826 | 0.74357 | 0.51676 |
| F | 0.35894 | 0.72443 | 0.49367 |
| B | 0.375 | 0.74461 | 0.49461 |
| Cu | 0.75597 | 0.5 | 0.5 |

**Supplementary Table 3 | Fractional atomic coordinates for catena-COF-806.**

| Catena-COF-806 | | | |
|---|---|---|---|
| Space group $P4_232$, $a$ = 27.8544 Å | | | |
| Atom | *x* | *y* | *z* |
| C | 0.98183 | -1.67901 | 0.0174 |
| C | 0.96366 | -1.63557 | 0.0351 |
| C | 0.98181 | -1.59202 | 0.01747 |
| C | 0.92829 | -1.6341 | 0.07064 |
| C | 0.91392 | -1.58994 | 0.08964 |
| C | 0.93421 | -1.54737 | 0.07203 |
| N | 0.96537 | -1.54949 | 0.03488 |
| C | 1.07142 | -1.50313 | -0.09915 |
| C | 1.07316 | -1.46071 | -0.07281 |
| C | 1.07094 | -1.4168 | -0.09635 |
| C | 1.0675 | -1.41507 | -0.14663 |
| C | 1.06956 | -1.4577 | -0.17287 |
| C | 1.0716 | -1.50154 | -0.14928 |
| H | 1.03295 | -1.71455 | -0.0313 |
| H | 0.9113 | -1.66877 | 0.08399 |
| H | 0.88586 | -1.58862 | 0.1193 |
| H | 1.07639 | -1.46206 | -0.03211 |
| H | 1.0719 | -1.38205 | -0.0749 |
| H | 1.06957 | -1.45657 | -0.2137 |
| H | 1.07343 | -1.53621 | -0.1708 |
| N | 1.63647 | -1.17012 | 0.43817 |
| C | 1.64369 | -1.21116 | 0.4214 |
| C | 1.65454 | -1.21375 | 0.37246 |
| C | 1.65514 | -1.25734 | 0.34919 |
| C | 1.64594 | -1.29962 | 0.37453 |
| C | 1.63503 | -1.29725 | 0.42377 |
| C | 1.63303 | -1.2528 | 0.44691 |
| H | 1.66294 | -1.17967 | 0.35157 |
| H | 1.66316 | -1.25901 | 0.30917 |
| H | 1.62784 | -1.33154 | 0.44478 |
| H | 1.62276 | -1.2505 | 0.48638 |
| C | 0.57198 | 0.3279 | 0.86946 |
| C | 0.14815 | 0.14815 | 0.14815 |
| O | -0.22567 | 0.96478 | -0.38544 |
| H | 0.21187 | 0.08164 | 0.36909 |
| O | 0 | -0.5 | -0.25 |
| H | 0.62452 | 0.37548 | 0.62452 |
| O | 0.34325 | 0.15675 | 0.75 |
| F | -1.02627 | -0.21113 | 0.54762 |
| F | -1.05097 | -0.26523 | 0.60568 |
| B | 0.25 | 0.44235 | -0.05765 |
| Cu | 0.5 | 0 | 0 |

**Supplementary Table 4 | Fractional atomic coordinates for catena-COF-807.**

| Catena-COF-807 | | | |
|---|---|---|---|
| Space group $P4_232$, $a$ = 26.1114 Å | | | |
| Atom | *x* | *y* | *z* |
| C | 0.97754 | -1.68817 | 0.01133 |
| C | 0.95499 | -1.64473 | 0.02295 |
| C | 0.9775 | -1.60118 | 0.01139 |
| C | 0.91078 | -1.64326 | 0.04661 |
| C | 0.89149 | -1.5991 | 0.06058 |
| C | 0.91604 | -1.55653 | 0.04966 |
| N | 0.95669 | -1.55865 | 0.02324 |
| C | 1.093 | -1.50691 | -0.0698 |
| C | 1.1365 | -1.48299 | -0.06417 |
| C | 1.14157 | -1.43641 | -0.08124 |
| C | 1.10316 | -1.41359 | -0.10463 |
| C | 1.06102 | -1.43923 | -0.11338 |
| C | 1.05595 | -1.48571 | -0.09614 |
| H | 1.04066 | -1.72371 | -0.02031 |
| H | 0.89063 | -1.67793 | 0.05441 |
| H | 0.85598 | -1.59778 | 0.08075 |
| H | 1.16778 | -1.50159 | -0.04562 |
| H | 1.17694 | -1.41658 | -0.0763 |
| H | 1.03071 | -1.42204 | -0.13469 |
| H | 1.0216 | -1.50655 | -0.10348 |
| N | 1.59424 | -1.16563 | 0.41578 |
| C | 1.60818 | -1.21712 | 0.40142 |
| C | 1.65523 | -1.23324 | 0.4082 |
| C | 1.66769 | -1.27969 | 0.39683 |
| C | 1.63314 | -1.31155 | 0.37938 |
| C | 1.58574 | -1.29556 | 0.37251 |
| C | 1.5736 | -1.24798 | 0.38272 |
| H | 1.68354 | -1.2079 | 0.42319 |
| H | 1.70627 | -1.29224 | 0.40165 |
| H | 1.55727 | -1.32137 | 0.35865 |
| H | 1.53569 | -1.2344 | 0.37584 |
| C | 0.60822 | 0.36791 | 0.86666 |
| H | 0.85862 | 0.6444 | 0.15825 |
| C | 0.13207 | 0.13207 | 0.13207 |
| O | 1.27176 | 0.63976 | -0.01704 |
| O | 0.25 | 0.40249 | -0.09751 |
| O | 0.59869 | 0.40131 | 0.59869 |
| O | 0.79977 | 0.25 | 0.29977 |
| F | 1.00132 | 0.77791 | 0.54525 |
| B | 0 | 0.75 | 0.5 |
| Cu | 0.5 | 0 | 0 |

Framework Flexibility

All three catena-COFs possess flexible frameworks which can respond to guest molecules such as organic solvents. The flexibility was confirmed by the observation of a variation in PXRD patterns of those samples with addition or removal of solvents such as THF (Supplementary Figs. 41–44).

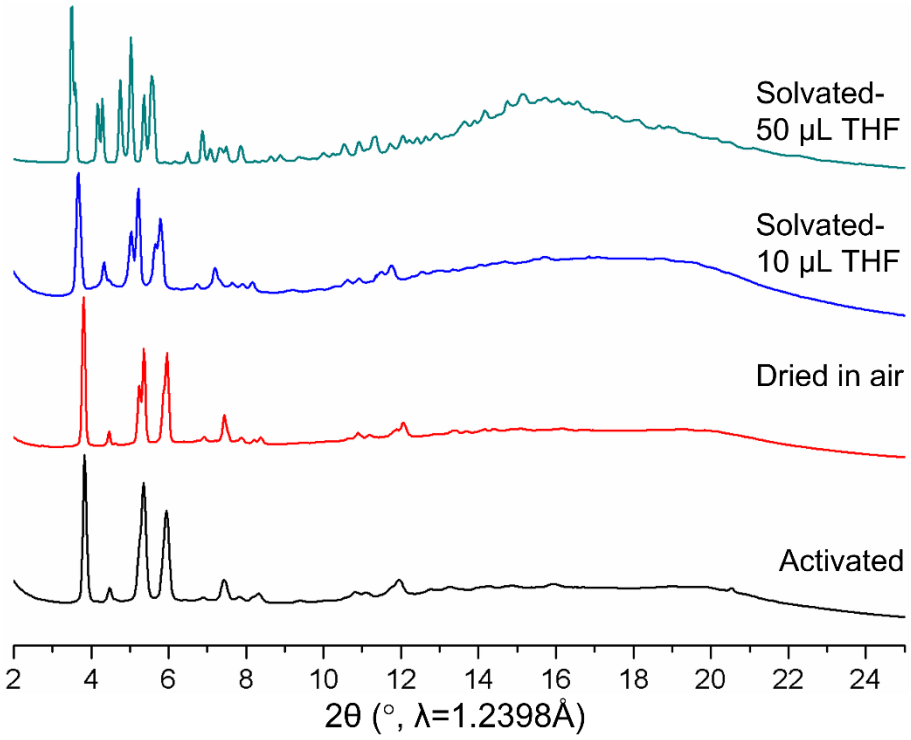


**Supplementary Fig. 41 | Comparison of PXRD patterns of catena-COF-805 samples containing different amounts of guest molecules.** Black: PXRD pattern of the activated catena-COF-805 which was processed according to the activation procedures listed in section S2. Red: PXRD pattern of catena-COF-805 which was only dried in air after solvents exchange and without drying at high temperature. Blue: PXRD pattern of the solvated catena-COF-805 which was prepared by adding 10 μL THF into the activated sample to keep it moist. Turquoise: PXRD pattern of the solvated catena-COF-805 which was prepared by adding 50 μL THF into the activated sample to ensure the sample was fully immersed in THF. All the samples were sealed in capillaries to prevent moisture absorption or solvent volatilization. The datasets were collected with the synchrotron x-ray beam as described in Instrumentation.

It is shown that: 1) As the amount of THF increasing, the peak positions continuously move to lower Bragg angles. 2) With the amount of THF increasing, the number of reflection peaks increases by splitting, i.e., the degree of peak splitting become larger along with the increase of THF amounts in catena-COF-805. Note that in the PXRD pattern of activated sample (black), there is an inconspicuous shoulder peak at ~5.0°, which may be caused by a few residual guest molecules such as water in catena-COF-805. 3) As commonly observed in porous flexible materials[10], the

relative peak intensities are different between the patterns of activated and solvated samples, for example, the intensity of peak/peaks at ~4.4° increased with the guest molecules increasing.

All the information implies a framework flexibility of catena-COF-805 responding to THF, including unit cell expansion (caused peak shift) and possible framework distortion (caused peak splitting). The distortion may result in reduced structural symmetry, which was supported by Pawley refinement for PXRD of solvated catena-COF-805 with lower symmetry (Supplementary Fig. 42). Note that these facts also sustained that the minor difference between the calculated and experimental PXRD should be caused by guest molecules which cannot be fully removed from the sample (Supplementary Figs. 43–45).

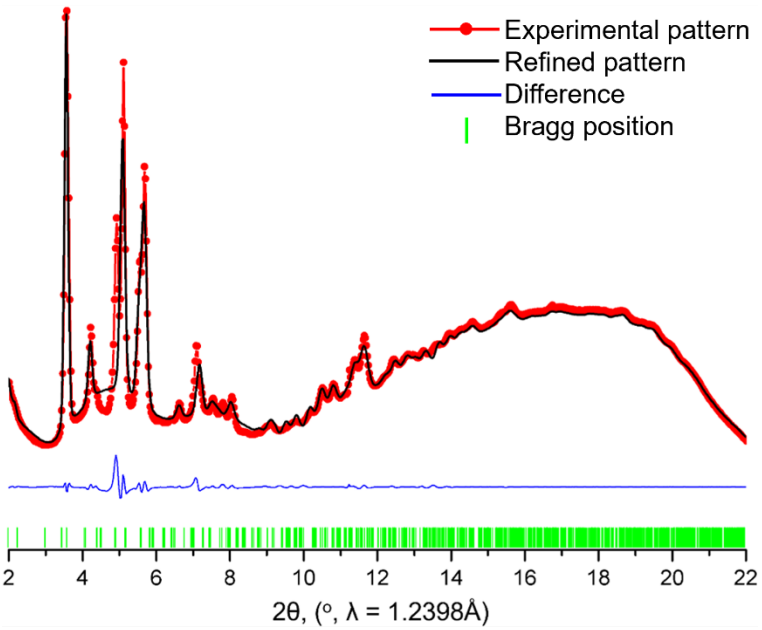


**Supplementary Fig. 42 | Pawley refinement of solvated catena-COF-805 with 10 μL THF.** Experimental PXRD pattern, red; refined pattern, black; difference pattern, blue; observed positions of Bragg reflections, green. As discussed above, the existence of solvents most probably induced the framework distortion and resulted in a reduced structural symmetry. Thus, the Pawley refinement was carried out in the space group of *F*222 (No. 22), resulting in unit cell parameters of $a$ = 55.8309(4) Å, $b$ = 55.8304(8) Å and $c$ = 55.4322 (4) Å with $R$p = 0.75% and $wR$p = 2.34%, which validated our hypothesis.

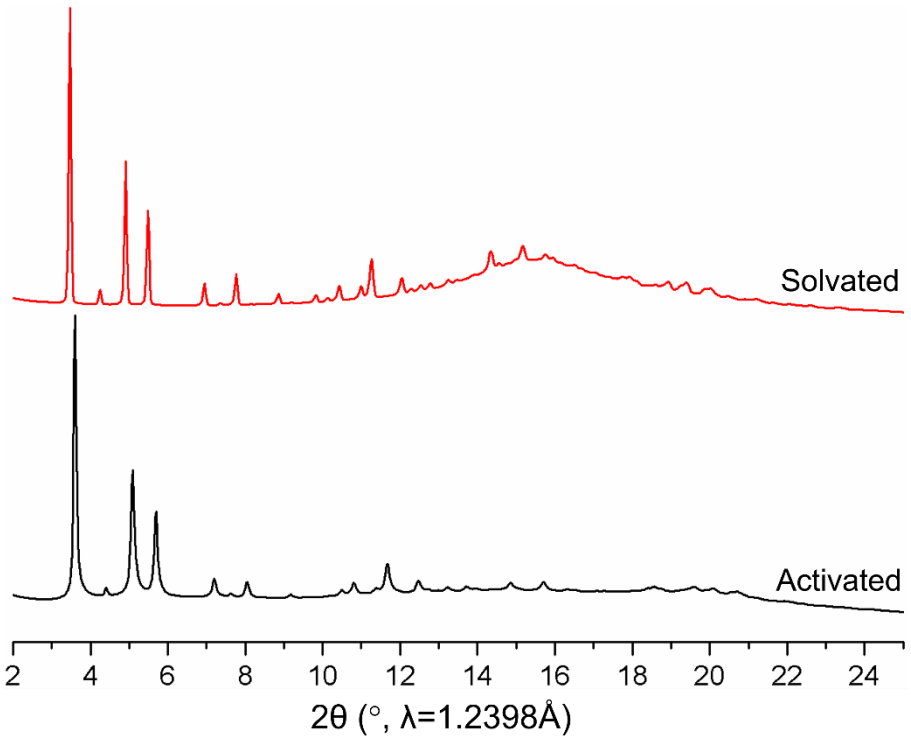


**Supplementary Fig. 43 | Comparison of PXRD patterns of activated catena-COF-806 (black) and THF solvated catena-COF-806 (red).** The activation of catena-COF-806 was processed according to the procedures listed in section S2 while the solvated catena-COF-806 was prepared by adding 50 μL THF into the activated sample to make sure that the catena-COF-806 was fully immersed in THF.

Similar to catena-COF-805, -806 also has a framework flexibility respond to THF since the shift in reflection peaks of solvated catena-COF-806 to lower angles indicates the expansion of unit cell with guest molecules. However, unlike catena-COF-805, no big difference can be found regarding the relative peak intensity and peak splitting between the patterns of activated and solvated samples, which means structure distortion caused by THF could be negligible in catena-COF-806. Benefiting from the minor structural changes and high crystallinity, Rietveld refinement was carried out for catena-COF-806 with constraints (Supplementary Fig. 39).

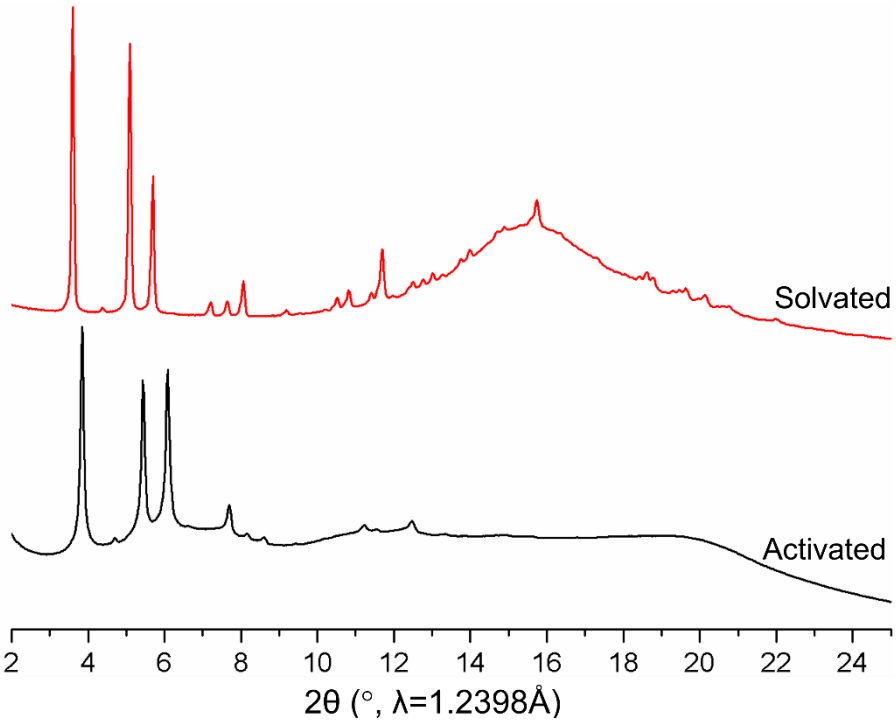


**Supplementary Fig. 44 | Comparison of PXRD patterns of activated catena-COF-807 (black) and THF solvated catena-COF-807 (red).** The activation of catena-COF-807 was processed according to the procedures listed in section S2 while the solvated catena-COF-807 was prepared by adding 50 μL THF into the activated sample to make sure the sample was fully immersed in THF.

Similar to the cases of catena-COF-805 and -806, the shift of reflection peaks related to unit cell expansion can also be found when comparing PXRD patterns of activated and solvated catena-COF-807. Interestingly, variation in relative peak intensity can be observed here like that in catena-COF-805, while no splitting peaks can be found on the pattern of solvated catena-COF-807 compared with that of activated catena-COF-807, which is similar to the case of catena-COF-806. These differences imply that the framework flexibility of catena-COF-807 should be in between catena-COF-805 and -806.

## Section 10. Demetalation and Remetalation Experiments

Taking catena-COF-806 as the example, the demetalation and remetalation experiments were carried out under the reported[1] and further optimized conditions.

**1) Demetalation.** A reaction tube was charged with 10.0 mg catena-COF-806 powder, 2.0 mL KCN solution (0.5 M) in a mixture of MeOH and $H_2O$ (*v*/*v* = 1:1). The suspension was stirred and heated at 75°C. The solution was replaced by a fresh KCN solution (caution: toxic hazard) of 0.5 M every 24 h and this procedure was repeated for three times. Then the separated solid which was further identified as demetalated catena-COF-806 was washed with $H_2O$, MeOH, EtOH, and dried at 120°C for 12 h. The demetalated sample was observed to be khaki in color, in contrast to the reddish-brown of metalated sample (Supplementary Fig. 45). Inductively coupled plasma atomic emission spectroscopy (ICP-AES) was used to determine the copper component (Cu%) in different catena-COF-806 samples, showing that Cu% is 5.21% (calcd. 5.12%) in metalated catena-COF-806 and 0.46% in demetalated catena-COF-806. This means that 90% Cu was removed from the original metalated catena-COF-806. SSNMR and FT-IR spectroscopies were applied to confirm that the interlocking covalent polyhedra of catena-COF-806 were kept intact without covalent bonds breaking after demetalation (Supplementary Figs. 46, 47), which was further supported by the results of a control experiment (Supplementary Scheme 1 and Fig. 48). TGA also confirmed that the framework of interlocking covalent polyhedra was maintained after demetallation (Supplementary Fig. 49). SEM was also used to characterize the crystal morphology after demetalation (Supplementary Fig. 50). The absence of Cu(I) imparted a high degree of structural freedom onto the polyhedra interlocked by mechanical bonds, which was substantiated by the observation of decreasing framework crystallinity after demetalation (Supplementary Fig. 51).

**2) Remetalation.** 8.0 mg demetalated catena-COF-806 was dispersed in anhydrous $CHCl_3$ under $N_2$, to which was added 1.0 mL solution of $[Cu(CH_3CN)_4]BF_4$ in $CH_3CN$ (0.01 M). This mixture was stirred for 12 h at room temperature and the remetalated catena-COF-806 was obtained with reddish-brown color recovered (Supplementary Fig. 45). The Cu% in remetalated catena-COF-806 was determined as 5.78% by ICP analysis, which is ~130% of Cu content in original metalated catena-COF-806, indicating that more Cu was captured by the material. The crystallinity cannot return to that of the original metalated catena-COF-806 (Supplementary Fig. 51). Although more diluted $[Cu(CH_3CN)_4]BF_4$ solutions were used in further remetalation experiments to reduce the Cu content, the crystallinity still cannot return.

**3) Partial demetalation.** To better understand the demetalation and remetalation processes, further exploration was carried out to partially remove the Cu ions with milder demetalation conditions such as a lower reaction temperature (e.g., room temperature or 50°C), reduced reaction time (e.g., 12 or 24 h), or diluted KCN solution (e.g., 0.008 M). From ICP analysis, we found that ~60%–70% of Cu in the original catena-COF-806 can be removed at room temperature in 3 days, or at 75°C in 12 h, or with 0.008M KCN solution at 75°C in 3 days. Different from the above result where >90% Cu was removed, the crystallinity of original catena-COF-806 can be preserved somewhat after partial demetalation (Supplementary Fig. 51).

**4) Remetalation for partially demetalated catena-COF-806.** All the partially demetalated catena-COF-806 samples from different demetalation conditions were remetalated in $[Cu(CH_3CN)_4]BF_4$ solutions with different concentrations (e.g., 0.0025 M and 0.005 M, both lower than the reported 0.01 M). Despite the fact that their crystallinity could not be recovered to the original metalated state after remetalation (Supplementary Fig. 51), the Cu ions were left in the materials. Hence, we recrystallized these samples in 1,4-dioxane with small amounts of 6 M HOAc aq. for 3 days at 120$^{o}$C. The crystallinity can be recovered after recrystallization (Supplementary Fig. 51). Note that without the remetalation step, the partially demetalated catena-COF-806 cannot be recovered to crystalline with the same 'recrystallization' process. Besides, the recrystallization cannot occur if there was no acid present. Interestingly, the crystallinity of >90% demetalated catena-COF-806 cannot be recovered after processing with the same procedures of remetalation and 'recrystallization'. The demetalation, remetalation and recrystallization experiments on catena-COF-805 and -807 yielded similar results with catena-COF-806. A schematic diagram of all these processes is proposed in Supplementary Fig. 52.

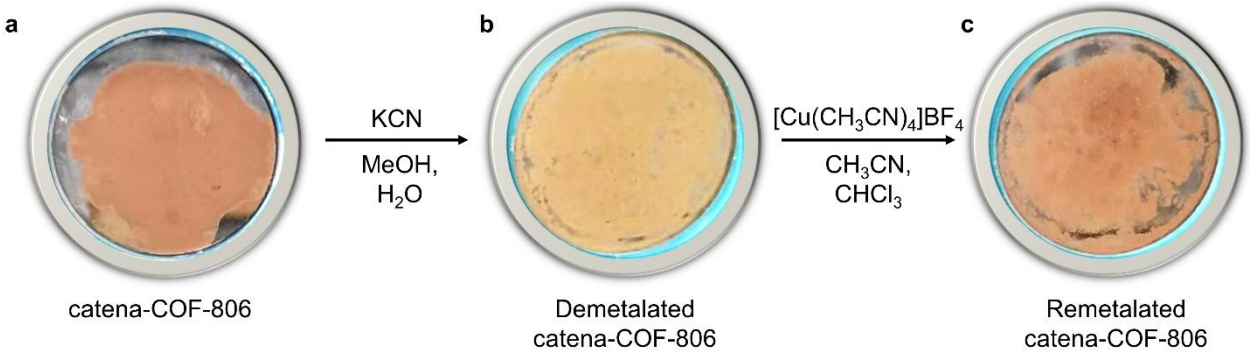


**Supplementary Fig. 45 | The original metalated (a), demetalated (b) and remetalated** (**c**) **catena-COF-806.** The powders of different catena-COF-806 samples were splitting on the PXRD sample holders for taking images. The demetalated catena-COF-806 (b) is khaki in color while metalated (a) and remetalated (c) samples are the same reddish-brown.

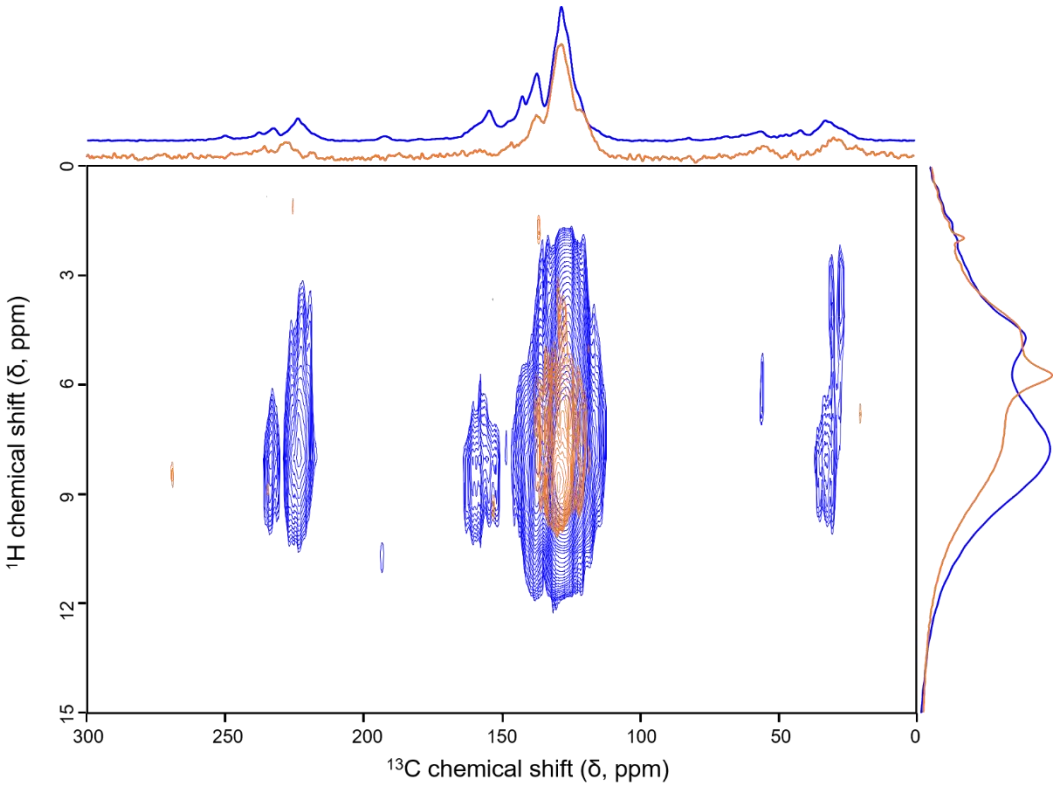


**Supplementary Fig. 46 | The overlaid 2D $^{1}$H-$^{13}$C HETCOR spectra with 1D $^{13}$C CP/MAS (top) and $^{1}$H spectra (right) of the original metalated (blue) and demetalated (orange) catena-COF-806.** The similar resonance signals and correlation signals can be observed, which indicates that metalated and demetalated catena-COF-806 have the same organic composition and covalent bonding. The overlaid cluster of signals appearing at $^{13}$C chemical shift of 154–156 ppm which shows a correlation with a $^{1}$H chemical shift of ~9.0 ppm, is assigned to the carbon of imine group (–CH=N), demonstrating that the imine linkages in organic polyhedra were kept after demetalation. Note that the signals of demetalated catena-COF-806 are broader and weaker than those of metalated catena-COF-806 due to a non-crystalline property of the demetalated congener (Supplementary Fig. 51).

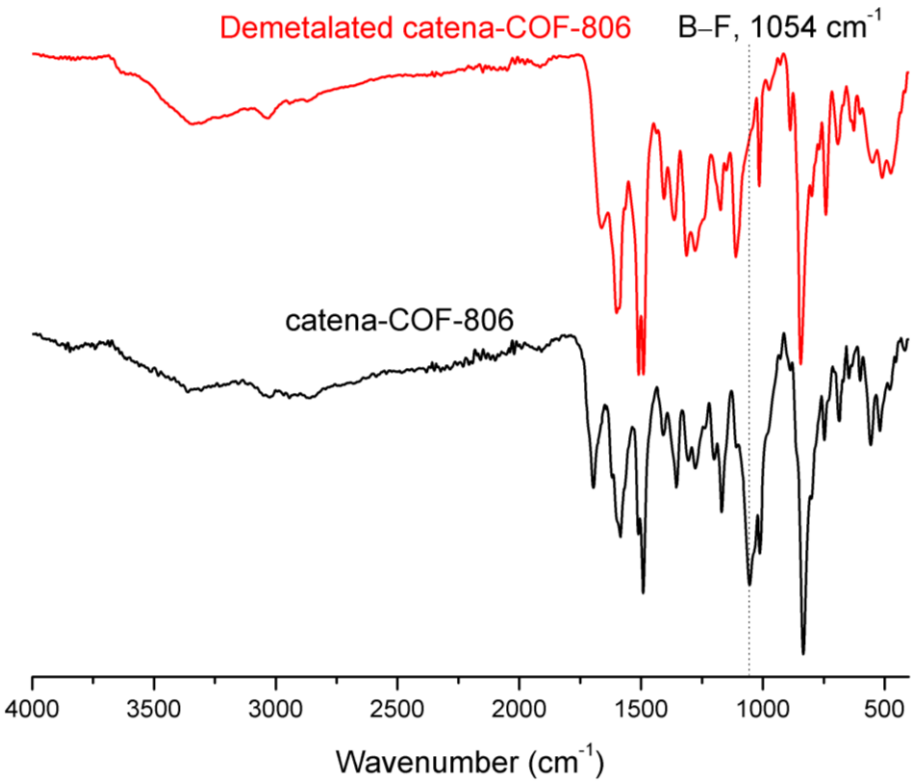


**Supplementary Fig. 47 | Comparison of the FT-IR spectra of the original metalated (black) and demetalated (red) catena-COF-806.** The signal at ~1054 $cm^{-1}$, which is assigned to be B−F stretching vibration of $BF_4$ anions, is found to exist in metalated catena-COF-806 but is absent in demetalated catena-COF-806, indicating that the $BF_4$ anions were removed with Cu ions for charge balance. In addition, the compared FT-IR spectra have nearly the same vibration signals, which demonstrates the presence of the same organic building blocks and covalent bonding between demetalated and metalated catena-COF-806, indicating that the framework of interlocking covalent polyhedra was maintained after demetalation. Note that the signal of the terminal −CHO group (~1697 $cm^{-1}$) which belongs to unlinked PDB molecules at the surface or the defects of material, disappeared in spectrum of demetalated catena-COF-806 (red), indicating that the independent PDB molecules were removed after the demetallation process. The resulted defects might partially increase the possibility of unsuccessful remetalation. The results of a control experiment (Supplementary Scheme S1 and Fig. 48) further confirmed that the demetalated catena-COF-806 was indeed comprised of interlocking organic polyhedra (all closed structures) instead of other structures with terminal groups.

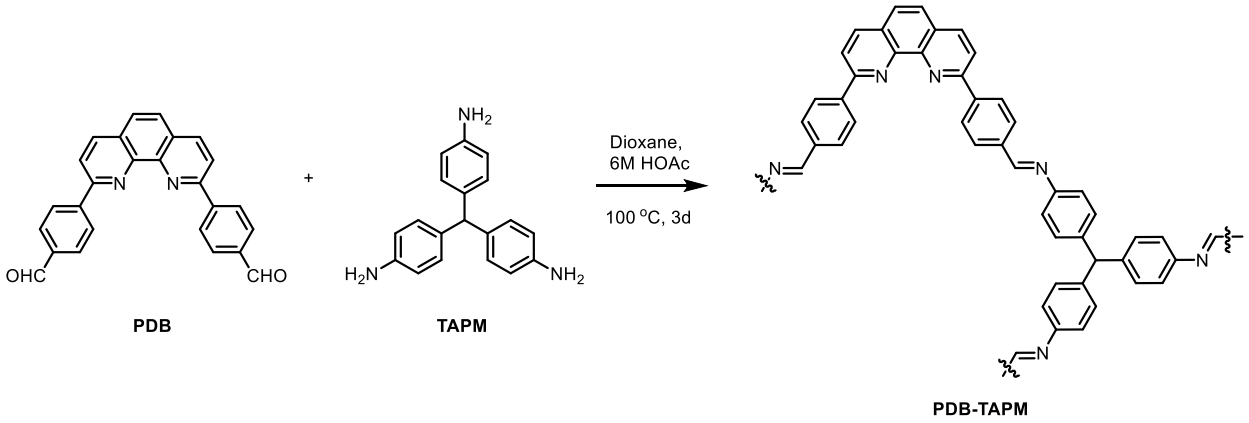


**Supplementary Scheme 1 | The synthetic approach for the control experiment.** An amorphous solid termed PDB-TAPM was synthesized at 100 °C by linking PDB (23.3 mg, 0.06 mmol) with TAPM (11.5 mg, 0.04 mmol) in 1.0 mL dioxane through imine condensation in the absence of metal ion templating. 6M HOAc (0.2 mL) was used as catalyst. After heating the reaction for 3 days, the produced solid was separated and washed with acetone and $CHCl_3$. The dried sample was used for comparison with the demetalated catena-COF-806 (Supplementary Fig. 48).

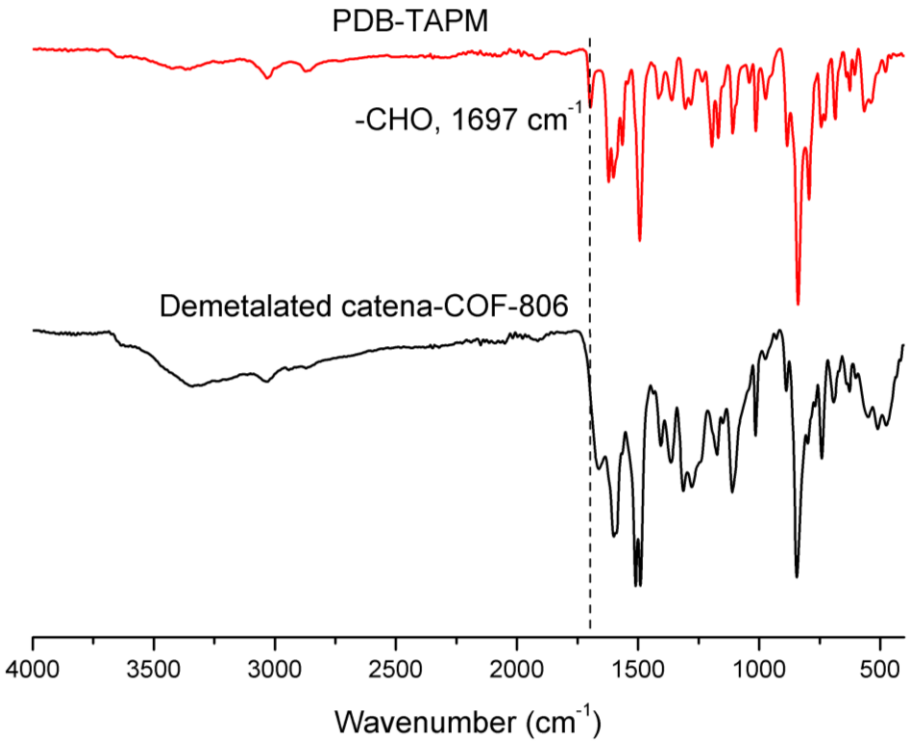


**Supplementary Fig. 48 | Comparison of the FT-IR spectra of the demetalated catena-COF-806 (black) and PDB-TAPM (red).** As shown in Scheme 1, PDB-TAPM was produced by linking of 4,4'-(1,10-phenanthroline-2,9-diyl)dibenzaldehyde (PDB) with tris-(4-aminophenyl)methane (TAPM) by imine condensation without metal ion templating. The signal of terminal −CHO group (~1697 $cm^{-1}$) which is assigned to unreacted aldehyde moieties of PDB is observed in PDB-TAPM but is absent in demetalated catena-COF-806. This confirmed that demetalated catena-COF-806, in contrast to the structure of PDB-TAPM with randomly distributed terminal groups, is comprised of intact interlocking polyhedra. While the wavenumbers for most signals of the two samples are similar, there are still detailed differences between the two FT-IR spectra. This further supports the fact that the demetalated catena-COF-806 and PDB-TAPM have similar components but different connection patterns between PDB and TAPM linkers.

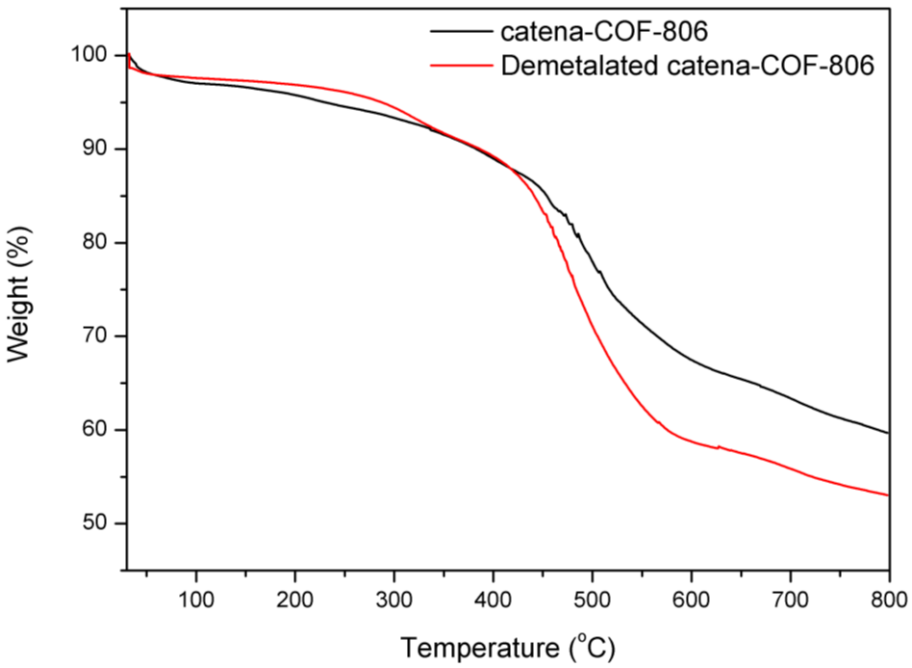


**Supplementary Fig. 49 | Comparison of the TGA curves of the original metalated (black) and demetalated (red) catena-COF-806.** The similar decomposition temperatures of ~450°C for the original and demetalated samples further confirmed that the framework of interlocking covalent polyhedra was maintained after demetalation.

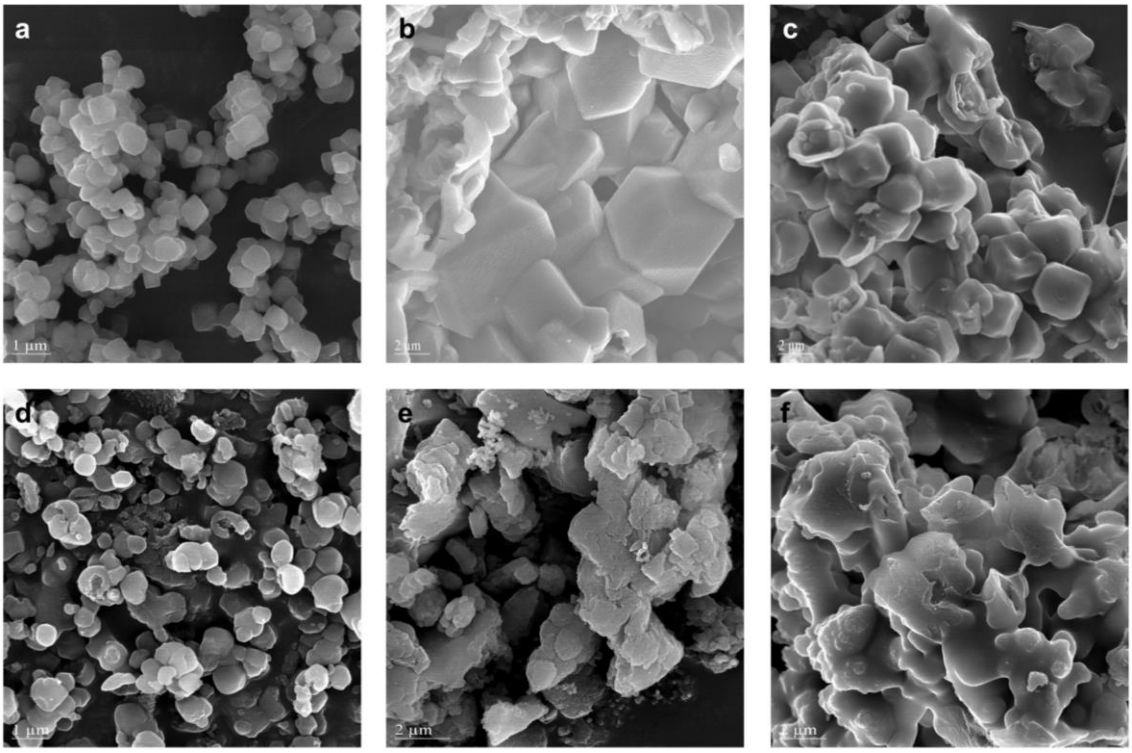


**Supplementary Fig. 50 | SEM images of the original metalated and demetalated catena-COFs.** **a**–**c**, The original metalated catena-COF-805, -806, and -807, respectively. **d**–**f**, Demetalated catena-COF-805, -806, and -807, respectively. Comparing with the original catena-COFs, similar crystal morphologies and sizes were basically maintained after demetalation. However, demetalated COFs have less distinct crystal edges and corners, especially for larger-sized catena-COF-806 and -807. Most of catena-COF-806/-807 crystals were broken after demetalation. This implied that the main frameworks could be kept but the inner structures were distorted or partially collapse, matching with the results of the PXRD analysis (Supplementary Fig. 51).

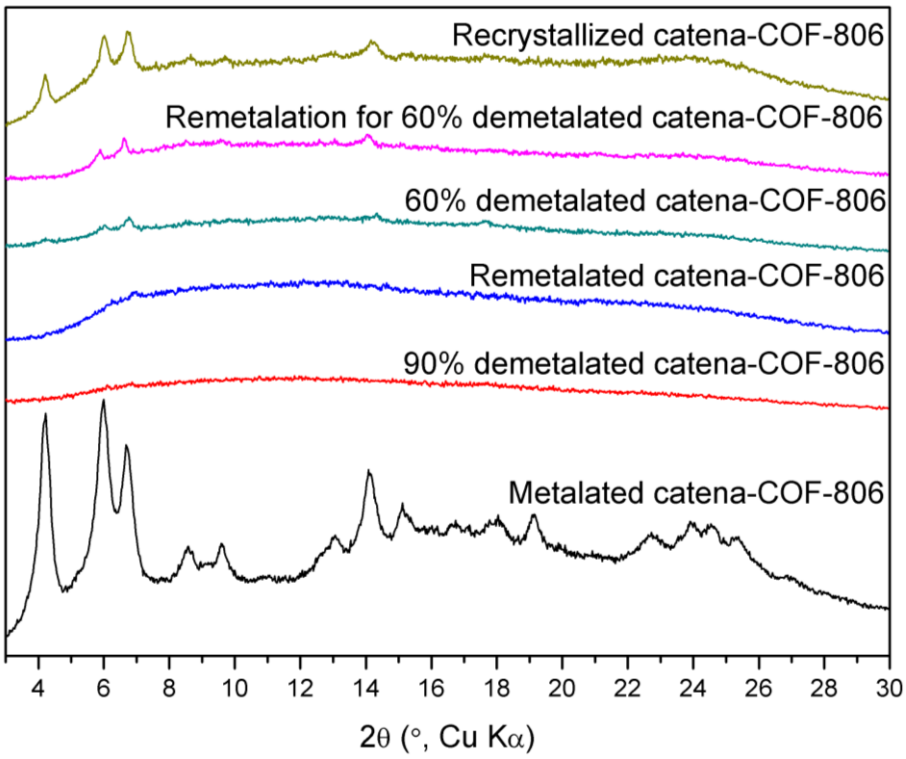


**Supplementary Fig. 51 | Comparison of PXRD patterns of the original metalated catena-COF-806 (black), 90% demetalated catena-COF-806 (red), remetalated catena-COF-806 (blue), 60% demetalated catena-COF-806 (turquoise), remetalated sample from 60% demetalated catena-COF-806 (pink) and recrystallized catena-COF-806 (olive).** The datasets were collected at a Rigaku MiniFlex 600 Benchtop diffractometer with Cu K$\alpha$ radiation of $\lambda$ = 1.5418 Å at 40 kV and 15 mA. A fast scan of step size = 0.02° and an exposure time = 0.5 s per step was used.

It is shown that: 1) The crystallinity of catena-COF-806 lost upon demetalation (>90%) and the crystallinity cannot be restored after remetalation. 2) The crystallinity of original catena-COF-806 was preserved a little after partial demetalation (~60%), but the crystallinity still cannot be recovered to the original state after remetalation. 3) The crystallinity increased after the further recrystallization for the sample which was 60% demetalated and then remetalated. Although the reflection intensity of recrystallized catena-COF-806 is observed to be weaker than the original sample due to the sample loss during the multiple steps of reactions (demetalation→remetalation→recrystallization), the recrystallized sample has a higher intensity than the previous remetalated one, indicating that crystallinity can be recovered. Note that the crystallinity cannot be recovered for the sample which was 90% demetalated and then remetalated through the same 'recrystallization' process used for the 60% demetalated sample. A proposed explanation for all these processes is presented in Supplementary Fig. 52.

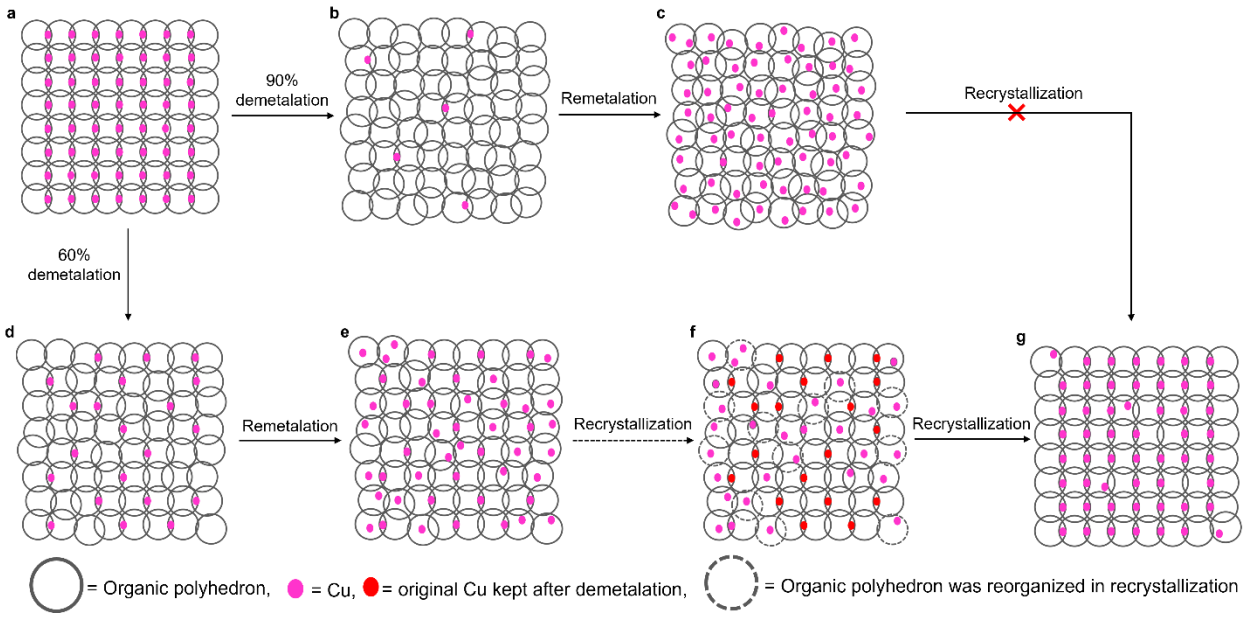


**Supplementary Fig. 52 | Proposed scheme for all the demetalation, remetalation, and recrystallization processes.** The polyhedra are represented by gray circles (solid and dashed), while Cu ions are represented by pink and red oval spots. **a**, In the original metalated catena-COF-806 with high crystallinity, the polyhedra were interlocked with each other in a regular arrangement by the supporting of Cu ions. **b**, Removal of >90% of Cu ions resulted in a mutual dislocation between these 0D interlocking polyhedra since they can move freely within the confines of their mechanically linked counterpart without breaking chemical bonds, thus yielding an irregular molecular arrangement, i.e., loss of crystallinity. **c**, The crystallinity cannot be recovered after the remetalation and even after a so-called 'recrystallization' process (discussed further below), which means the polyhedra and Cu ions cannot return to the original regular arrangements. This is different from COF-505 which consists of interlacing 1D threads[1] and COF-500 comprised of interlocked 1D ribbons[11]. Catena-COFs were formed by interlocking of discrete 0D polyhedra, which possess a higher potential for mobility than the extended 1D threads and ribbons. The malposition between tremendous of the 0D polyhedra was very difficult to be repaired by adding Cu ions again (remetalation), and the original periodicity of polyhedra arrangement was not easy to be regenerated especially when the original symmetries of these crystals were very high ($F4_132$ for catena-COF-805 and $P4_232$ for -806/-807, while the reported COF-505 and COF-500 were *Cc*2*a* and *C*222, respectively). The possible dislocation and distortion of the polyhedra after demetalation were supported by molecular dynamic simulation results as shown in Supplementary Fig. 53. **d**, The crystallinity can be retained partially after a 60% demetalation, which means partial regular arrangements of polyhedra and Cu ions were kept while the rest of them were irregular. **e**, After remetalation was carried out for the 60% demetalated catena-COF-806, the crystallinity cannot be recovered except Cu was left in the material as disorders (confirmed by ICP analysis). **f**, In the recrystallization process, the retained crystalline parts (represented by the red spots and dashed circles) might be used as crystal seeds, which induced the reorganization

of the organic polyhedra (dashed circles) around the seeds in the presence of acid. Most of the crystallinity can be recovered after recrystallization (**g**). Note that >90% demetalated sample cannot be recovered by the similar ‘recrystallization’ process most possibly because of the lack of crystal seeds as in the partially demetalated sample.

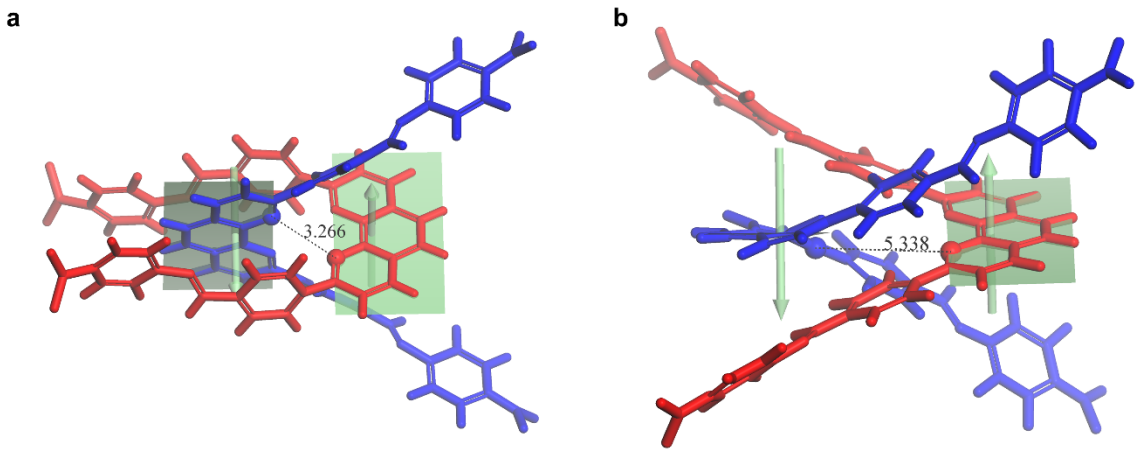


**Supplementary Fig. 53 | Compared local structures of (a) experimental model of catena-COF-805 where Cu is omitted for clarity and (b) remetalated catena-COF-805 model after energy optimization by molecular dynamic simulation.** To further investigate the structure of remetalated catena-COFs, energy minimization was carried out on a subset of eight interlocking polyhedra with Forcite Module by using universal force field in Materials Studio. The dihedral angle between two crossing phenanthroline planes of two interlocking polyhedra in catena-COF-805 changed from 102.5° (a) in the metalated progenitor to 17.0° (b) in the demetalated structure. Furthermore, the minimum distance between nitrogen atoms of two interlocking phenanthroline moieties were elongated from 3.3 Å in the metalated structure (a) to 5.3 Å in the demetalated one (b), thus corroborating the expected deviation of the idealized binding sites for complete remetalation. It is conceivable that all these conformation changes across the vast number of interlocking polyhedra caused major structural deformation, thus imposing a high activation energy on the remetalation with Cu ions to fully recover the original conformation of the crystalline framework.

## Section 11. THF Sorption

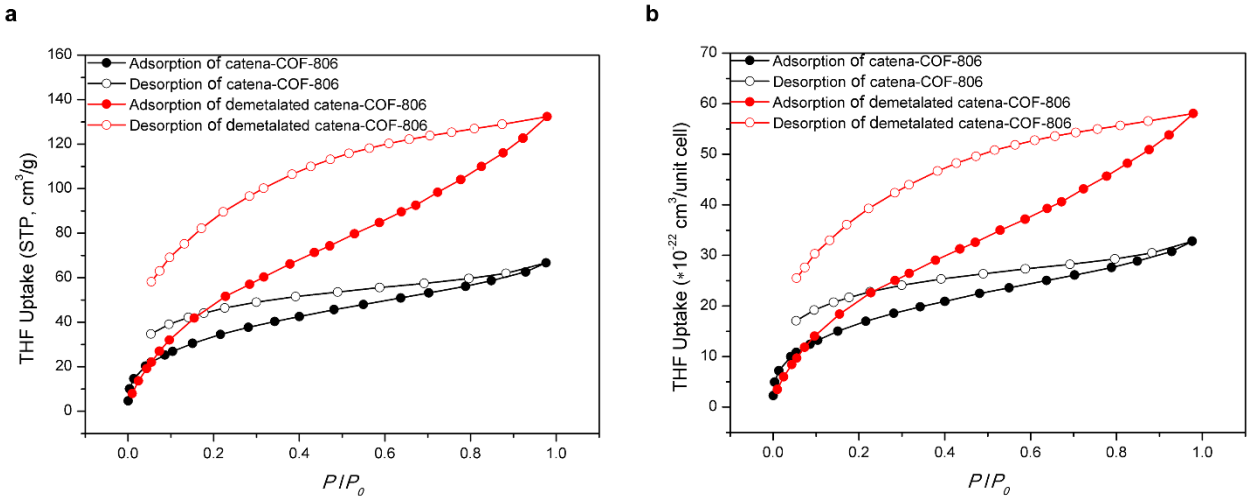


**Supplementary Fig. 54 | THF vapor sorption isotherms of the original metalated catena-COF-806 (black) and demetalated catena-COF-806 (red). a**, The recorded THF vapor sorption isotherms of the original metalated catena-COF-806 (black) and 90% demetalated catena-COF-806 (red). **b**, Normalized THF vapor sorption isotherms of the original metalated catena-COF-806 (black) and 90% demetalated catena-COF-806 (red). Since the metalated and demetalated catena-COF-806 have different molecular weights, the recorded THF uptakes were normalized to display the uptake per unit cell.

It is shown that metalated catena-COF-806 exhibits an approximate type I adsorption isotherm with a characteristic microporous filling below $P/P_0$ = 0.1 (black), while the adsorption curve of the demetalated catena-COF-806 exhibits a linear isotherm profile (red). This implies that the demetalated catena-COF-806 possesses a higher flexible framework which can be expanded by taking up THF molecules until the saturated uptake reaches to ~132 $cm^3\ g^{-1}$ (~$58\times10^{-22}$ $cm^3$ per unit cell). Although the metalated catena-COF-806 also exhibits some degree of flexibility which can be observed in its PXRD pattern upon soaking in THF (Supplementary Fig. 43), it possesses a less flexible framework which exhibits a THF uptake of ~27 $cm^3\ g^{-1}$ (~$13\times10^{-22}$ $cm^3$ per unit cell) at $P/P_0$ = 0.1, and a saturated uptake of ~67 $cm^3\ g^{-1}$ (~$33\times10^{-22}$ $cm^3$ per unit cell) at $P/P_0$ = 0.98. Additionally, the saturated uptake of demetalated catena-COF-806 is approximately two times larger than that of the catena-COF-806 at $P/P_0$ = 0.98. Benefiting from its higher flexibility from mechanically interlocking of the polyhedra, the demetalated catena-COF-806 can be expanded further to accommodate more guest molecules than its metalated analogue.

## Section 12. Mechanical Properties

Catena-COF-806 samples were dispersed in ethanol using an ultra-sonication bath for 0.5 h. A thin layer of crystal bond was applied on a magnetic plate at 100°C before drop-casting of the COF-ethanol dispersion on the plate. With a few drops of sample dispersion, the plate was quickly cooled to room temperature and dried at ambient conditions overnight for indentation. The nanoindentation was performed with a Hysitron TI-950 Triboindenter as described in Instrumentation. A Berkovich tip (TI-0039-1, 50 nm tip radius) was used to indent catena-COF-806 and its demetalated analogue after scanning the area to localize the tip position. The reduced modulus and hardness were measured based on the Oliver and Pharr method[12] under quasi-static indentation mode with a holding time of 30 sec prior to unloading. The reduced modulus is defined as $1/E_r = (1 - \nu_{sample}^2)/E_{sample} + (1 - \nu_{indenter}^2)/E_{indenter}$, where the modulus of elasticity ($E$) and Poisson's ratio ($\nu$) of the indenter are 1140 GPa and 0.07, respectively. The modulus of elasticity of the sample, $E_{sample}$, was evaluated assuming Poisson's ratio of the sample, $\nu_{sample}$, is 0.38, which is a typical value for polymers. The maximum load was set as of 100 μN with a loading rate of 20 μN/s. Scanning probe microscopy was used to verify the ~500 nm height of the pristine COF particles from the substrate prior to performing the nanoindentation.

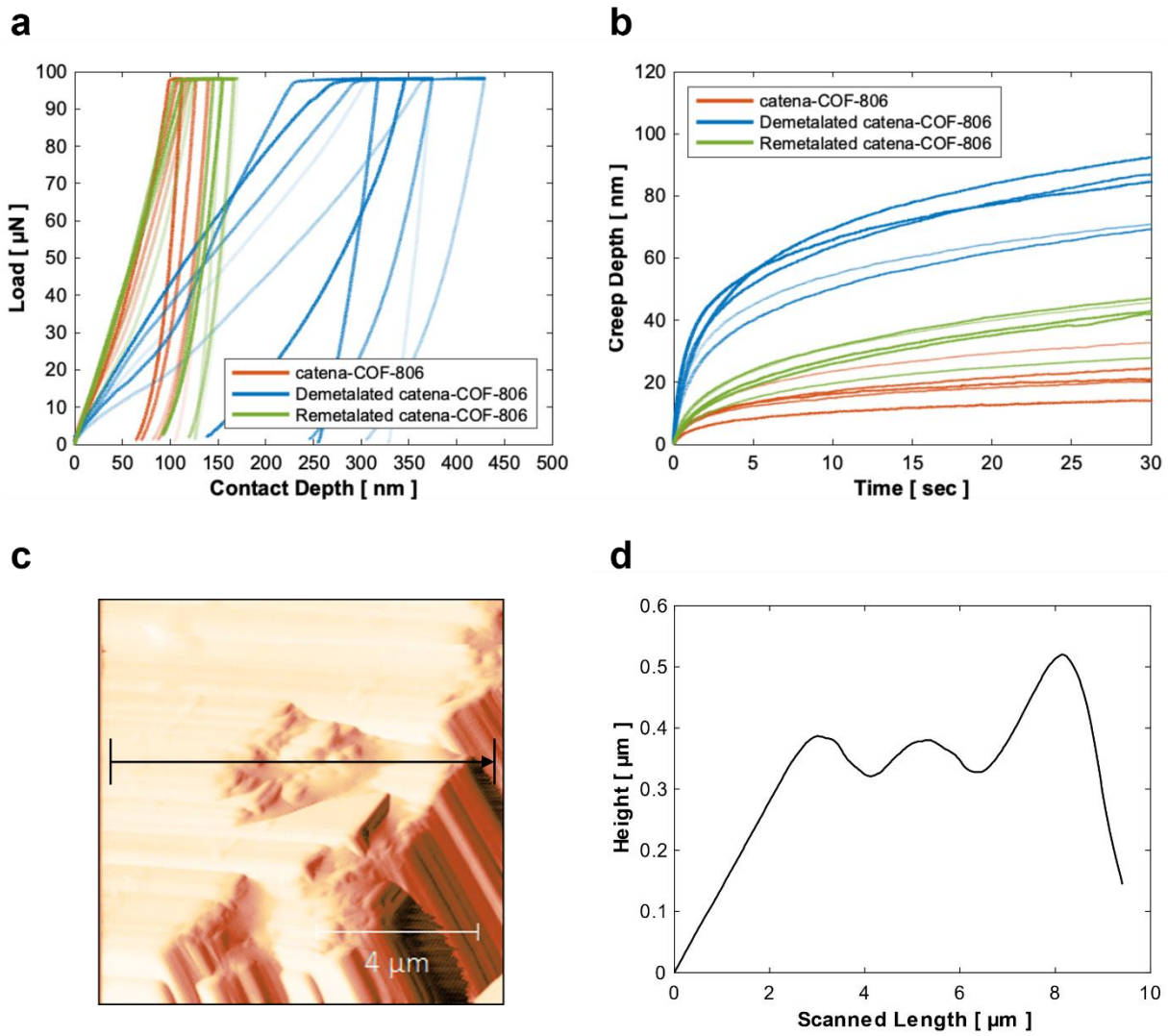


**Supplementary Fig. 55 | Nanoindentation results of the metalated, 90% demetalated and remetalated catena-COF-806. a**, Load-depth curves of the metalated catena-COF-806 (various shades of orange), the demetalated catena-COF-806 (various shades of blue), and the remetalated catena-COF-806 (various shades of green). The maximum loads of 100 µN were held for 30 sec prior to unloading. **b**, Depth-time curves for the metalated catena-COF-806 (various shades of orange), the demetalated catena-COF-806 (various shades of blue) and the remetalated catena-COF-806 (various shades of green) at a maximum load of 100 µN for 30 sec. **c**, A scanning probe microscopy image of the metalated catena-COF-806. **d**, The cross-sectional height profile along the direction shown in c. The measured elastic modulus and hardness were reported in the main text and in Supplementary Table 5.

**Supplementary Table 5 | Nanoindentation results of the metalated, 90% demetalated and remetalated catena-COF-806.**

| Sample / Properties | Metalated catena-COF-806 | Demetalated catena-COF-806 | Remetalated catena-COF-806 |
|---|---|---|---|
| Elasticity (*E*, GPa) | 3.81 | 1.41 | 2.61 |
| Hardness (*H*, MPa) | 154.7 | 55.8 | 96.1 |
| Std. | 0.07 (*E*), 27.7 (*H*) | 0.55 (*E*), 8.7 (*H*) | 0.64 (*E*), 29.5 (*H*) |

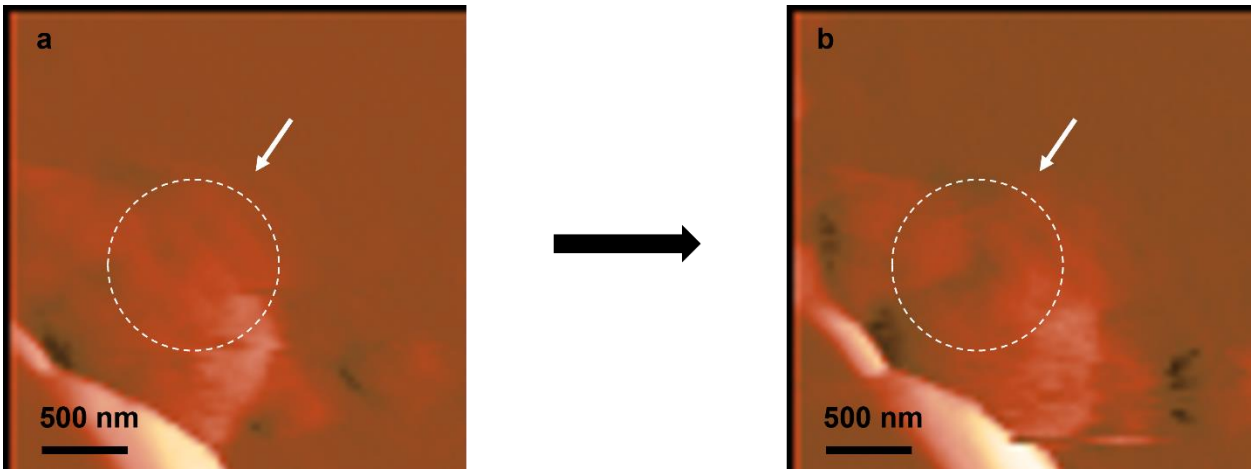


**Supplementary Fig. 56 | Comparison of scanning probe microscopy images of a catena-COF-806 particle before (a) and after (b) indentation.** The indentation impression can be observed in the bright dashed circle after experiment.

## Section 13. Degree of Catenation (DC)

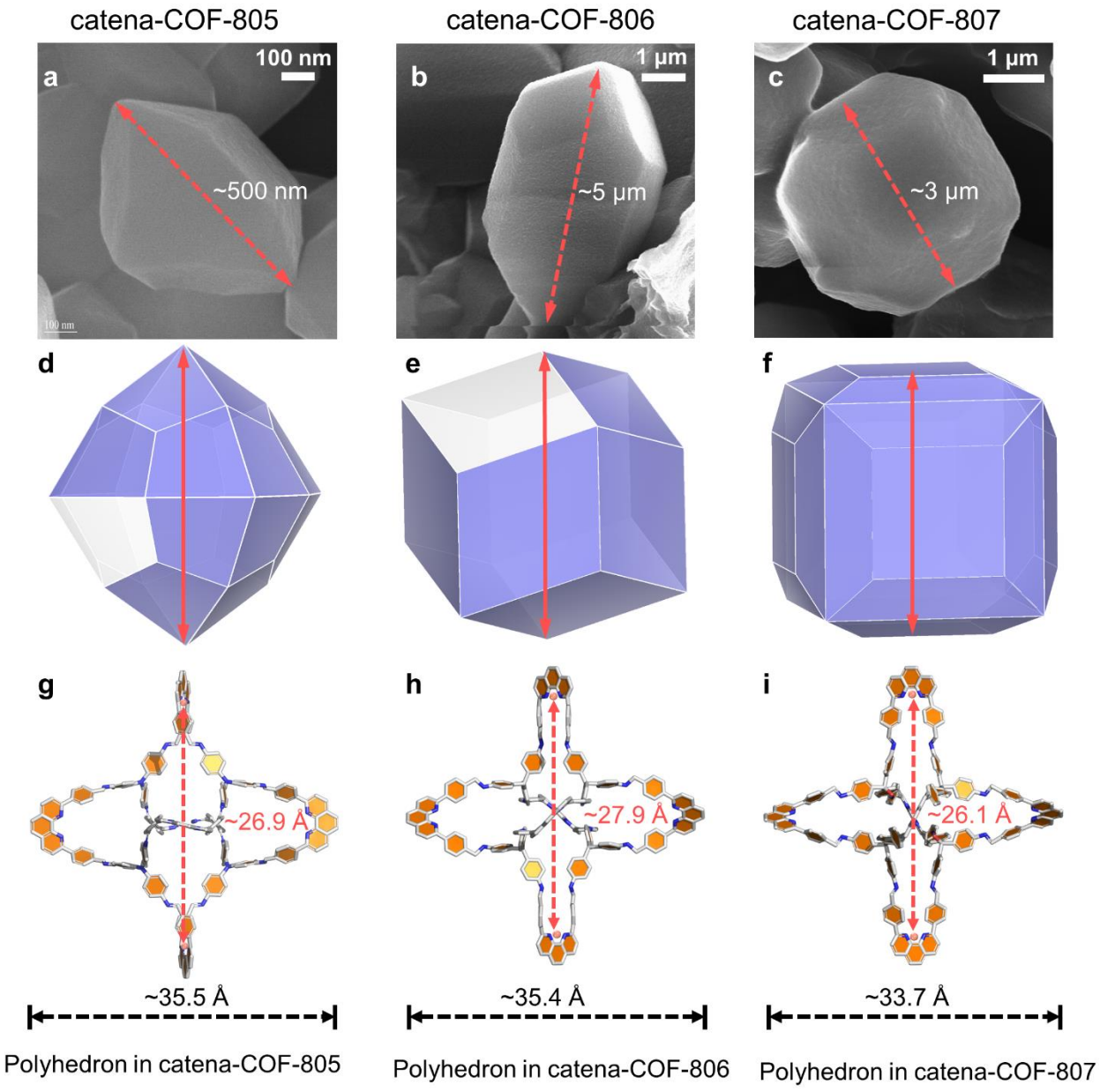


**Supplementary Fig. 57 | SEM images (a–c), simulated crystal morphologies (d–f), and structural details of polyhedra size (g–i) of catena-COF-805 (left), -806 (middle) and -807 (right), respectively.** It is observed from the SEM images that the maximum dimensions of the crystals are ~500 nm for catena-COF-805 (a), ~5 μm for catena-COF-806 (b) and ~3 μm for catena-COF-807 (c), respectively, same as they are shown in Supplementary Fig. 18. These crystals all have ideal morphologies with 4-fold, 3-fold and 2-fold axis along <100>, <111> and <110>, respectively, matching perfectly with their internal symmetries where the space groups of three catena-COFs (-805, -806 and -807) are $F4_132$, $P4_232$ and $P4_232$, respectively, which possess the same point symmetry of 432. These morphologies also matched well with the simulation results

(d–f) which were conducted with Morphology module in Materials Studio according to the Bravais-Friedel-Donnay-Harker (BFDH) rule[13–15]. The labeled red arrows in d–f indicate the direction of organic polyhedra interlocking, which are the same as the direction of they are labeled with red arrows in g–i. As shown in g–i, the maximum dimensions of different organic polyhedron units of catena-COF-805, -806 and -807 are ~35.5 Å, ~35.4 Å and ~33.7 Å, respectively, while the distances between two interlocking crossing centers (*i.e.*, distance between two Cu ions) are ~26.9 Å, ~27.9 Å and ~26.1 Å for catena-COF-805, -806 and -807, respectively. The distance value of 26.9 Å is half of the unit cell parameter *a* of catena-COF-805, and the other two distance values (27.9 Å and 26.1 Å) are the same as unit cell parameters (*a*) of catena-COF-806 and -807, respectively.

The degree of catenation (DC) in a crystal can thus be calculated by comparing the crystal sizes (e.g., along the direction of polyhedra interlocking) with the distances between two interlocking crossing centers (*i.e.*, $\frac{1}{2}a$ or *a*). Specifically, in a 500 nm-sized catena-COF-805 crystal, it can be calculated that there are 187 interlocking polyhedra along one direction, which means the DC of polyhedra units will be over 5 million in a three-dimensional 500 × 500 × 500 $nm^3$ crystal. Similarly, in a 5 μm-sized catena-COF-806 crystal, there are ~1800 interlocking polyhedra along one direction and over 5 billion of interlocking polyhedra in a 5 × 5 × 5 $\mu m^3$ crystal. For a catena-COF-807 crystal of 3 μm, the DC of interlocking polyhedra was calculated as ~1000 along one direction and ~1 billion in a 3 × 3 × 3 $\mu m^3$ crystal. These numbers are orders of magnitude higher than that of the reported longest organic poly[*n*]catenane chain ($n = 130$)[16].

## References


1. Liu, Y., Ma, Y., Zhao, Y., Sun, X., Gándara, F., Furukawa, H., Liu, Z., Zhu, H., Zhu, C., Suenaga, K., Oleynikov, P., Alshammari, A. S., Zhang, X., Terasaki, O. & Yaghi, O. M. Weaving of organic threads into a crystalline covalent organic framework. *Science* **351**, 365–369 (2015).

2. Gemmi, M. & Oleynikov, P. Scanning reciprocal space for solving unknown structures: energy filtered diffraction tomography and rotation diffraction tomography methods. *Z. Kristallogr.* **228**, 51–58 (2013).

3. Lee, M. & Goldburg, W. I. Nuclear-magnetic-resonance line narrowing by a rotating rf field. *Phys. Rev.* **140**, A1261 (1965).

4. Bielecki, A., Kolbert, A. C. & Levitt, M. H. Frequency-switched pulse sequences: Homonuclear decoupling and dilute spin NMR in solids. *Chem. Phys. Lett.* **155**, 341–346 (1989).

5. O'Keeffe, M. Peskov, M. A., Ramsden, S. J. & Yaghi, O. M. The reticular chemistry structure resource (RCSR) database of, and symbols for, crystal nets. *Acc. Chem. Res.* **41**, 1782–1789 (2008).

6. Liu, Y., O'Keeffe, M., Treacy, M. M. J. & Yaghi, O. M. The geometry of periodic knots, polycatenanes and weaving from a chemical perspective: a library for reticular chemistry. *Chem. Soc. Rev.* **47**, 4642–4664 (2018).

7. Lewandowska, U., Zajaczkowski, W., Corra, S., Tanabe, J., Borrmann, R., Benetti, E. M., Stappert, S., Watanabe, K., Ochs, N. A. K., Schaeublin, R., Li, C., Yashima, E., Pisula, W., Müllen, K. & Wennemers, H. A triaxial supramolecular weave. *Nat. Chem.* **9**, 1068–1072 (2017).

8. Thompson, B. & Hyde, S. T., A theoretical schema for building weavings of nets via colored tilings of two-dimensional spaces and some simple polyhedral, planar and three-periodic examples. *Isr. J. Chem.* **58**, 1144–1156 (2018).

9. Smeets, S., McCusker, L. B., Baerlocher, C., Elomari, S., Xie, D. & Zones, S. I. Locating organic guests in inorganic host materials from x-ray powder diffraction data. *J. Am. Chem. Soc.* **138**, 7099–7106 (2016).

10. Schneemann, A., Bon, V., Schwedler, I., Senkovska, I., Kaskel, S. & Fischer, R. A. Flexible metal–organic frameworks. *Chem. Soc. Rev.* **43**, 6062–6096 (2014).

11. Liu, Y., Diercks, C. S., Ma, Y., Lyu, H., Zhu, C., Alshmimri, S. A., Alshihri, S. & Yaghi, O. M. 3D covalent organic frameworks of interlocking 1D square ribbons. *J. Am. Chem. Soc.* **141**, 677–683 (2019).

12. Oliver, W. C. & Pharr, G. M. An improved technique for determining hardness and elastic modulus using load and displacement sensing indentation experiments. *J. Mater. Res.* **7**, 1564–1583 (1992).

13. Bravais, A. *Etudes Cristallographiques* (Gauthier Villars, Paris, 1866).

14. Friedel, G. Études sur la loi de Bravais, *Bull. Soc. Franc. Mineral.* **30**, 326–455 (1907).

15. Donnay, J. D. H. & Harker, D. A new law of crystal morphology extending the Law of Bravais. *Am. Mineral.* **22**, 446–467 (1937).

16. Wu, Q., Rauscher, P. M., Lang, X., Wojtecki, R. J., de Pablo, J. J. Hore, M. J. A. & Rowan, S. J. Poly[*n*]catenanes: synthesis of molecular interlocked chains. *Science* **358**, 1434–1439 (2017).